ДОКЛАДЫ
АКАДЕМИИ НАУК СССР

SOVIET PHYSICS

"Doklady"

VOLUME 2 NUMBER 1

A Translation

of the

"Physics Section"

of the

Proceedings of the Academy of Sciences of the USSR

(RUSSIAN ORIGINAL VOL. 112, NOS. 1-6)

Published by the
AMERICAN INSTITUTE OF PHYSICS
INCORPORATED

SOVIET PHYSICS
"Doklady"

A translation of the "Physics Section" of the Proceedings of the Academy of Sciences of the USSR.

A publication of the

AMERICAN INSTITUTE OF PHYSICS

Governing Board

ALLEN V. ASTIN
WALTER S. BAIRD
JESSE W. BEAMS
HANS A. BETHE
RAYMOND T. BIRGE
RICHARD H. BOLT
FRANKLIN D. DEXTER
IRVINE C. GARDNER
SAMUEL A. GOUDSMIT
CHARLES KITTEL
HUGH S. KNOWLES
WINSTON E. KOCK
R. BRUCE LINDSAY
WILLIAM F. MEGGERS
WALTER C. MICHELS
R. RONALD PALMER
ROBERT F. PATON
JOSEPH B. PLATT
RALPH A. SAWYER
HENRY D. SMYTH
MARK W. ZEMANSKY

Officers and Staff

FREDERICK SEITZ
Chairman, Governing Board
ELMER HUTCHISSON
Director
HENRY A. BARTON
Associate Director
WALLACE WATERFALL
Executive Secretary
MARK W. ZEMANSKY
Treasurer
THEODORE VORBURGER
Advertising Manager
RUTH F. BRYANS
Publication Manager
KATHRYN SETZE
Assistant Treasurer
ALICE MASTROPIETRO
Circulation Manager
EUGENE H. KONE
Director of Public Relations

American Institute of Physics Advisory Board on Russian Translations

ROBERT T. BEYER, *Chairman*

FREEMAN DYSON, DWIGHT GRAY, MORTON HAMERMESH, VLADIMIR ROJANSKY

Advisory Editor, Soviet Physics—"Doklady": VLADIMIR ROJANSKY, Ramo-Wooldridge Corporation, Los Angeles, California

SOVIET PHYSICS—"Doklady" is a bi-monthly journal published by the American Institute of Physics for the purpose of making available in English reports of current Soviet research in physics as contained in the "Physics Section" of the Proceedings of the Academy of Sciences of the USSR. The Proceedings appears thirty-six times per year and the "Physics Sections" are accumulated and English translations of them are published in six issues per year.

Transliteration of the names of Russian authors follows the system employed by the Library of Congress.

This translating and publishing project was undertaken by the Institute in the conviction that dissemination of the results of research everywhere in the world is invaluable to the advancement of science. The National Science Foundation of the United States encouraged the project initially and is supporting it in large part by a grant. Translation and printing are being handled by Consultants Bureau, Inc.

The American Institute of Physics and its translators propose to translate faithfully all of the scientific material in the "Physics Section" of the Proceedings of the Academy of Sciences of the USSR appearing after January 1, 1956. The views expressed in the translated material, therefore, are intended to be those expressed by the original authors, and not those of the translators nor of the American Institute of Physics.

One volume is published annually. Volume 2 will consist of six issues and will contain all scientific material published in the "Physics Section" of the original Russian journal during the 1957 calendar year.

Subscription Prices:

Per year (6 issues)	
United States and Canada	$25.00
Elsewhere	27.50
Back Numbers	
Single copies	$ 5.00

Subscriptions should be addressed to the American Institute of Physics, 335 East 45th Street, New York 17, New York.

Copyright by American Institute of Physics 1957

SOVIET PHYSICS

"Doklady"

VOLUME 2, NUMBER 1 JANUARY-FEBRUARY, 1957

A STUDY OF THE EXPLOSIVE SHOWERS PRODUCED BY HIGH-ENERGY COSMIC RAYS

V. V. Alpers, I. I. Gurevich, V. M. Kutukova, A. P. Mishakova
B. A. Nikol'skii and L. V. Surkova

(Presented by Academician A. I. Alikhanov August 28, 1956)

This article gives preliminary results of the study of explosive showers induced by high-energy cosmic ray particles; the 29 showers which were studied were obtained in a nuclear film stack. The stack consisted of 100 layers each 10 cm in diameter and 450 μ thick. We used Type "R" Cine-photographic Research Institute emulsions. The stack was irradiated in the stratosphere at 27 km for 7 hours during May 1955.

TABLE 1

Shower Number	Primary Particles	Ω_*, deg	n_h+n_g	n_s	$\vartheta_{1/2}$, deg	ρ for $k=12$	ρ for $k=6$
1	—		9+14	22	20	0.7	0.54
2	α	0	12+12	50	20	0.97	0.99
3	—		1+1	31	35	0.53	0.95
4	α	3	10+10	26	10	0.12	0.52
5	—		13+13	89	25	0.65	0.8
6*	Z	12,5	14+8	52	15	0.001	0.00001
7*	p	9,5	10+7	25	10	0,09	0.02
8	—		12+7	16	20	0,4	0,8
9	Z	12	12+4	90	27	0.8	0.85
10	n		6+9	22	10	0.85	0.8
11*	Z	2	6+16	78	22	0.037	0,09
12	—		3+2	7	7.5	0,25	0.67
13*	p	0	5+3	23	20	0.1	0,09
14	p	9	3+0	8	5	0.8	0.98
15	p	12	5+2	10	2,5	0.4	0.42
16	—		11+8	12	7.5	0.45	0.12
17	—		9+13	13	10	0.3	0,54
18*	p	1,5	2+4	24	4	0.0028	0.09
19	—		4+7	10	15	0,86	0.95
20	—		10+10	17	9	0.25	0.54
21	—		13+12	22	15	0.02	0.54
22	n		6+2	15	15	0.53	0.08
23	—		13+8	20	25	0.61	0.67
24*	Z	11,5	1+7	93	13	0.05	0,06
25	n		6+2	7	5	0.85	0.91
26	p	0	8+8	26	15	0.12	0,67
27	Z	0	8+9	18	20	0,4	0.9
28	—		7+12	13	32	0.44	0.54
29	—		11+13	13	1	—	—

The emulsions were area scanned with an enlargement of 10 × 15 × 1.5 using MBI-2 microscopes. Explosive showers were recorded with the number of relativistic particles $n_s \geq 5$ in a very narrow cone (black and gray tracks were not discriminated) as well as "jets" containing $n_s \geq 3$ relativistic particles.

The scanning of 26.5 cm^3 of emulsions revealed 27 explosive showers and 29 jets. When the jets were traced through the stack it was found that 2 of them originated in stars while the remaining 27 jets were electron-photon showers.

The 29 explosive showers which were thus observed were analyzed microscopically with an enlargement of 90 × 15 × 1.5. We determined the primary particle which generated the shower, the number of relativistic particles in the shower and the angular distribution of the shower particles with respect to the shower axis. Angles in the plane of an emulsion (α) and the dip angles (β) were measured within 1°. The angular distribution of shower particles with respect to the shower axis was determined by an instrument which had been especially constructed by V. V. Alpers. Each shower particle was plotted on an aluminum sphere and the angles α and β were measured by two special scales. The space angles of the shower particles plotted on the sphere were determined by the use of an additional hemisphere made of plexiglas bearing latitudinal (ϑ) and longitudinal (φ) angles. For each shower we determined the angle $\vartheta_{1/2}$ containing half of the shower particles as well as the distribution with respect to the angles ϑ and φ. We also determined the angle Ω between the axis of symmetry of a shower and the direction of the primary particle whenever the latter could be determined reliably. The experimental data are summarized in Table 1, where n_s is the number of relativistic tracks in the shower and n_h and n_g are the number of black and gray tracks in the star, respectively.

Figure 1 is a graph showing the dependence of n_s on $\vartheta_{1/2}$. Each shower is represented by a point. The figure distinguishes the points for which the nature of the primary particle could be determined reliably. In Fig. 1 the showers produced by heavy particles form a separate region and are characterized by a considerably larger number of shower particles.

If it is assumed that the observed showers resulted from nucleon-nucleon collisions it will be expected that in the center-of-mass system of the two colliding particles, the angular distribution of the shower particles will be symmetrical with respect to the angle $\theta_{c\ m} = \pi/2$. On this hypothesis the experimentally measured angle $\vartheta_{1/2}$ corresponds in the center-of-mass system of the two colliding particles to the angle $\theta_{c\ m} = \pi/2$.

The formulas for transformation to the center-of-mass system in the case of extremely relativistic shower particles will then be:

$$\cot \vartheta = \gamma_c \frac{\cos\theta + 1}{\sin\theta}, \tag{1}$$

$$\gamma_c = \cot \vartheta_{1/2}, \tag{2}$$

where ϑ is the angle of a shower particle in the laboratory system, θ is the angle in the center-of-mass system $\gamma_c = \left[\frac{1}{\sqrt{1-\beta^2}},\right]$ and β is the velocity of the center-of-mass.

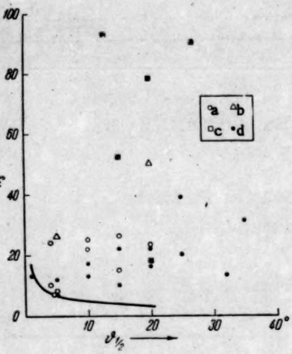

Fig. 1. Dependence of n_s on $\vartheta_{1/2}$ for the observed showers: a) showers produced by neutrons or protons; b) showers produced by alpha particles; c) showers produced by heavy particles; d) showers for which the nature of the primary particle was not determined (a nucleon or alpha particle). The solid curve represents the dependence of n_s on $\vartheta_{1/2}$ according to Fermi's theory Eq. (4).

On the other hand the number of shower particles according to Fermi's thermodynamical theory is associated with the energy of the colliding particles in the center-of-mass system by the formula

$$n_s = k\left(\frac{E}{2mc^2}\right)^{1/4} = k\gamma_c^{1/2}, \tag{3}$$

where E is the energy in the laboratory system, k = 1-2.

Thus, on the assumption of a nucleon-nucleon mechanism of shower production we can write the following relation between n_s and $\vartheta_{1/2}$:

$$n_s = k\sqrt{\cot \vartheta_{1/2}}. \tag{4}$$

Figure 1 gives the dependence of n_s and $\vartheta_{1/2}$ on the assumption that k = 2.

It can be seen from Fig. 1 that some showers satisfy (4) and can thus be attributed to nucleon-nucleon interactions. However, as will be seen hereafter, the angular distributions of shower particles are in disagreement with this conclusion.

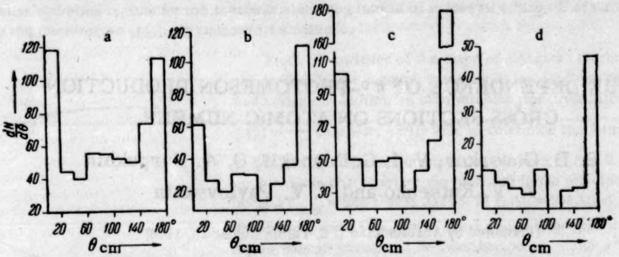

Fig. 2. Angular distributions of shower particles: a) showers produced by heavy particles; b) produced by nucleons; c) produced by nucleons and alpha particles; d) showers which according to (4) can be attributed to nucleon-nucleon interactions (see Fig. 1)

Equations (1) and (2) can be used to obtain for each shower the value of γ_c and the corresponding angular distribution $f(\theta)$ in the center-of-mass system. Figure 2 gives the combined angular distributions obtained in this manner. The figure shows that all showers produced by nucleons and alpha particles are characterized by appreciable asymmetry with respect to the angle $\theta = \pi/2$, which is in disagreement with the model of shower production by nucleon-nucleon interactions. It should be noted that the angular distribution $f(\theta)$ for showers produced by heavy particles was symmetrical with respect to $\theta = \pi/2$, although this conclusion is not very definite in view of the small number of observed cases.

In studying the distribution of shower particles with respect to the azimuthal angle φ we found that some showers showed considerable asymmetry of angular distribution $f(\varphi)$.

The values of P in Table 1 are the Pearson probabilities of observing a given asymmetry of distribution, $f(\varphi)$, for each shower on the hypothesis that the values obtained for the asymmetry result from statistical fluctuations. The Pearson probabilities $P(\chi^2)$ were determined from tables of values of χ^2, calculated from the formula

$$\chi^2 = \frac{k}{N}\Big(\sum_{i=1}^{h} n_i^2\Big) - N,$$

where N is the total number of particles in a shower; k is the number of divisions of the angle φ; n_i is the number of shower particles in the i-th division $\Delta\varphi$.

It should be noted that in a number of instances, the values of P for $k = 6$ and $k = 12$ are considerably different from each other (see showers 6, 7, 18, 21, 22). This results from the relatively small number of particles in the observed showers and is evidence of insufficient accuracy in determining P. In 6 instances the observed asymmetry corresponds to $P \leq 0.1$ for $k = 6$ and $k = 12$ (these showers are indicated in Table 1 by asterisks). Of course, the ultimate explanation of the existence of showers with azimuthal asymmetry of relativistic particles will require a considerable increase in the number of observed cases, and the data of Table 1 must be regarded as only preliminary results.

It must be noted that large asymmetry is observed both for showers produced by heavy particles and for showers produced by nucleons. Table 1 also shows that in a number of instances, there are appreciable angles between the direction of the primary particle and the axis of symmetry of the shower (the angle Ω).

In conclusion, the authors wish to thank D. M. Samoilovich and E. S. Barinova for developing the nuclear emulsions, and L. A. Smirnova for assistance with the microscope work.

Received July 10, 1956

THE DEPENDENCE OF π^0-PHOTOMESON PRODUCTION CROSS SECTIONS ON ATOMIC NUMBER

B. B. Govorkov, V. I. Gol'danskii, O. A. Karpukhin
A. V. Kutsenko and V. V. Pavlovskaia

(Presented by Academician I. E. Tamm August 15, 1956)

The dependence of cross sections for the production of π^0-mesons (σ_{π^0}) by bremsstrahlung quanta on the atomic number A, has been investigated in [1-5] with maximum bremsstrahlung energy varying from 170 to 340 Mev, while the π^0-mesons were recorded through one photon [2, 4, 5], or two photons [1, 3] emitted in their decay. Each of these methods of detecting π^0-mesons has its advantages and disadvantages. The recording of a single photon enables us to strongly increase the statistical accuracy although it is possible at the same time, to record photons scattered elastically or inelastically by nuclei. The recording of two photons permits the distinguishing of π^0-meson production against the background of other processes although at a given position of two counters only π^0-mesons of a very definite energy are observed; this circumstance reduces the efficiency of recording of π^0-mesons from complex nuclei (for which, in the case of inelastic photoproduction, there is no unique relation between the angle of emission and energy) compared with π^0-mesons from hydrogen.

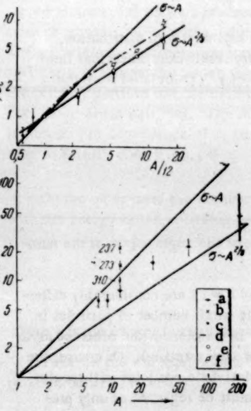

Fig. 1. Dependence of π^0-photomeson production cross sections on atomic number according to the literature:
a) [1] 260 Mev; b) [2], 237-310 Mev; c) [3], (265 ± 15) Mev; d) [4], 170-340 Mev; e) [5], 260 Mev; f) [5], 200 Mev.

Among the shortcomings of previous investigations of the dependence $\sigma_{\pi^0} = f(A)$ one must also mention the fact that the relation between the cross sections for complex nuclei and hydrogen was either not studied at all [3, 4], or determined from difference measurements with paraffin and graphite targets [1, 2, 5] with quite small accuracy. A summary of the data obtained in [1-5] is given in Fig. 1.

In order to determine accurately the dependence of π^0-meson photoproduction cross sections on atomic number in a broad range, we carried out a number of experiments and investigated with special care the region of small A. For this purpose we compared the π^0-meson yield from liquid oxygen, liquid nitrogen and liquid hydrogen in a PS-4 cylindrical foam polystyrene target (of the following dimensions: inside diameter 108 mm, outside diameter 208 mm, wall thickness 40 mg/cm^2). The background of the empty target was 1.6% for oxygen, and from 8 to 33% of hydrogen, so that it was easy to obtain results of high accuracy. For the transition to heavier targets in a single series of experiments we used two graphite targets. One of these, a cylinder of 106 mm diameter, was inserted into the foam polystyrene target, thus permitting a direct comparison of π^0-meson photoproduction in carbon with hydrogen, nitrogen and oxygen. The other graphite target, which was flat with the thickness 3.3 g/cm^2, was placed at 45° to the bremsstrahlung beam with the same geometrical arrangement as targets of aluminum (1.79 g/cm^2), iron (1.30 g/cm^2), copper (1.27 g/cm^2), cadmium (0.928 g/cm^2) and lead (0.541 g/cm^2). Thus, it was possible to compare the cross sections for π^0-meson photoproduction in the above-mentioned complex nuclei with hydrogen.

The experiments were performed using the 265 Mev synchrotron of the Physical Institute of the Academy of Sciences USSR. In order to lessen the overloading of individual counters and coincidence circuits we used an operating regime for the accelerator whereby, instead of sudden switching off of the accelerating voltage on the resonator, we gradually reduced its amplitude.

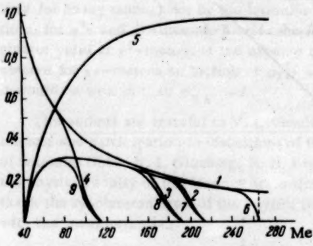

Fig. 2. Various data on the bremsstrahlung spectrum and the efficiency of gamma recording in our experiments

From a knowledge of the shape of elongated synchrotron pulses, that is, the electron spectrum at incidence on the target, and taking the undistorted bremsstrahlung spectrum in the form $f(E) = \frac{a}{E}$, we were easily able to determine the form of the γ-ray spectra in our experiments, as is shown in Fig. 2. Curve 1 in this figure characterizes the spectrum in the principal experiments ($E_{max} = 256$ Mev); Curves 2 ($E_{max} = 200$ Mev), 3 ($E_{max} = 180$ Mev) and 4 ($E_{max} = 97$ Mev) give the spectra for additional measurements which will be described below. The π^0-meson yield was recorded by observing one of the photons from their decay with a telescope consisting of four liquid scintillation counters filled with a solution of terphenyl and toluene (3 g/l). Two telescopes were used simultaneously at the same, or at different angles (90° and 135°).

Following the first counter of each telescope, connected for anticoincidences, we placed a lead converter (6.2–7 g/cm^2); between the third and fourth counters we placed an aluminum filter of thickness 5.4–6 g/cm^2. The gamma threshold, determined by thickness of the second and third counters and of the filter was ~40 Mev for both telescopes.

TABLE 1

Relative cross sections for photoproduction of π^0-mesons

Nucleus	E_{max} = 256 Mev		E_{max} = 200 Mev		E_{max} = 180 Mev
	90°	135°	135°	90°	90°
	Without corrections for other screening processes				With Corrections
H^1	1	1	1	1	1
C^{12}	12.7±0.1	12.0±0.4	22.1±1.4	23.2±2.2	23.9± 2.6
N^{14}	15.1±0.1	15.5±0.5	23.2±1.5	30.3±2.9	31.4± 3.4
O^{16}	17.1±0.2	16.5±0.5	29.5±1.9		
Al^{27}	22.1±0.2	26.0±0.9	40.5±2.9	55.5±5.3	53.8± 6.2
Fe^{56}	38.3±0.4	39.8±1.4	60.4±5.2	82.5±8.2	71.1± 8.7
Cu^{64}	44.7±0.5	41.0±0.5	82.0±6.8	88.0±8.9	73.6± 9.2
Cd^{112}	62.3±0.5	67.6±2.6	109 ±13	135 ±15	101 ±16.0
Pb^{207}	105.2±1.2	91 ±4.5	176 ±31	234 ±26	152 ±28

The dependence of gamma counting efficiency of both telescopes on photon energy E is shown in accordance with the relation $\epsilon \sim 1 - e^{-\frac{E-40}{40}}$ given in [2] (where telescopes of the same kind were used) by Curve 5 of Fig. 2.

The experimental results and statistical errors are shown in Table 1. Small corrections (9-15%) were made in the data to allow for the difference in photon absorption in liquid hydrogen, nitrogen and oxygen targets and in a round graphite target.

The principal source of systematic errors may have been the recording of photons from elastic scattering, whose cross section is approximately $\sim(Z^2/A)^2$, and other processes which screened the effect.

In order to take these errors into account, we performed additional experiments at $E_{max} = 97$ Mev; in order to extrapolate the data from these experiments to higher energies we assumed that the cross section of the various screening processes remains constant from 40 to 260 Mev and that their yield per effective quantum increases

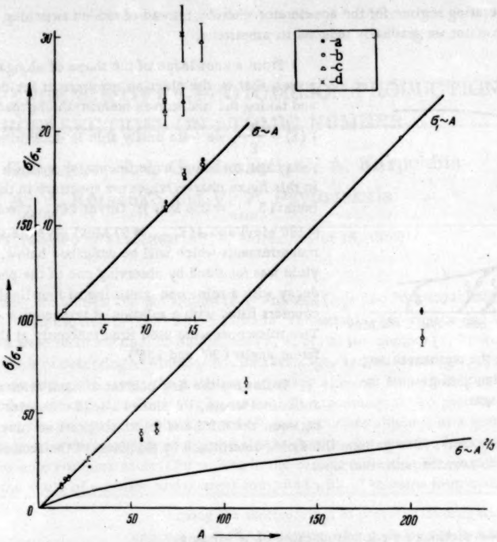

Fig. 3. Dependence of photoproduction cross sections for π^0-mesons on nuclear mass number (our data): a) 90°, 256 Mev; b) 135°, 256 Mev; c) 135°, 200 Mev; d) 90°, 180 Mev.

proportionately to the area under Curves 6-9 of Fig. 2, which represent the product of the bremsstrahlung spectrum by the efficiency of gamma counting. The correction for screening processes at $E_{max} = 265$ Mev does not exceed 9%; for $E_{max} = 180$ Mev, the corrections are indicated in the table. Independently of any screening processes, it follows from our experiments that for light nuclei at least up to oxygen, the cross section for photoproduction of π^0-mesons increases approximately as $\sigma_{\pi 0} \sim A$ (and even somewhat more strongly) and that only thereafter is a relation close to $\sigma_{\pi 0} \sim A^{2/3}$ established (see Fig. 3).

The relation $\sigma_{\pi 0} = f(A)$ can be explained qualitatively by the fact that mesons are produced throughout the entire volume of a nucleus but are then reabsorbed so that only a fraction of the mesons emerge. This interpretation is given in [1, 4] as well as in [6], where the optical model is used as a basis for determining the reabsorption range of pions in the form $\sigma_\pi = f(A)$.

However, for a quantitative examination of meson reabsorption one must take into account three circumstances which have, thus far been neglected:

1. The π^+-meson photoproduction yield in the energy range under consideration is several times greater than the yield for π^0-mesons.

2. The probability of meson scattering by nucleons of the nucleus is not only smaller, but even greater than the probability of charge exchange (and, evidently, than the probability of meson reabsorption through interactions with pairs or groups of nucleons).

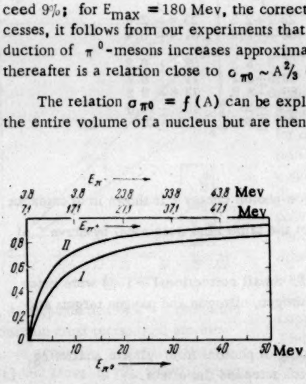

Fig. 4. Ratio of charge exchange cross sections for neutral and charged mesons: 1) $\sigma_{\pi^2 n}/\sigma_{\pi^- p}$; 2) $\sigma_{\pi^2 p}/\sigma_{\pi^+ p}$

3. Due to the endothermic character of charge exchange with π^0-mesons, the cross sections for the reactions $\pi^- + p \rightarrow \pi^0 + n$ and, especially, $\pi^+ + n \rightarrow \pi^0 + p$ at low meson energies considerably exceeded the cross sections for the inverse processes (Fig. 4).

The existence of strong scattering (point 2) indicates the possibility of analyzing meson reabsorption (at least for heavy nuclei) not by the formulas of the optical model, but rather by a system of two diffusion equations, for π^0- and $\pi^\pm$-mesons. Due to the facts mentioned in points 1 and 3, charge exchange must result in a greater yield of π^0-mesons at the expense of $\pi^\pm$-mesons, so that in the absence of meson absorption we would observe for π_0-mesons an increse of $\sigma_{\pi 0}$ with A, which would be stronger than $\sigma_{\pi 0} \sim A$, while for $\pi^\pm$-mesons it would be weaker than $\sigma_{\pi \pm} \sim A$.

The authors are grateful to V. I. Veksler, Corresponding Member of the Academy of Sciences USSR for his interest and participation in discussions of the results, to A. I. Shal'nikov, Corresponding Member of the Academy of Sciences USSR, N. I. Ginzburg, N. N. Khoroshilov and other members of the Low Temperature Department of the Physics Faculty of the Moscow State University for assistance in the work with liquid hydrogen. We also thank the synchrotron crew of the Physics Institute and our Bulgarian colleague, Milko Borislov, who assisted with the measurements.

Received August 14, 1956

LITERATURE CITED

[1] W. H. Panofsky, J. N. Steinberger and J. Steller, Phys. Rev. 76, 180 (1952).

[2] G. Cocconi and A. Silverman, Phys. Rev. 88, 1230 (1952).

[3] R. Meunier, P. Barringer and L. S. Osborne, Bull. Am. Phys. Soc., Ser. II, 1, No. 4, EA6, EA7 (1956).

[4] J. D. Anderson, R. W. Kenney and C. A. Macdonald, Phys. Rev. 100, 1798, I, 4 (1955); Bull. Am. Phys. Soc., Ser. II, 1, No. 5, E8, (1956).

[5] A. S. Belousov, E. I. Tamm and E. V. Shitov, All-Union Conference on the Physics of High-Energy Particles (Acad. Sci. USSR Press, 1956) p. 93, (Russian Translation).

[6] K. A. Brueckner, R. Serber and K. Watson, Phys. Rev. 84, 258 (1951).

FINE STRUCTURE AND LAMB SHIFT OF THE $2s_{1/2}$ LEVEL OF THE TRITIUM T_α LINE λ 6560 A

P. S. Kireev

(Presented by Academician A. A. Lebedev April 25, 1956)

An investigation of the fine structure of lines of the third hydrogen isotope, tritium, is of considerable scientific interest. The theory of the fine structure and Lamb shift of the levels $ns_{1/2}$ can be checked for tritium lines with greater accuracy than for the lines of hydrogen or deuterium since the Doppler breadth of tritium lines is 1.73 and 1.22 times smaller, respectively, than the widths of lines emitted by hydrogen and deuterium under identical conditions. It is of great interest to investigate the intensities of the fine structure components of tritium lines and the isotope shift resulting from the different masses of H, D and T. There is practically no information in the literature concerning spectroscopic investigations of tritium lines.

In the present work we investigated the fine structure of T_α(λ 6560 A), the first line of the Balmer series of tritium, the intensities of the fine structure components and the isotope shift $H_\alpha - T_\alpha$.

Table 1 gives the structure of T_α, based on Dirac's theory of the electron. The separation of the components from the most intense component a is given according to Dirac's theory and with allowance for the Lamb shift of the terms $2s_{1/2}$ and $3s_{1/2}$. The intensities of the components are given in arbitrary units based on Dirac's theory of radiation. Table 1 contains data on the fine structure of the α-line of the Balmer series of any hydrogen isotope. For the shift of the terms $2s_{1/2}$ and $3s_{1/2}$, we have taken the values 0.035 and 0.010 cm^{-1} [1] (Fig. 1).

TABLE 1

Desig-nation	Transition	(Dirac) $1\cdot10^{-3}$ см$^{-1}$	$\delta\nu$ Lamb shift $1\cdot10^{-3}$ см$^{-1}$	I_{theor}
a	$3d_{5/2} - 2p_{3/2}$	0,0000	0,0000	9.00
g	$3d_{3/2} - 2p_{1/2}$	328.6	328.6	5.00
f	$3p_{3/2} - 2s_{1/2}$	328.6	293.6	2.08
e	$3p_{1/2} - 2s_{1/2}$	220.8	185.8	1.04
d	$3s_{1/2} - 2p_{1/2}$	220.8	230.8	0.10
	$3d_{3/2} - 2p_{3/2}$	—36.0	—36.0	1.00
c	$3s_{1/2} - 2p_{3/2}$	—144.2	—134.2	0.195

In this work the light source was a U-shaped discharge tube with a capillary of about 3 mm diameter and ~ 120 mm long, the tube was carefully evacuated while the walls and electrodes were heated; it was then filled with pure tritium to 2-3 mm Hg pressure. Tritium radiation was excited by a current of a few milliamperes (2.5-10 ma) from a high-voltage transformer connected to the tube in series with a resistance of ~ 200,000 ohms.

The fine structure of T_α was resolved by a Fabry-Perot interferometer with different spacings placed before the slit of an ISP-51 spectrograph with an $f = 270$ mm camera. The interference pattern was projected on the slit of the spectrograph by an $f = 300$ mm objective. The reflection coefficient of the interferometer mirrors in the investigated region was 0.92. The source, placed in a vertical position, was immersed in liquid nitrogen to reduce the Doppler breadth of the lines. Light from the source was directed to the interferometer by a rotatable prism. Secondary images from the interferometer were collected by a second slit placed behind the rotatable prism and projected on the spectrograph slit by auxiliary objectives. The spectrum was photographed on highly sensitive panchromatic film with exposures from 2-3 to 30-40 minutes. The spectrograms were measured with an IZA-2 comparator and the results were interpreted by the (tabular) method of exact fractions.

Control photographs taken with interferometers of different spacings showed that T_α consists of three well resolved components. The majority of the photographs were taken with a 7.0 mm interferometer spacing and 0.7148 cm^{-1} dispersion. After the tube had been operated for some time, the spectrum showed traces of hydrogen; this was controlled by photographing the emission of hydrogen in a hollow cathode. Thereupon, T_α was photographed with interferometer spacing of 4.0 and 5.0 mm; in this instance, the line H_α is between the orders of T_α. A very small quantity of hydrogen aided the more exact measurement of the separations of components in H_α and T_α (Figs. 2 and 3).

The mean values of the separations between complexes (a group of unresolved components will be called a complex) a–e, e–g and a–g are 192.3, 129.0, and 321.3 (in units $1 \cdot 10^{-3}$ cm^{-1}). These results do not agree with Dirac's fine structure theory because of the shift of the $2s_{1/2}$ and $3s_{1/2}$ levels with respect to $2p_{1/2}$ and $3p_{1/2}$. To obtain the magnitude of the shift, we can use a calculation from the position of the center of gravity on the assumption that the center of gravity of a complex is given by the maximum blackening and that the location of maximum blackening is determined only by the components in a given complex. We neglect the influence of neighboring complexes in first approximation. Denoting the shift of the $2s_{1/2}$ level by x and assuming that the shift of the $3s_{1/2}$ term follows the n^{-3}-law, we can obtain the shift x by comparing the experimentally determined separations between complexes with their theoretical values. In this case we obtain for x (in units $1 \cdot 10^{-3}$ cm^{-1}): $x = 35.4$, $x = 34.9$, $x = 36.4$, which values were obtained from the separations a–e, a–g, g–e, respectively, taking into account the theoretical values of the component intensities. The average shift of the $2s_{1/2}$ level is $35.5 \cdot 10^{-3}$ cm^{-1}, which is in good agreement with the theory of $ns_{1/2}$ shifts in hydrogen and deuterium [1]. But for a more exact calculation of the level shifts, the influence of neighboring complexes must be taken into account. The effect of complex g on complex e can be allowed for by assuming that the lines have a pure Doppler shape. Taking the experimental halfwidths and line intensities, which differ from the theoretical values (see below), we can obtain the shift of the $2s_{1/2}$ level as 0.037 cm^{-1}. The influence of neighboring components on the location of the maximum in the case of a Doppler contour is very strongly dependent on the halfwidth; therefore, the shift in this case is determined to an accuracy of 0.002-0.003 cm^{-1}. Thus, we can state that the shift of $2s_{1/2}$ lies within the limits $0.033 < \delta E_{2S} < 0.039$ cm^{-1}. In order to obtain a more exact value, we must reduce the line width by cooling the hydrogen.

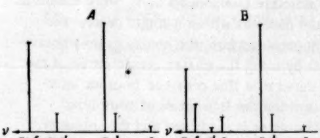

Fig. 1. Structure of the T_α line from the Dirac theory (A) and with allowance for the Lamb shift of the levels $ns_{1/2}$ (B)

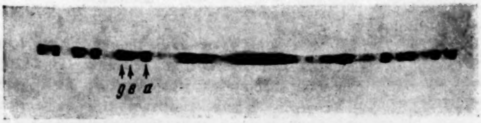

Fig. 2. Structure of T_α. Interferometer spacing t = 7.0 mm.

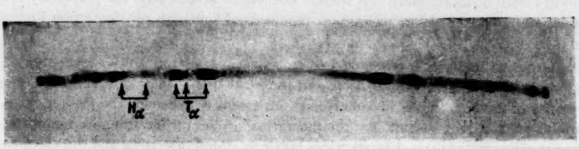

Fig. 3. Isotope shift $T_\alpha - H_\alpha$. Interferometer spacing t = 4.0 mm.

The $H_\alpha - T_\alpha$ isotope shift was investigated by Pomerance and Terranova [2] using a spectrograph and diffraction grating with 0.14 mm/A dispersion. They obtained a $H_\alpha - T_\alpha$ separation of (2.36 ± 0.05) A or (5.475 ± 0.116) cm^{-1}. The use of an interferometer permits a considerable reduction of measuring errors and gives a more precise result.

The measurement of separations between corresponding components was obtained in our work from spectrograms taken with an interferometer of 4.0, 4.3 and 5.0 mm spacing. The isotope shift between corresponding components of H_α and T_α (in air) was found to be $\delta\nu = (5.5321 \pm 0.0025)\ \mathrm{cm}^{-1}$. Considering the refractive index of air, and introducing a correction for the isotope shift in a vacuum, we obtained $\delta\nu = (5.5305 \pm 0.0025)\ \mathrm{cm}^{-1}$, which is greater by $0.006\ \mathrm{cm}^{-1}$ than the theoretical value [3] assuming a simple mass effect. The discrepancy lies within the limits of error, but the explanation is not known.

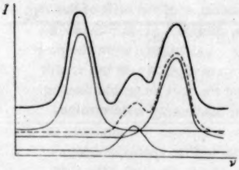

Fig. 4. Curve of the intensity of T_α and its resolution into the contours of complexes. Interferometer spacing t = 7.0 mm

The intensities of the fine structure components of T_α were measured from the ratios of the areas of the contours within a single order. For this purpose the photomicrogram obtained from the spectrogram was converted into a curve of intensities by using the characteristic curve of the film S(log I). But the intensity curve of a line obtained from an interferometer cannot be used to determine the intensities of complexes since the dispersion of an interferometer is nonlinear and the intensity curve cannot be resolved into the contours of complexes. Therefore, the intensity curve obtained from a spectrogram is converted into a curve with linear dispersion. Figure 4 gives the intensity curve of T_α with ϵ the order of interference counted from a certain maximum. In order to determine the relative intensities of complexes from a combined intensity curve, the contours of complexes are separated (in Fig. 4 the contours of complexes are denoted by light lines). The ratio of the areas of complex contours within a single order ($\Delta\epsilon = 1$) gives the relative intensity of the complexes, and the area of a complex is proportional to the sum of intensities of the components in the complex. As unity, we have taken the intensity of complex *a*, which consists of components *a*, *b*, *c*. As Table 2 shows, the intensity of complex *g*, which consists of components *g* and *f*, is somewhat higher than the theoretical value; the intensity of complex *e*, which consists of components *e* and *d*, is almost twice as great as the theoretical value.

TABLE 2

Complex	Composition of complex	I_{exp}	I_{theor}
a	*a, b, c*	1.000	1.000
g	*g, f*	0.772	0.694
e	*e, d*	0.218	0.112

The raised values of the intensities of *e*, *d* and *g*, *f* results from processes in the light source. Self-absorption of light in the source cannot be responsible for the anomalous distribution of intensities in line components because self-absorption should reduce the intensities of *e* and *f*, since they result from an atomic transition into the state $2s_{1/2}$ which is metastable, and thus these components should show considerably greater self-absorption than the others. Observations by photographing light through the capillary agree with observations of light along the capillary within the limits of error. Thus our results for tritium confirm in several ways the previously observed strong dependence of the relative intensities of fine structure components of hydrogen and deuterium lines on the conditions of excitation [4].

It is striking that increased intensity is observed for components associated with *s*-levels, which experience considerable vacuum shift. This was observed by us [5] for the He II line λ 4686 A. Kuhn and Series [6], observed increased intensity of the *e* complex in deuterium; this intensity exceeded the theoretical value by a factor of 1.7. All of this permits us to assume that the theoretical values of fine structure intensities are incorrect because they do not allow for additional interactions between atomic electrons and the electromagnetic and electron-positron vacuum, as a result of which, the transition probability for components associated with s-levels increases, thus increasing the intensities of these components compared with the remainder, for which such interactions are less pronounced. We may possibly have in this case a peculiar "vacuum effect" for intensities superimposed on effects associated with the conditions of excitation. A final explanation can be obtained following a detailed investigation of the variation of intensities with different conditions of excitation in order to take into account the dependence on excitation conditions and the distinguishing of a possible "vacuum effect for intensities" in pure form.

In conclusion, I wish to thank F. A. Korolev for his interest and assistance and D. D. Ivanenko, similarly.

M. V. Lomonosov Moscow State University
Received April 24, 1956

LITERATURE CITED

[1] Recent Developments in Quantum Electrodynamics, Collection, (Foreign Lit. Press, 1954) (Russian Translation).

[2] H. Pomerance and D. Terranova, Am. J. Phys. 18, 466 (1950).

[3] C. E. Moore, Atomic Energy Levels, 1 (Washington, 1949), pp. 1-3.

[4] H. Bethe, Quantum Mechanics of One- and Two-Electron Problems (1935) (Russian Translation).

[5] P. S. Kireev, Doklady Akad. Nauk SSSR 106, 4, 630 (1956). *

[6] H. Kuhn and C. W. Series, Proc. Roy. Soc. (London) A 202, 127 (1950).

---

*[Soviet Physics-Doklady, p. 74].

ON THE ROLE OF BOUND STATES IN PHOTOPRODUCTION*

A. A. Logunov, B. M. Stepanov and A. N. Tavkhelidze

(Presented by Academician N. S. Bogoliubov July 12, 1956)

In the present note we propose to examine the role of bound states in the dispersion relations of photoproduction processes. This is an important question, since it is connected with an analysis of the unobservable energy region in the dispersion relations. The photoproduction threshold in the coordinate system $(\mathbf{p}+\boldsymbol{\varphi})=0$ is $(1+\frac{\mu^2}{4\mathbf{p}^2})\,|\mathbf{p}|$.** We shall consider the region of energies E for which $E < |\mathbf{p}| + \frac{\mu^2}{4|\mathbf{p}|}$ and where, consequently, the formation of "bound" states is possible.

The antihermitian part of the photoproduction amplitude can be represented as

$$
\begin{aligned}
A_{\xi,\,\omega}(E,\ \lambda\mathbf{e}) = \pi \sum_n \langle \dot{\Psi}_{-\mathbf{p},\,s'} J_{\rho'}(0)\, \Psi_{n,\,\lambda\mathbf{e}-\varepsilon\rho} \rangle \langle \dot{\Psi}_{n,\,\lambda\mathbf{e}-\varepsilon\mathbf{p}}\, I_m(0)\, \Psi_{\mathbf{p},\,s} \rangle \times \\
\times\, \delta\left(E - \sqrt{M_n^2 + \lambda^2 + \varepsilon^2\mathbf{p}^2} + \sqrt{M^2 + \mathbf{p}^2}\right) - \\
- \pi \sum_n \langle \dot{\Psi}_{-\mathbf{p},\,s'}\, I_m(0)\, \Psi_{n,\,-\lambda\mathbf{e}+\varepsilon\mathbf{p}} \rangle \langle \dot{\Psi}_{n,\,-\lambda\mathbf{e}+\varepsilon\mathbf{p}}\, J_{\rho'}(0)\, \Psi_{\mathbf{p},\,s} \rangle \times \\
\times\, \delta\left(E + \sqrt{M_n^2 + \lambda^2 + \varepsilon^2\mathbf{p}^2} - \sqrt{M^2 + \mathbf{p}^2}\right). \qquad (1)
\end{aligned}
$$

We assume that between M and $M+\mu$ there are no bound states of the meson-nucleon system. In other words, $M_n \geq M+\mu$ for $n \geq 1$ ($n = 0$ corresponds to a single-nucleon state of the system). We consider the region of recoil momenta $\mathbf{p}^2 < M\mu/2$. It is then easily shown that the integration interval in the dispersion Relations (10) of reference [1] divides into two parts:

$$
0 < E' < \frac{M\mu + {}^1\!/_4\mu^2 - \mathbf{p}^2}{\sqrt{M^2 + \mathbf{p}^2}} < E' < \infty. \qquad (2)
$$

In the first region a non-vanishing contribution to the integral comes only from single-nucleon states. States with $n \geq 1$ contribute to the integral only in the second region. Strictly speaking, the second region still retains a portion of the unobservable energy region. But its contribution can be made sufficiently small if the recoil momentum is suitably fixed.

The expression for $A_{\xi,\,\omega}$ in the first energy region can be written as:

---

* Presented at the All-Union Conference on the Physics of High-Energy Particles May 15, 1956.

** We retain the notation and terminology of [1].

$$A_{\xi,\,\omega}(E,\ \lambda \mathrm{e}) =$$

$$= -\pi \frac{M^2 - {}^1\!/_4\mu^2}{M^2 + \mathbf{p}^2} \sum_{s''} \langle \Psi_{-\mathbf{p},\,s'} I_m (0)\, \Psi_{-\lambda\mathrm{e}+\varepsilon\mathbf{p},\,s''} \rangle \langle \Psi_{-\lambda\mathrm{e}+\varepsilon\mathbf{p},\,s''} J_{\rho'} (0)\, \Psi_{\mathbf{p},\,s} \rangle$$

$$\delta \left(E - \frac{\mathbf{p}^2 + {}^1\!/_4\mu^2}{\sqrt{M^2 + \mathbf{p}^2}} \right). \qquad (3)$$

Let us consider the mean values of the currents herein. For example, we shall calculate the average of the meson current $I_{\rho'}(0)$. The average electromagnetic current is calculated similarly.

We have: $\langle \dot{\Psi}_{\mathbf{p}',\,s'} I_{\rho'}(x)\, \Psi_{\mathbf{p},\,s} \rangle = e^{i(p'-p)x} \langle \dot{\Psi}_{\mathbf{p}',\,s'} I_{\rho'}(0)\, \Psi_{\mathbf{p},\,s} \rangle$;

and on the other hand : $\langle \dot{\Psi}_{\mathbf{p}',s'}\ I_{\rho'}(x)\, \Psi_{\mathbf{p},s} \rangle = i \langle \dot{\Phi}_{p',s'} \dfrac{\delta S}{\delta \varphi_{\rho'}(x)} \Phi_{p,s} \rangle$.

Introducing the Fourier transformation

$$\varphi_{\rho'}(x) = \frac{1}{(2\pi)^4} \int e^{iqx} \varphi_{\rho'}(q)\, dq,$$

we obtain

$$\delta(p' - p + q) \langle \dot{\Psi}_{\mathbf{p}',\,s'} J_{\rho'}(0)\, \Psi_{\mathbf{p},\,s} \rangle = i \langle \dot{\Phi}_{p',\,s'} \frac{\delta S}{\delta \varphi_{\rho'}(q)} \Phi_{p,\,s} \rangle.$$

The last expression can be represented symbolically in the form of the following sum of diagrams:

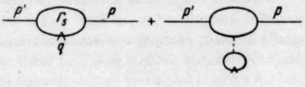

Here Γ_5 is the strongly bound part. If instead of the symbol $\wedge$ there were free meson lines here the sum under consideration would be

$$\gamma_5^{\rho'}(p,\ p',\ q)\, \Delta_c^{\rho'}(q).$$

Since we lack a free meson line, the expression obtained must be multiplied by $(\mu^2 - q^2)$.

Normalizing the Green's functions at $p'^2 = M^2$, $p^2 = M^2$, $q^2 = \mu^2$, with conservation of energy and momentum we obtain finally

$$\langle \dot{\Psi}_{p's'} J_{\rho'}(0)\, \Psi_{p,\,s} \rangle = g\ \langle \bar{u}_{s'}(p')\, \gamma^5 \tau^{\rho'} u_s(p) \rangle. \qquad (4)$$

As can easily be seen g is the renormalized pseudoscalar coupling constant of the meson and nucleon fields.

For the electromagnetic current

$$\langle \Psi_{p',\, s'} I_m (0)\, \Psi_{p,\, s} \rangle = \\ = \langle u_{s'}(p') \left\{ e \frac{1+\tau_3}{2} \gamma^m + \frac{1}{2} \hat{\mathfrak{M}} \, [(k\gamma),\ \gamma^m] \right\} u_{s}(p) \rangle, \qquad (5)$$

where $\hat{\mathfrak{M}} = \mu_p \frac{1+\tau_3}{2} + \mu_n \frac{1-\tau_3}{2}$; e is the renormalized electronic charge; μ_p and μ_n are the anomalous magnetic moments of a proton and neutron.

With the aid of (4) and (5) it is not difficult to write in final form the dispersion relations for photoproduction taking account of "bound" states and eliminating the unobservable energy region. A complete analysis of the dispersion relations in the approximation of a fixed source gives results equivalent to those of Low and Chew [2].

We are deeply grateful to Academician N. N. Bogoliubov for directing this work.

M. V. Lomonosov Moscow State University

Received July 4, 1956

LITERATURE CITED

[1] A. A. Logunov, and B. M. Stepanov, Doklady Akad. Nauk SSSR 110, 3, 368 (1956).*

[2] G. F. Chew and F. E. Low, Phys. Rev. 101, 1579 (1956).

---

*[Soviet Physics-Doklady, p. 552].

ON THE OBSERVATION OF MAGNETIC VISCOSITY IN FERRITES AT LOW TEMPERATURES

R. V. Telesnin and I. A. Lednev

(Presented by Academician I. K. Kikoin November 7, 1956)

At low temperatures the magnetic viscosity of the majority of ferromagnetic substances and particularly of ferrites is strongly increased [1, 2]. This may be observed in a very simple manner. Around a toroidal ferrite sample with high initial permeability $\mu_0 \approx 2000$ gauss/oersted we place two coils: a primary magnetizing and a secondary measuring coil; the voltage from the secondary coil is fed through an electron-tube integrator or ordinary RC integrating circuit and amplifier to the vertical input of an oscilloscope. The sweep voltage is applied to the oscilloscope in the usual manner from a resistance connected in series with the magnetizing coil of the toroid [3]. A low-frequency current such as 50 cps is sent through the magnetizing coil. The current amplitude is such that the ferrite is in a field H', at which there is intersection of the static magnetization curves taken at room temperature and at the temperature of liquid nitrogen (Fig. 1). Then the values of the static magnetic permeability at these two temperatures are identical and reduction of the induction B at very low frequencies and low temperatures can be caused only by magnetic viscosity.

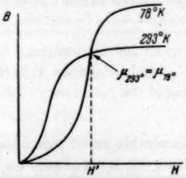

Fig. 1

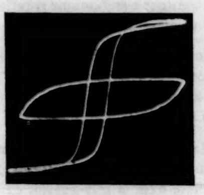

Fig. 2

Figure 2 shows oscillograms of the hysteresis loop of a ferrite with $\mu_0 = 2000$ at 293° K (narrow high loop) and 78° K (broad low loop). It can be seen that the reduction of induction due to viscosity is of very considerable magnitude; this must be taken into account in designing apparatus containing ferrites for operation at very low temperatures.

M. V. Lomonosov Moscow State University

Received August 30, 1956

LITERATURE CITED

[1] R. V. Telesnin and E. F. Kuritsyna, Doklady Akad. Nauk SSSR 75, 6, 797 (1950).

[2] E. F. Kuritsyna, Doklady Akad. Nauk SSSR 84, 1, 45 (1952).

[3] G. Hund, High Frequency Measurements (1931) (Russian translation).

ON THE SOLUTION OF A PROBLEM WITH THE SCHROEDINGER EQUATION IN INFINITE THREE-DIMENSIONAL SPACE

M. Burnat

(Presented by Academician S. L. Sobolev November 22, 1956)

Scattering is one of the very important problems of quantum mechanics. This requires the solution of the equation

$$-\Delta u + q(x)u - \lambda^2 u = 0, \tag{1}$$

over all Euclidean space and satisfying certain conditions at infinity and in the neighborhood of singular points of $q(x)$ if such exist. The number λ^2 is assumed to be real and not identical with the eigenvalues of (1).

The question of the existence and unique solution of the scattering problem was first investigated with complete rigor for a continuous potential $q(x)$ by A. Ia. Povzner [1].

In the present article we examine the case in which the potential $q(x)$ has singularities. Equation (1) is considered in three-dimensional Euclidean space. The proof of existence and uniqueness is based on an investigation of the resolvent kernel. Proof is given of a number of properties of the resolvent and the kernel is evaluated in the vicinity of singular points.

Theorem 1. Let $q(x)$ be continuous in E except for a finite or enumerable set of points having only isolated limit points (at infinity and in the vicinity of singular points no limitations are placed on the behavior of $q(x)$. Furthermore, let there exist a self-adjoint extension Af of the operator $Bu = -\Delta u + qu$. Then for any regular point λ of the operator Af its resolvent is

$$R_\lambda u = \int\limits_E H(x, y; \lambda)\, u(y)\, dy; \tag{2}$$

$$\int\limits_E |H(x, y; \lambda)|^2\, dy < N(Z, \lambda), \quad x \subset Z, \tag{3}$$

where Z is any bounded region which does not contain singular points.

In order to determine the more detailed characteristics of the resolvent nucleus, and first of all its value in the vicinity of singular points of $q(x)$ certain limitations must be imposed on $q(x)$.

Let $q(x)$ with the exception of a finite number of singular points $P_1, \ldots, P_n$, be continuous with a continuous first derivative and

$$q(x) \underset{x\to\infty}{=} O\left(\frac{1}{|x|^{3.5+\varepsilon}}\right), \tag{4}$$

where ϵ is an arbitrary positive number, and in the vicinity of the singular points

$$q(x) \underset{s=1,2,\ldots,n}{=} O\left(\frac{1}{|x-P_s|^{\alpha_s}}\right), \quad \alpha_s < 1.5. \tag{5}$$

We shall hereinafter always assume that $q(x)$ satisfies these conditions. Then the operator $Bu = -\Delta u + qu$ has [2] zero defect indices and thus a unique self-adjoint extension Af. We shall consider the resolvent of this self-adjoint extension below.

It can be proved that the kernel $H(x, y;\ \lambda^2)$ for $y \neq P_s$ satisfies the integral equation

$$f(x) + \frac{1}{4\pi}\int_E \frac{e^{-i\lambda|x-s|}}{|x-s|}\, q(s) f(s)\, ds = \frac{e^{i\lambda(x-y)}}{4\pi|x-y|}. \tag{6}$$

For the further investigation of the resolvent Banach spaces are introduced.

Let y be any point which does not coincide with P_s ($s = 1, 2, \ldots, n$), and K_s be nonintersecting spheres whose centers are at the points P_s and which do not contain the point y. Let the incomplete normalized linear space $B^0_{y,K_1\ldots K_n}$ consist of all functions of the form

$$f(x, y) = \frac{a}{|x-y|} + u(x),$$

where a is a constant; $u(x)$ is continuous in E; $u(x) \to 0$ uniformly as $x \to \infty$ and

$$\|f\|_{B^0_{y,K_1\ldots K_n}} = |a| + \sup_{x \subset E - \sum_s K_s} |u(x)| + \left(\sum_{s=1}^{n} \int_{K_s} u^2(x)\, dx\right)^{1/2}. \tag{7}$$

Completion of the space $B^0_{y,K_1\ldots K_n}$ will be denoted by $B_{y,K_1\ldots K_n}$.

We introduce the complete space B_y which consists of the same set of functions as $B^0_{y,K_1\ldots K_n}$, with its norm given differently:

$$\|f\|_{B_y} = |a| + \sup_{x \subset E} |u(x)|. \tag{8}$$

Finally B will denote the subspace of B_y which is obtained from B_y when we set $a = 0$. It can be proved that in these spaces Fredholm's alternative is valid for the integral operator in (6). Making use of the fact that the operator under consideration has zero defect indices this alternative can be formulated in terms of the spectrum of the self-adjoint extension Af. Indeed,

$$f(x) + \frac{1}{4\pi}\int_E \frac{e^{i\lambda(x-s)}}{|x-s|}\, q(s)\, f(s)\, ds = g(x) \tag{9}$$

for any g(x) in the considered spaces then and only then has a unique solution (belonging to the appropriate spaces) when λ^2 is not an eigenvalue.

Since the resolvent kernel satisfies (6) and $H(x, y;\ \lambda^2) \subset B_{y, K_1 \ldots K_n}$, from the uniqueness of the solution of (6) and the fact that

$$B \subset B_y \subset B_{y, K_1 \ldots K_n}, \tag{10}$$

it follows that

$$H(x, y;\ \lambda^2) \subset B_y; \tag{11}$$

$$h(x, y;\ \lambda^2) \subset B, \tag{12}$$

where $h(x, y;\ \lambda^2) = H(x, y;\ \lambda^2) - \dfrac{1}{4\pi(x-y)}$.

It follows from the above that the integral operator of (9) for λ^2 which is not an eigenvalue of Af has bounded inverses in the considered spaces. On this basis we evaluate the kernel in the vicinity of the singular points. Thus, for example, the following theorem is valid.

Theorem 2.

$$|h(x, y;\ \lambda^2)| \underset{s=1,2,\ldots,n}{<} \begin{cases} M, & \alpha_s < 1; \\ \dfrac{M}{|y - P_s|^{\alpha_s - 1}}, & \alpha_s > 1; \\ M\,|\ln|y - P_s||, & \alpha_s = 1, \end{cases} \tag{13}$$

where $x \subset E$; M is a constant; α_s are the indices in Equation (5).

We similarly make the corresponding evaluations for the derivatives of the resolvent kernel.

It can also be proved that when λ^2 is regular and approaches a point λ_0 of the purely continuous spectrum of the operator Af, then $H(x, y;\ \lambda^2)$ for x and y in any bounded region not containing singular points of q(x) uniformly approaches a certain function $H(x, y;\ \lambda^2)$.

We introduce the set of functions $K_{\alpha_1 \ldots \alpha_n}$ [$\alpha_1, \ldots, \alpha_n$ are the indices of (5)] consisting of all functions which satisfy the conditions:

(1) v(x) is doubly differentiable continously in $E - \sum_{s=1}^{n} P_s$;

(2) v(x) satisfies the radiation conditions;

$$(3)\quad v(x) \underset{s=1,2,\dots,n}{=} O\left(\frac{1}{|x-P_s|^{3-\alpha_s-\varepsilon}}\right), \quad \frac{\partial v}{\partial x} \underset{s=1,2,\dots,n}{=} O\left(\frac{1}{|x-P_s|^{2-\varepsilon}}\right), \tag{14}$$

where ϵ is an arbitrary positive number.

The solution of (1) will be obtained in the form

$$u(x) = e^{i\lambda(\omega, x)} + v(x),$$

where $v(x) \subset K_{\alpha_1 \dots \alpha_n}$ and ω is a given unit vector. Then (1) is reduced to

$$-\Delta u + q(x)v - \lambda^2 v = -q(x)e^{i\lambda(\omega, x)}. \tag{15}$$

On the basis of the properties of the resolvent we can prove the following theorem:

Theorem 3. If $q(x)$ satisfies the Conditions (4) and (5) then (15) for λ^2 which does not coincide with an eigenvalue of the operator Af has in the class $K_{\alpha_1 \dots \alpha_n}$ a unique solution of the form

$$v(x) = -\int_E \tilde{H}(x, y; \lambda^2)\, e^{i\lambda(\omega, y)} q(y)\, dy, \tag{16}$$

where $\tilde{H}(x, y; \lambda^2)$ for regular λ^2 is the kernel of the resolvent and for λ^2 belonging to the continuous spectrum coincides with the limit of the kernel which was mentioned above.

Furthermore,

$$v(x) \underset{\substack{x \to P_s \\ s=1,2,\dots,n}}{=} O(1), \quad \frac{\partial v}{\partial x} \underset{s=1,2,\dots,n}{=} \begin{cases} O(1) & \alpha_s < 1, \\ O\left(\frac{1}{|x P_s|^{\alpha_s - 1}}\right), & \alpha_s > 1; \\ O(\ln|x - P_s|), & \alpha_s = 1. \end{cases} \tag{17}$$

The behavior of the solution and of the resolvent kernel at infinity (radiation conditions) can be studied as in reference [2].

A. A. Zhdanov Leningrad State University

Received October 5, 1956

LITERATURE CITED

[1] A. Ia. Povzner, Math. Collection (U.S.S.R.) 32, (74), 1 (1953).

[2] K. Friedrichs, Math. Ann. 109, 4-5 (1934).

PHOTOLUMINESCENCE OF THALLOUS CHLORIDE

A. S. Vysochanskii

(Presented by Academician A. N. Terenin November 21, 1956)

The study of luminescence in thallium halides in the crystalline state is of great interest in connection with the investigation of alkali-halide phosphors activated by thallium. In addition, thallium halides are in many respects similar to silver halides so that an understanding of their characteristics could improve understanding of the processes which take place in photographic materials.

The photoluminescence of thallous chloride was first observed by Randall [1], who determined that TlCl emits blue light at -183°. No more detailed information regarding the photoluminescence of thallous chloride had been published by the time that our investigation was completed in February 1953. In June 1953, the article of Gobrecht and Becker [2] appeared in which an attempt was made to account for the blue radiation from thallous chloride by the presence of a small amount of water.

Having studied, in addition to the luminescence of thallous chloride, the absorption of light, the luminescence excitation spectrum and the temperature dependence of the luminescence spectrum, we have come to different conclusions.

1. Preparation of samples.

The original materials used in preparing thallous chloride were the triply recrystallized chemically pure salts $TlNO_3$ and NH_4Cl or KCl. The precipitate was carefully washed and dried. All operations were performed in darkness or in dark red light.

For the investigation of the absorption spectrum, the samples were prepared in the form of thin films of thallous chloride deposited on a quartz backing by thermal atomization in a high vacuum.

The excitation and luminescence spectra were studied in powdered phosphors, fused films, sublimated phosphors and solidfied melts of thallous chloride. The films were prepared by the method of Levitskaia and Korolev [3], the sublimates were prepared by the method of F. D. Klement [4] and the melts were prepared by melting the salt in a quartz crucible. The specimens were prepared under dark red light.

2. The absorption spectrum of thallous chloride phosphors.

A "Beckman" spectrophotometer was used to investigate the absorption spectrum from 2200 to 4600 A. In this region, in addition to the intrinsic absorption peak observed by Hilsch and Pohl [5] at 2490 A we observed two absorption peaks at 3520 and 3800 A. These peaks were weak in samples which had not been subjected to light and are considerably strengthened if before the measurement the sample is irradiated with ultraviolet light from a mercury lamp (Fig. 1, 1) before irradiation; 2) after irradiation). Both of these absorption peaks are observed in measuring the absorption by the irradiated half of a sample compared with the nonirradiated half (Fig. 1, 3).

As it is known that thallous chloride when sublimated or illuminated is partly decomposed with the release of chlorine we believe that the absorption peaks at 3520 and 3800 A are associated with the appearance of excess thallium in the TlCl lattice. This hypothesis is supported by the fact that when an irradiated sample is exposed to chlorine the peaks diappear.

The absorption spectrum of thallous chloride at the temperature of liquid nitrogen was investigated by S. Nikitin and R. Reiss [6]. But these authors measured absorption only in unilluminated samples in which the concentration of excess thallium is considerably lower and its absorption bands are weak. They also confined their investigation to 0.1μ films. Under these conditions it is difficult to detect the absorption bands of excess thallium, and all the more so because an absorption band which they detected at 3597 A and attributed to excitons lies between the absorption bands of excess thallium. These are presumably the reasons why these investigators did not detect the absorption bands of excess Tl at the temperature of liquid nitrogen.

3. Luminescence excitation spectrum of thallous chloride.

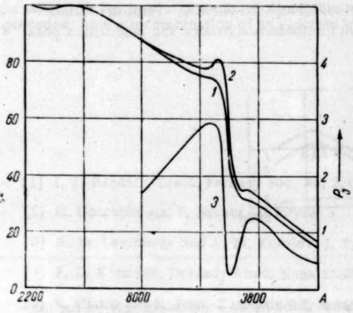

Fig. 1.

The luminescence excitation spectrum was investigated with the apparatus represented in Fig. 2. Separate narrow portions of the continuous spectrum from the krypton lamp X were obtained from the monochromator M and directed by the prism P_1 into the Dewar D containing the sample. The luminescent light from the sample was directed by the prism P_2 through the lens L_1 which focused it on the opening of the photometer Ph. The second field of the photometer was illuminated by a comparison source C through milk glass G and the filter F which equalized the colors of the comparison fields. Light from the source C was attenuated by the neutral wedge K whose transmission was measured for different wedge positions recorded by the scale S. The relative energy distribution at the monochromator output was determined by a photoelectric amplifier.

We first measured photometrically the reflection spectrum of the sample; then liquid air was poured into the Dewar and photometric readings were taken of the excited luminescence together with the reflected light. If n_1 is the transmission of the wedge when the compared fields are equally illuminated for the measurement of reflected light and n_2 for measuring luminescence together with reflection, then $n_2 - n_1 = \frac{I}{I_C}$, where I is the luminescence intensity of the sample and I_C is the intensity of the source C, which is constant. By obtaining this ratio for different wavelengths of exciting light and dividing it by the relative energy for these wave lengths we obtain the relative intensity I_p of luminescence of the sample as calculated for equal incident energy. These

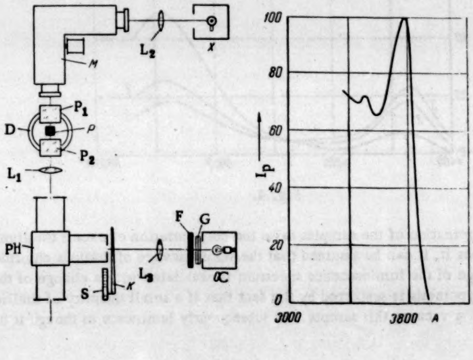

Fig. 2.

results are given in Fig. 2 which shows that the peaks of excited luminescence of thallous chloride are near 3520 and 3800 A, which is where the absorption bands of excess thallium are observed at room temperature. We believe that this is not a chance coincidence and can be explained by the fact that the absorption spectrum of excess thallium in thallous chloride depends slightly on reduced temperatures, that is, the absorption bands of thallous chloride are evidently only slightly shifted at the temperature of liquid air.

4. Luminescence spectra of thallous chloride phosphors.

The luminescence spectra were recorded in two ways: with a sensitive visual spectrophotometer [7] and by photographing. The relative energy distribution in the luminescence spectra of different thallous chloride phosphors are shown in Fig. 3: Curve 1 represents melts, Curve 2 represents fused films and Curve 3 represents powdered phosphors. The curve for sublimated phosphors almost coincides with Curve 2. Thus, the luminescence spectra of all types of thallous chloride phosphors have two luminescence bands: the blue with a peak at about 4650 A and the red with a peak near 6300 A. The intensity of the bands depends strongly on the thermal treatment of the sample and ultraviolet irradiation. Fig. 4 shows the luminescence spectra of fused samples: Curve 3 before heating, Curve 2 after heating at 400° for 10 minutes and Curve 1 after heating at the same temperature for 30 minutes. A comparison of the curves shows that increased heating time attenuates the blue luminescence and strengthens the red. The same change of luminescence spectrum is observed when the time of ultraviolet illumination of a sample is increased. After prolonged heating or illumination the samples are very much darkened and lose their ability to luminesce. Treatment of such samples with chlorine or hydrochloric acid returns them to their original luminescent condition.

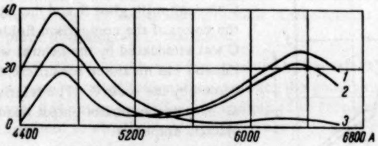

Fig 3.

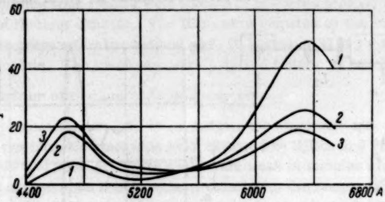

Fig. 4.

Since heating and illumination of the samples raise the concentration of excess thallium in the TlCl lattice and chlorination reduces it, it can be assumed that the luminescence of thallous chloride is caused by excess thallium and the change of the luminescence spectrum is associated with a change of the thallium concentration in TlCl. This hypothesis is supported by the fact that if a small quantity of thallium is deposited on an unilluminated sample in a vacuum this sample will subsequently luminesce as though it had been heated or irradiated.

Investigation of the luminescence spectrum of thallous chloride at different temperatures showed an optimum luminescence temperature for both bands: the blue luminescence is brightest at -160° and the red at -145°. At lower temperatures the band intensities are reduced. With increasing temperature the band peaks are somewhat shifted towards longer wavelengths.

Thallous chloride phosphors also exhibit phosphorescence of the same spectral composition as luminescence under excitation; it is also possible to observe a scintillation of the phosphor. The investigations showed that the luminescence spectra in all cases are independent of the wave length of exciting light.

We believe that the above facts enable us to conclude that thallous chloride is a typical crystalline phosphor in which the role of activator is played by excess thallium atoms which are absorption centers of exciting light as well as luminescence centers; absorption results in an internal photoelectric effect and luminescence is preceded by the recombination of an electron in the conduction band with an excess thallium ion.

Received June 19, 1956

LITERATURE CITED

[1] I. T. Randall, Trans. Faraday Soc. 35, 2, (1939).

[2] H. Gobrecht and F. Becker, Z. Physik 5, 135 (1953).

[3] A. M. Levitskaia and A. M. Korolev, J. Tech. Phys. (U.S.S.R.) 7, 7 (1937).

[4] F. D. Klement, Doklady Akad. Nauk SSSR 46, 295 (1945).

[5] R. Hilsch and R. Pohl, Z. Physik 48, 384 (1928).

[6] S. Nikitin and R. Reiss, Compte Rend 242, 1003 (1956).

[7] A. S. Vysochanskii, Odessa State University 3, 69 (1951).

π PRODUCTION IN CARBON BY 308 MEV π MESONS

V. V. Krivitskii and A. A. Reut*

(Presented by Academician L. A. Artsimovich November 14, 1956)

The investigation of meson production by mesons at energies close to the threshold for meson production is of considerable interest for an understanding of the nature of the interactions between pions and nucleons or mesons. There are a number of articles [1-3] concerning this problem but it must be noted that in all of these papers, the production processes were studied in photographic emulsion nuclei so that it was impossible to determine which nucleus was involved in the interaction.

In the present work we investigated the production of positive pions in carbon by negative pions. The experiment is shown diagrammatically in Fig. 1. A π^--beam at 308 ± 12 Mev was deflected by the magnetic field of the synchrocyclotron and entered a collimator of 50 mm diameter and 2.7 m length, passing through the yoke of the accelerating magnet [4]. After traversing the collimator the π^--mesons struck the target in which positive pions were produced (the target consisted of a graphite cylinder with 60 mm diameter and 40 mm thickness placed on the collimator axis). The π^--beam was then deflected by an auxiliary magnet and recorded by a monitor consisting of two scintillation counters.

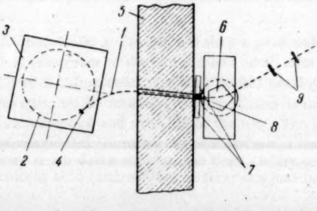

Fig. 1. Diagram of experiment: 1) pions, E= = 308 Mev; 2) protons, E ≃ 670 Mev; 3) accelerating chamber; 4) target; 5) yoke of synchrocyclotron magnet; 6) auxiliary magnet; 7) photographic plates; 8) graphite target; 9) telescope.

The π^--energy was determined by the range in copper and by a current-bearing filament in a magnetic field. Indefiniteness in the value of the energy was caused by nonuniformity of the energy in the initial beam, slowing down of mesons in the target and inaccuracy in determining the ranges.

For the purpose of determining the intensity of the π^--beam, we used electron-sensitive photographic plates placed inside the collimator. In this work we used beams whose intensity was approximately 150 and 300 cm^{-2}–sec^{-1}.

Positive pions were recorded in 280μ emulsions fastened on aluminum wedges. The geometry of the experiment (Figs. 1 and 2) was such that the plates recorded mainly π^+ mesons which left the target at an average angle of 90° with the direction of the π-beam.

The number of π-mesons stopped in the emulsion was determined from the number of $(\pi - \mu)$ decays. Only those $(\pi - \mu)$ decays were counted in which the μ track did not leave the emulsion; otherwise, the decay was considered doubtful. The efficiency of recording of $(\pi - \mu)$ decays by the emulsions used was calculated at 0.25.

It is important to note that while in the experiments involving emulsion nuclei we can speak of meson production only when two pions are observed, the method which we have described permits us to do so when a single π^+ meson is observed (in this case the emulsion is simply an "indicator" of π^+ mesons). To be sure, the appearance of a π^+ meson when carbon is irradiated with π^--mesons can also result from two successive first order processes $(\pi^- \to \pi^0, \pi^0 \to \pi^+)$ in the same nucleus (sign reversal of pion charge), but the probability of such events is apparently small and they can therefore, be neglected. When hydrogen is irradiated with π^--mesons this possibility is, of course, absent.

---

* Deceased;

The plates were scanned microscopically with 300 x magnification. In 300 cm^2 of emulsion we found 16 $(\pi - \mu)$ decays. The results are given in Fig. 3. The largest number of observed $(\pi - \mu)$ decays correspond to 30-50 Mev as the energy of the created π^+ mesons. This result is basically the result of the experimental conditions: mesons below 30 Mev were stopped in the target itself or in the wedges and were therefore not recorded by the emulsions; mesons above 50 Mev were recorded in small numbers because of the geometry of the experiment (small solid angle). Therefore, the calculation took account of only 12 cases of $(\pi - \mu)$ decay corresponding to the energy range 30-50 Mev in which the meson production cross section was assumed to be constant.

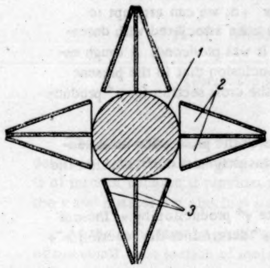

Fig. 2. Geometry of the experiment. 1) graphite target; 2) aluminum wedges; 3) photographic plates.

The differential cross section for meson production by mesons was calculated from the formula

$$\frac{d^2\sigma}{dE\,d\omega} = \frac{N_{\pi^+}}{N_{\pi^-}\,nt\,d\,|dE/dR|_E\,\eta}\,\frac{1}{(\overline{S/r^2})},$$

where N_{π^+} is the number of observed $(\pi - \mu)$ decays; N_{π^-} is the π^- flux; $\underline{n}$ is the effective number of target nuclei; $\underline{t}$ is the exposure time; $\underline{d}$ is the emulsion thickness; $[dE/dR]_E$ is the energy loss in the emulsion by π^+-mesons with energy E [5]; η is the recording efficiency of the emulsions for $(\pi - \mu)$ decays; $(\overline{S/r^2})$ is the average solid angle in which stopped π^+-mesons were recorded.

The cross section calculated from the above formula for E = 40 Mev at 90° to the direction of the π^--beam is

$$\frac{d^2\sigma}{dE\,d\omega} = (2.6 \pm 1.3) \cdot 10^{-30}\ \text{CM}^2\ \text{Sterad}^{-1}\ \text{Mev}^{-1}.$$

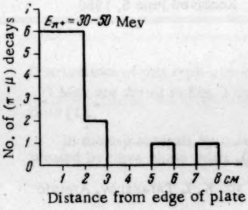

Fig. 3. Distribution of $(\pi - \mu)$ decays in photographic plates.

The indicated error of measurement of the cross section includes the statistical error as well as the errors in determining π^--beam intensity and the geometrical factors.

Since the π^+ production spectrum is unknown and could not be determined with sufficient accuracy by the method described above, further calculations were based on the spectrum calculated from perturbation theory [6]. Perturbation theory is, of course, inapplicable in the present case, but arbitrary choice of the spectrum has little effect on the results for the given accuracy of measurement.

Integration over the spectrum gives a cross section for π^+ production by π^--mesons at 90° with the value

$$\left(\frac{d\sigma}{d\omega}\right)_{90^\circ} = (2.1 \pm 1.1) \cdot 10^{-28}\ \text{cm}^2\ \text{Sterad}^{-1}.$$

Assuming that the angular distribution of π^+-mesons is isotropic the total cross section for meson production by mesons in carbon nuclei is $\sigma_C = (2.6 \pm 1.3)\ 10^{-27}\ \text{cm}^2$.

It should be noted that the π^+-mesons recorded by emulsions could be produced not only by π^--mesons but also by neutrons possessing energy sufficient for meson production (~ 300 Mev). The admixture of neutrons in the beam was determined from the number of "neutron stars" (that is, stars which showed no track of an incident meson * in a specially-prepared electron sensitive emulsion which we then placed in the collimator and

---

* The cross sections of star production for neutrons and pions in this estimate were assumed to be equal.

amounted to 10%. It must be kept in mind that the collimator was directed towards the center of the circulating proton beam in the synchrocyclotron so that the overwhelming majority of the neutrons which entered it possessed energies insufficient to produce pions. If we use data on meson production by neutrons [7] we are able to conclude that in our case the contribution of neutrons to π^+ production is quite insignificant and can be neglected.

Knowing the total cross section for meson production by mesons and assuming that π^+ production in a nucleus can take place only by protons according to the reaction $\pi^- + p \rightarrow \pi^+ + \pi^- + n$, we can attempt to evaluate the cross section for π^+ production by a nucleon. However, difficulties arise associated with determination of the absorption coefficient of a meson in the same nucleus in which it was produced. A rough estimate based on data concerning meson ranges in nuclear matter leads to the conclusion that in the present case the carbon nucleus absorbs about 50 % of the mesons produced in it. Then the cross section for π^+ production by negative pions per nucleon is $\sigma_{\pi^- \rightarrow \pi^+} \sim 10^{-27}\ \mathrm{cm}^2$.

This value can be compared with the data in [2], where there is an estimate of the production cross section per nucleon of charged mesons by π^- mesons with 500 Mev energy. These investigators conclude that the cross section at this energy lies within the limits 3.5 – 10.0 mb.

It is proposed to use the above-described experimental scheme to investigate π^+ production by π^- mesons in liquid hydrogen. It is important that in this case the identification of only a π^+ determines the reaction $\pi^- + p \rightarrow \pi^+ + \pi^- + n$.

The results lead us to the conclusion that in experiments on the elastic scattering of π^- mesons in hydrogen (using scintillation counters) it is necessary at 300 Mev to consider inelastic processes.

In conclusion we wish to express our deep gratitude to B. Pontecorvo for directing this work and for his constant assistance, and to E. L. Grigor'ev and V. M. Sidorov for discussing the results and for a number of valuable suggestions. We are also very thankful to N. N. Antonova for a great deal of assistance with the scanning of the plates.

Institute for Nuclear Problems,
Academy of Sciences USSR

Received June 5, 1956

LITERATURE CITED

[1] W. F. Fry, Phys. Rev. 91, 1576 (1953).

[2] M. Blau and M. Caulton, Phys. Rev. 96, 150 (1954).

[3] N. A. Mitin and E. L. Grigor'ev, Doklady Akad. Nauk SSSR 103, 219 (1955).

[4] A. E. Ignatenko, V. V. Krivitskii, A. I. Mukhin, B. Pontecorvo, A. A. Reut and K. I. Tarakanov, Atomic Energy J. 1956, No. 5, 5.

[5] H. Bradner, F. M. Smith, W. H. Barkas and A. S. Bishop, Phys. Rev. 77, 462 (1950).

[6] L. I. Lapidus, Dissertation, Inst. for Nuclear Prob. Acad. Sci. USSR, 1953.

[7] V. M. Sidorov, J. Exptl.-Theoret. Phys. (U.S.S.R.) 28, 727 (1955).

PHASES OF MESON-NUCLEON SCATTERING UP TO 310 Mev

A. I. Mukhin, I. V. Popova and G. N. Tentiukova

(Presented by Academician L. A. Artsimovich November 14, 1956)

The interaction of π^+ mesons with hydrogen at energies below 200 Mev has been studied more or less in detail by a number of investigators. The investigation of meson-nucleon scattering from ~200 to ~300 Mev is of interest because it provides a possibility of observing interactions between mesons and protons not only in the s and p states but also in d states.

At the same time, a phase analysis at these energies can still be carried through relatively simply because of the small cross section of inelastic processes.

The present short note gives results obtained from an analysis of data on π^+ scattering in hydrogen, performed both on the assumption that the contribution of d states to scattering is negligibly small, that is, that scattering occurs only in s and p states (s-p analysis) and on the contrary assumption that the contribution of d states can be appreciable (s-p-d analysis).

When the interaction of a π^+ meson with hydrogen occurs only in s and p states, the angular distribution of scattered mesons in the center-of-mass system can be written in the form

$$\lambda^{-2}\frac{d\sigma}{d\Omega} = A + B\cos\theta + C\cos^2\theta.$$

Distributions of this type with coefficients obtained by the method of least squares at 176, 200, 240, 270 and 307 Mev are shown in Fig. 1 by solid lines together with the experimentally measured values of the cross sections [1].*

In the s-p analysis by means of an electronic calculating machine the differential cross sections were expressed by three phase shifts α_3, α_{31} and α_{33}. The minimum value was sought for the quantity

$$M = \sum_i \left\{\frac{f_i(\alpha_3, \alpha_{31}, \alpha_{33}) - \sigma_i}{\Delta\sigma_i}\right\}^2,$$

which characterizes the degree of deviation of the curve $f_i(\alpha_3, \alpha_{31}, \alpha_{33})$ calculated in terms of the scattering phases, from the experimental values σ_i of the cross sections with error $\Delta\sigma_i$. As a first approximation in the calculations, the phases beginning with α_3 were alternately varied within given limits by one degree; this cycle was repeated a few times until the reduction of M ceased. The variation then was performed with one half degree, etc., until a given accuracy of calculation was attained. The "optimum" scattering phases obtained in this manner are given in Table 1.

---

* A detailed escription of the experimental side of the study of π^+-hydrogen scattering has recently been published [J. Exptl.-Theoret. Phys. (U.S.S.R.) 31, 371 (1956)] which, however, does not contain complete results of a phase analysis at all energies.

With respect to the validity of the s-p analysis up to ~300 Mev it follows from what has been said above that the linear dependence of α_3 on momentum is not preserved at energies above 200-240 Mev.

On the other hand, although there is no strong experimental indication for its necessity,* it is of interest to determine whether the linear dependence of the s phase on meson momentum is preserved when the analysis takes higher angular moments ($\ell = 2$) into consideration. In view of this, the experimental data of [1] as well as of [3-7] were reanalyzed with the aid of a rapid electronic calculator on the assumption that the description of pion scattering requires the consideration of d waves as well as s and p waves (s-p-d analysis). If s, p and d waves are involved in the scattering then, in addition to the three phase shifts α_3, α_{31} and α_{33} already given, the shifts δ_{33} and δ_{35} also differ from zero in value; these correspond to d states with total angular momentum $^3/_2$ and $^5/_2$.

TABLE 1

S-p analysis. Phases of π^+ mesons scattered by protons (in degrees).

Meson Energy (Mev)	Rapid Electronic Computer		
	α_3	α_{31}	α_{33}
126	—10.6	—19.5	69.0
700	— 9.1	10.0	102.0
240	—18.1	— 2.6	114.7
270	—20 2	— 6.7	129.3
307	—23.3	— 8.4	133.2

In these calculations as in the case of the s-p analysis we sought the minimum of

$$M = \sum_i \left\{ \frac{f_i(\alpha_3, \alpha_{31}, \alpha_{33}, \delta_{33}, \delta_{35}) - \sigma_i}{\Delta\sigma_i} \right\}^2, \text{ where } f_i(\alpha_3, \alpha_{31}, \alpha_{33}, \delta_{33}, \delta_{35})$$

is a function which expresses the cross section in terms of five phase shifts and σ_i is the experimental cross section with error $\Delta\sigma_i$.

The "optimum" scattering phases obtained from the s-p-d analysis are given in Table 2.

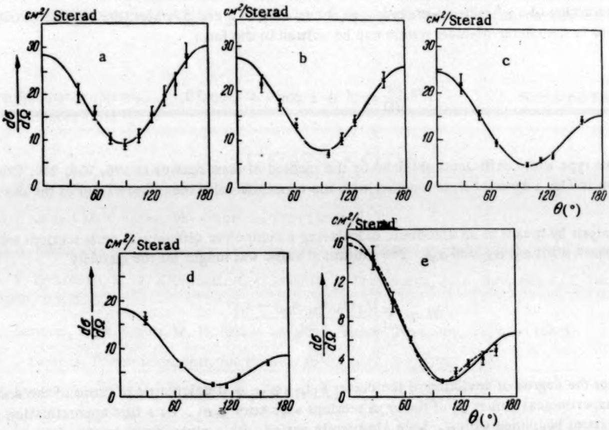

Fig. 1. Angular distributions of positive pions scattered elastically by hydrogen.
a) E = 176 Mev, b) E = 200 Mev, c) E = 240 Mev, d) E= 270 Mev, e) E= 307 Mev.

---

*Only data at 307 Mev indicate some difficulty in approximating the observed angular distribution by a function of the type A + B cosθ + C cos² θ, i. e., with only three free parameters.

TABLE 2

S-p-d analysis of π^+-proton scattering phases (in degrees)

Meson Energy (Mev)	α_3	α_{31}	α_{33}	δ_{33}	δ_{35}
113	−12.0	− 1.0	27.2	−1.6	0.6
120	−11.2	− 1.3	32.5	0.9	0
165	−18.0	− 6.0	62.2	1.0	− 5.7
176	−16.6	−15.2	68.8	1.7	− 2.3
189	−12.5	− 7.0	96.5	−3.0	− 3.7
200	− 6.7	8.9	102.7	7.0	− 0.3
240	−14.0	− 2.0	114.4	3.0	− 5.0
270	−13.6	− 4.3	128.8	4.3	− 6.9
307	−13.0	− 4.0	133.6	9.5	−10.0
310	−16.8	− 2.0	129.6	2.6	− 6.5

It is, of course, difficult to draw any reliable conclusions regarding the magnitude of the phase shifts of d waves on the basis of only the "optimum" solution given in Table 2. They show a tendency to increase (at least δ_{35}) at higher meson energies; this is an indirect argument but certainly not a proof that the contribution of d waves can no longer be neglected at energies of the order of 300 Mev.

In conclusion the authors wish to thank Academician A. A. Dorodnitsyn, Director of the Computing Center of the Academy of Sciences USSR, for making it possible to perform the calculations on the BESM, and B. Pontecorvo and L. I. Lapidus for discussions.

Received July 17, 1956

LITERATURE CITED

[1] A. I. Mukhin, E. B. Ozerov and B. Pontecorvo, Report at All-Union Conference on the Physics of High-Energy Particles, May 14-22, 1956.

[2] J. Orear, Phys. Rev. 96, 176 (1954).

[3] J. Orear, Phys. Rev. 96, 1417 (1954).

[4] L. Ferretti, E. Manaresi, G. Puppi and A. Ranzi, Nuovo cimento 1, 1238 (1955).

[5] H. L. Anderson and M. Glicksman, Phys. Rev. 100, 268 (1955).

[6] H. L. Anderson, W. C. Davidon, M. Glicksman and U. E. Kruse, Phys. Rev. 100, 279 (1955).

[7] E. L. Grigor'ev and N. A. Mitin, Report at All-Union Conference on the Physics of High-Energy Particles, May 14-22, 1956.

PROTON RELAXATION IN H_2O-D_2O MIXTURES CONTAINING PARAMAGNETIC IONS

A. I. Rivkind

(Presented by Academician M. A. Leontovich October 5, 1956)

In continuation of the study of the mechanism of spin relaxation in solutions of paramagnetic salts [1] we measured the longitudinal relaxation time T_1 of protons in solutions in which the relative quantity of relaxing H^1 nuclei was varied within wide limits by partially replacing ordinary (light) water H_2O with heavy water D_2O.

The results obtained for the solutions $MnCl_2$ 0.003 mol/l, $C(NO_3)_3$ 0.005 mol/l, $Cu(NO_3)_2$ 0.03 mol/l and $CoSO_4$ 0.25 mol/l are given in Fig. 1. The curves show that as the proton concentration is reduced there is very pronounced lengthening of the time T_1. When 90% of all the protons are replaced with deuterons ($\alpha = 0.9$) T_1 increases by more than one order of magnitude.

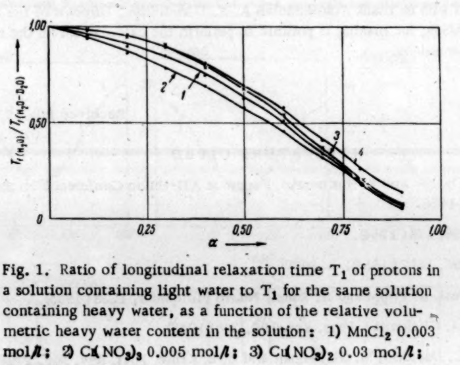

Fig. 1. Ratio of longitudinal relaxation time T_1 of protons in a solution containing light water to T_1 for the same solution containing heavy water, as a function of the relative volumetric heavy water content in the solution: 1) $MnCl_2$ 0.003 mol/l; 2) $C(NO_3)_3$ 0.005 mol/l; 3) $Cu(NO_3)_2$ 0.03 mol/l; 4) $CoSO_4$ 0.25 mol/l.

This effect is somewhat unexpected: it would seem that the relaxation time of protons should not depend on the isotopic composition of the solvent (water) and it is well known that T_1 in paramagnetic solutions is determined by the fluctuating magnetic dipole interaction between paramagnetic ions and protons of the solvent [2] (the magnetic interaction between nuclei is small and does not contribute appreciably to T_1). When H_2O molecules are replaced with D_2O there is no change in the structure of the solutions nor in the local magnetic fields generated by the ions. Moreover, numberous measurements in aqueous solutions have shown [2, 4] that even a very great reduction of the paramagnetic ion concentration N produces no anomaly in the relaxation process: the product T_1N remains practically constant as required by the theory [2].

In consideration of the above, it seems to us that there is only one possible explanation of the experiment: the equalization of the proton spin temperature T_S [5] in the immediate neighborhood of paramagnetic ions *

---

* This refers to the process of establishing thermodynamic equilibrium within the nuclear spin system.

is brought about not by Brownian motion of water molecules but by the molecular exchange of hydrogen ions. Neighboring molecules of water interchange protons through constantly formed and broken hydrogen bonds [6]. The introduction of heavy water into the solution, which because of lower chemical reactivity than ordinary water [7] slows down the proton exchange,* produces the observed increase of the time T_1.

We have already noted the influence of short-range order on proton relaxation in paramagnetic solutions [1]. It is evident that the stability of the hydrated atmosphere in the immediate vicinity of the paramagnetic ions is so high that the simple thermal transfer of water molecules cannot insure sufficient equalization of the spin temperature T_s in a time $\lesssim T_1$ (10^{-2} — 10^{-4} sec).

A preliminary calculation shows that the absence of effective Brownian translation in the first two or three layers of water molecules surrounding the ions is enough to explain the observed effect.

It follows from Fig. 1 that each of the four solutions investigated has its own individual curve. The differences do not lie within the limits of experimental error. In the solutions of doubly-charged ions Co^{2+} (N = 0.25 mol/l), Cu^{2+} (N = 0.03 mol/l) and Mn^{2+} (N = 0.003 mol/l) it can be explained qualitatively by the difference in concentrations N: with a larger number of paramagnetic ions in the solution the proton exchange must play a less important part since there is an increase in the relative number of protons which interact directly with paramagnetic ions. With regard to the chromium solution, the stronger dependence of T_1 on α compared with the maganese solution of similar concentration may be evidence of a somewhat greater hydrated atmosphere in the vicinity of triply-charged Cr^{3+} ions.

The results given above were obtained at room temperature in a constant magnetic field $H_0 \sim 230$ oersteds. The method of measurement was the same as in article [1]. Since the samples did not contain an identical number of protons a series of control experiments were performed to prove the strict linearity of the apparatus: the intensity of the resonance signal decreased linearly with reduction of the number of protons in the samples, provided that the relaxation time T_1 and the duty factor of the measuring coil remained unchanged.

Physico-Technical Institute
Kazan Branch, Academy of Sciences USSR

Received July 16, 1956

LITERATURE CITED

[1] A. I. Rivkind, Doklady Akad. Nauk SSSR 102, 6, 1107 (1955).

[2] N. Bloembergen, E. M. Percell and R. V. Pound, Phys. Rev. 73, 679 (1948).

[3] J. R. Zimmerman, J. Chem. Phys. 22, 950 (1954).

[4] P. Grivet, La Resonance Paramagnetique Nucleaire (Paris, 1955).

[5] N. Bloembergen, Physica 15, 386 (1949).

[6] N. D. Sokolov, Progr. Phys. Sci. (U.S.S.R.) 57, 2, 205 (1955).

[7] A. I. Brodskii, The Chemistry of Isotopes (Moscow, 1952) (Russian Translation).

---

* This can be shown from the theory of protolytic reactions [7].

THE EFFECT OF GAS ABSORPTION ON THE LUMINESCENCE OF ZINC OXIDE*

K. V. Tagantsev and Academician A. N. Terenin

In the present work luminescence intensities were measured by two procedures: 1) with continuous illumination; 2) with brief periods of illumination lasting 10 sec separated by dark intervals of not less than 5 min. The need for two illumination regimes is associated with the fact that prolonged illumination can, and indeed, as shown by our experiments, does produce a change of state of the adsorbent surface, as a result of photodesorption of gas, for example. Under brief periods of illumination there is a possibility of recording changes of state of the adsorbent surface which result only from dark adsorption of gases.

Procedure. The zinc oxide was prepared by burning metallic zinc in air inside a crucible furnace at 900° and was deposited on a glass plate in the form of an aqueous suspension. The plate and sample were placed in a glass vessel where they were aged in a high vacuum at 200 or 400°C for a few hours.

Luminescence of the ZnO was excited through use of light from an ARK-4 (220 w) mercury lamp through an UFS-3 ultraviolet filter. The differential photoelectric photometer which served to measured the luminescence intensities consisted of two STsV-3 antimony-cesium vacuum phototubes connected in opposition. The difference current was amplified by a dc amplifier. The greenish-yellow luminescence from the zinc oxide sample was focused by a glass lens on one phototube while luminescence from a comparison standard (a plate of uranium glass) was focused on the other tube.

In the figures given here I_0 denotes the initial luminescent intensity in the vacuum before admitting gas and under brief illumination; I denotes the changed luminescent intensity under the influence of the additional factors – gas adsorption and prolonged illumination.

Results. 1. It was established under brief illumination that the dark absorption of water vapor by a vacuum-aged sample, like the adsorption of dry oxygen, has an appreciable quenching effect on the luminescence (Fig. 1). The sample of ZnO quenched by water vapor was further quenched by oxygen (Fig. 1, Curve 3).

In one of the ZnO samples which was manufactured from different original materials, and possibly containing traces of organic matter, we observed very slight luminescence quenching by dry oxygen and considerable quenching by oxygen only in the presence of water vapor [11].

2. Especially strong quenching under brief illumination results from the adsorption of quinone vapor, which quenches ZnO luminescence even at a pressure of 0.1 mm (see Fig. 2). Quinone molecules possess electron affinity comparable with that of oxygen.

3. If oxygen at 1.5 mm is subjected to the weak electrodeless discharge of a Tesla coil, which is ordinarily used to test a vacuum, and then immediately or within one minute introduced into the vessel containing a luminescent ZnO sample, strong quenching takes place. Apparently the main quenching effect of active oxygen is associated with ozone formed in the discharge.

4. Measurements of the intensity of luminescence during prolonged illumination of a sample of ZnO which had absorbed gas, showed the strong effect of light on the system. In the presence of oxygen (80 mm pressure) we observe the growth of luminescence emmission in ZnO quenched by oxygen when passing from brief to

---

*Brief summary of a report at the 5th All-Union Conference on Luminescence at Tartu in June 1956. The present work is the direct continuation of a series begun by Terenin, Gachkovskii and Kasparov [1-3] during the 30's at the Physical Institute of the Leningrad University in which a study was made of luminescence quenching in solids by vapors and gases.

prolonged illumination (Fig. 3). This effect is reversible: after switching off the light the luminescence measured under brief illumination again drops to its initial level. The effect must be ascribed to the photodesorption of oxygen which has been observed by other methods [4, 5] and especially by the direct manometric measurements of Solonitsyn [6]. Similar stimulation of damped luminescence in passing from brief to continuous illumination is exhibited by ZnO which had adsorbed activated oxygen, water vapor and quinone vapor. We clearly are dealing here with photodesorption.

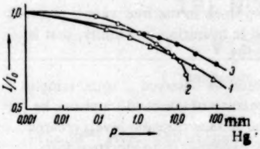

Fig. 1. Quenching of luminescence from ZnO following dark absorption of gases (brief illumination).
1) oxygen; 2) water vapor; 3) effect of oxygen on a sample previously quenched with water vapor (16 mm Hg pressure) in the presence of the latter.

Figure 4 shows the band scheme of energy levels according to the most recent ideas. The upper local levels, denoted by $Zn(Zn^{+}-e)$ in the figure, are created by excess zinc atoms which, according to Mollwo and Stockman [7] and Vergunas and Konovalov [8], are centers from which thermal conduction electrons are removed. The lower local levels, denoted by $Zn^{+}(Zn^{++}-e)$ in the figure, belong to excess singly-charged zinc ions which the same authors regard as centers of photoconduction and luminescence. In other words, the effect of light on Zn^{+} is to release electrons which enter the conduction band, and the recombination of an electron with Zn^{++} leads to an excited level and the emission of luminescent light energy (process E_m in Fig. 4).

By the adsorption of negatively charged molecules (O_2, H_2O, O_3) and quinone on the surface of ZnO additional electron traps are created. These levels are filled with electrons in the dark, which had come from the local levels of the Zn atoms, as is shown in the figure.

According to current ideas a double layer is thus formed on the surface of a semiconductor, which leads to the curving of the bands that is shown in the figure. The absorption of a light quantum which probably migrated to the surface as an exciton, detaches electrons from photoeffect centers of Zn^{+} and transfers the electrons to the conduction band (the arrow E_{xc} in the figure).

The potential barrier reduces the electron concentration of the boundary layer thus depressing the process of their recombination with ionized centers which is accompanied by luminescence emission. The ionized luminescence centers Zn^{++} recombine without radiation with electrons in traps created by the adsorption of negatively-charged molecules.

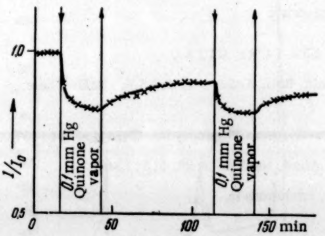

Fig. 2. Progress of quenching of ZnO luminescence by quinone vapor during brief illumination. The arrows pointing downward denote the time of admission of quinone vapor; the arrows pointing upward denote the beginning of pumping and freezing out of the vapor.

The indicated process leads, on the one hand, to the quenching of luminescence and on the other hand to a strengthened photoeffect resulting from increased electron lifetime in the conduction band. The last fact was discovered experimentally by Putseiko and Terenin [6] when negatively-charged gases were absorbed by ZnO. As electrons leave the adsorbed trapping levels, the barrier height will be reduced thus permitting electron migration to the surface and the filling of the emptying levels created by adsorption.

The growth of luminescence emission when a transition is made to continuous illumination is attributable to photodesorption in accordance with the above-mentioned photoelectric and manometric effects in ZnO. It can be assumed that a light quantum absorbed by the crystal and migrating to the surface as an exciton produces the discharge of a negative molecular ion of the surface and transfer of an electron to the conduction band. The change of the binding energy between the ion and the surface in this quantum transition follows the Franck-Condon principle. The extra kinetic energy communicated to the neutral ion in a direction perpendicular to the surface is clearly sufficient to overcome its bond with the adsorbent and to induce desorption [6]. Photodesorption destroys the surface levels which produce luminescence quenching.

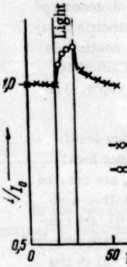

Fig. 3. Stimulation of Zn luminescence quenched by oxygen (80 mm Hg) in the transition from brief (a) to continuous (b) illumination.

A water molecule can also create a trap since in the free state it possesses electron affinity of the order of 1 ev [9] and in hydration its affinity, that is, the affinity of liquid water, is even higher [10].

The absence of quenching by dry O_2 which we observed in some samples and the quenching by oxygen only in the presence of adsorbed water can be explained as follows. In a given sample, the surface trapping levels created by the adsorption of O_2 are so high that they cannot capture electrons from the local levels of Zn atoms. When water is adsorbed, especially by capillary action, it is as though the O_2 molecules were hydrated with consequent [10] lowering of the negative ion energy level, which is equivalent to increased affinity of the original O_2 molecule. As a result, the vacant O_2 level on the surface is lowered enough to induce an electronic transition and the process of luminescence quenching as described above.

Physical Institute,
A. A. Zhdanov Leningrad State University

Received November 25, 1956

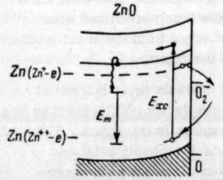

Fig. 4. Scheme of electronic transitions. It is assumed that the absorption (E_{xc}) centers in the photoeffect and in luminescence are $Zn^{+}(Zn^{++}-e)$ and that emission (E_m) occurs when these recombine with electrons from the conduction band.

LITERATURE CITED

[1] Gachkovskii and A. Terenin, Bull. Acad. Sci. U.S.S.R. OMEN Chem. Ser. 805 (1936).

[2] A. Terenin and V. Nachkovski, Acta Physicochim. URSS 4, 521 (1937).

[3] K. Ia. Kasparov, Doklady Akad. Nauk SSSR 28, 515 (1940).

[4] I. A. Miasnikov and S. Ia. Pshezhetskii, (S.S.S.R.) 8, 34 (1955).

[5] E. K. Putseiko and A. N. Terenin, Problemy Kinetiki i Kataliza (S.S.S.R.) 8, 53 (1955).

[6] A. N. Terenin, Problemy Kinetiki i Kataliza (S.S.S.R.) 8, 23 (1955).

[7] E. Mollwo and F. Stockman, Ann. Physik 3, 340 (1948).

[8] F. I. Vergunas and T. A. Konovalov, J. Exptl.-Theoret. Phys. (U.S.S.R.) 23, 712 (1952).

[9] A. N. Terenin, The Photochemistry of Dyes (1947) p. 203 (Russian Translation).

[10] R. Gurney, Ions in Solution (1938) pp. 65-67 (Russian Translation).

[11] A. Terenin, E. Putseiko and K. Tagantzev, J. phys. radium 17, 650 (1956).

THE NUCLEAR ISOMERISM OF $Hf^{180\,m}$

V. S. Gvozdev and L. I. Rusinov

(Presented by Academician I. V. Kurchatov November 17, 1956)

The Hf^{180} levels with excitation energies 93.3, 309.3, 641.7 and 1085.3 kev and spins 0+, 2+, 4+, 6+, 8+ [1] are rotational and are in accordance with recently developed ideas concerning the collective motion of nucleons in nuclei [2].

Above the energy level with spin 8+ there is a metastable level with total excitation energy 1142.9 kev and 5.5 hr halflife. The transition from this level to the 8+ level (E_γ = 57.6 kev) was identified as M3 from data concerning the lifetime and internal conversion coefficients [1]. But there are some indications that this identification is incorrect [3].

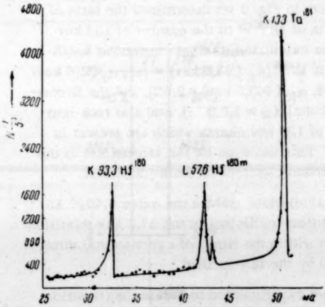

Fig. 1. Electron spectrum of $Hf^{180\,m}$, Hf^{181} and Ta^{181} from 20 to 70 kev. The horizontal axis indicates current in the electromagnet coil.

In the present article, for the purpose of establishing the multipole order of the radiation, we measured the L-shell internal conversion coefficients for the 57.6 kev isomeric transition in $Hf^{180\,m}$.

The electron spectra were measured in a beta-ray spectrometer with $\pi\sqrt{2}$ focusing angle.

As a radioactive source a layer of hafnium oxide 0.22 mg/cm² thick was deposited in vacuum on 4 μ aluminum foil and then irradiated with reactor neutrons for 18 hours. The source measured 17 × 1 mm².

Figure 1 shows the electron spectrum from 20 to 70 kev. Since the decay of $Hf^{180\,m}$ proceeds in stages, the electron spectrum in Fig. 1 makes it possible to determine α_L for the 57.6 kev transition. From the ratio of the areas of the conversion lines corresponding to the 57.6 and 93.3 kev transitions (with corrections for radioactive decay, energy range, self-absorption of electrons in the source and absorption in the counter film) and calculated data for K- and L-shell conversion [3, 4] for the 93.3 kev transition ($\alpha_K = 1.1$ and $\alpha_L = 1.7$) it is possible to determine the L-shell conversion coefficient for the 57.6 kev transition. For α_L the value 0.19± 0.10 was obtained.

This same coefficient α_L was also determined by comparing the number of L conversion electrons and gamma quanta associated with the 57.6 $Hf^{180\,m}$ transition. Since in these experiments different samples were used in the beta and gamma spectrometers the conversion coefficient was determined by using Ta^{181} emission. The number of L conversion electrons of the 57.6 kev transition in $Hf^{180\,m}$ was compared with the number of K conversion electrons of the 133 kev transition in Ta^{181} in one sample (0.22 mg/cm²) and the number of 57.6 kev quanta with the number of 133 kev quanta in the other (~2mg/cm²). Use was made of the value of α_K already measured for the 133 kev transition in Ta^{181}, which is 0.48± 0.02 [5].

Ta^{181} is formed by the β-decay of Hf^{181} $(T_{1/2} \approx 46$ days): Hf^{181} is obtained together with Hf$^{180\,m}$ in samples of natural isotopic composition through the (n, γ) reaction. Our measurements gave the cross section for Hf$^{180\,m}$ production as equal to ~0.6 barns. The internal conversion coefficient for this transition ($E_\gamma = 133$ kev) was measured by comparing the number of K conversion electrons with the number of electrons in the beta spectrum. The α_K measurements agreed with [5] in yielding the value 0.5.

From the conversion electron spectrum in Fig. 1 we determined the ratio of the number of L-shell conversion electrons of Hf for the 57.6 kev transition to the number of K-shell conversion electrons for the 133 kev transition of Ta, for several values of the time.

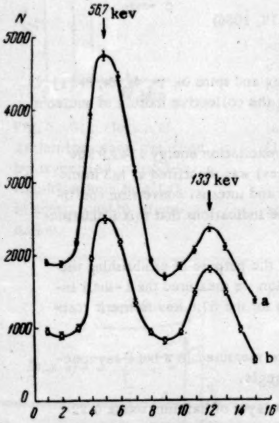

Fig. 2. Gamma spectra of Hf$^{180\,m}$ and Ta^{181} from 30 to 160 kev.

A scintillation spectrometer was used to measure the gamma spectra of Hf$^{180\,m}$ and Ta^{181} from 30 to 160 kev (Fig. 2). Because of the inadequate resolving power of the gamma spectrometer the characteristic x-ray emission associated with all transitions in Hf^{180} and Ta^{181} is superimposed on the investigated 57.6 kev gamma radiation of Hf$^{180\,m}$. The 136-kev gamma line of Ta^{181} is superimposed on the 133-kev gamma line. In addition, the gamma spectrum contains the 93.3 kev gamma rays of Hf^{180}. The number of quanta in the 57.6 kev peak associated with Hf$^{180\,m}$ decay was determined by subtracting the gamma spectrum of Ta^{181} (Fig. 2, curve b) measured after the Hf$^{180\,m}$ decay from the combined gamma spectrum of Hf$^{180\,m}$ and Ta^{181} (Fig. 2, curve a).

From the gamma spectrum in Fig. 2 we determined the ratio of the number of 57.6 kev quanta of Hf$^{180\,m}$ to the number of 133 kev quanta of Ta^{181}. We used the calculated internal conversion coefficients [4] for E-2 transitions in Hf^{180} [α_K (93.3 kev) = 1.1, α_K (216 kev) = 0.14, α_K (332.4 kev) = 0.04, α_K (443.6 kev) = 0.02], and the fluorescence yield of the hafnium K shell ($\omega = 0.94$) [3], and also took into account the relative number of 136 kev quanta which are present in the 133 kev gamma line [5]. This was done for the same times as the ratio of the numbers of conversion electrons for these transitions.

Our measurements and calculations yielded the value 0.23 ± 0.15 for the L-shell internal conversion coefficient in the 57.6 kev transition of Hf$^{180\,m}$. This value agrees within the limits of experimental error with the value of α_L obtained by the first method.

For a more detailed investigation of the decay scheme of Hf$^{180\,m}$ we experimented to obtain the transition from the level with 1142.9 kev excitation energy to the level with 641.7 kev excitation energy (spin 6+). The transition energy should be 501.2 kev. This transition was investigated with a scintillation gamma spectrometer with a 20-channel amplitude analyzer. The resulting gamma spectrum is given in Fig. 3. According to Fig. 4 the number of 443.6 kev transitions is equal to the number of 57.6 kev transitions. Therefore, the ratio of the numbers of quanta with 443.6 and 501.2 kev energy, considering the small conversion coefficients for these transitions, gives the ratio of the probabilities of transitions with 501.2 and 57.6 kev. From a comparison of the gamma line areas in Fig. 3 the ratio of the probabilities of these two transitions is 0.15 ± 0.05.

In calculating the internal conversion coefficient α_L for the 57.6 kev transition it was necessary, in connection with the data above, to make a correction for the parallel 501.2 kev transition. The value 0.22 ± 0.10 was obtained for the conversion coefficient.

A comparison of the obtained conversion coefficient with values calculated from the tables [3] by distant extrapolation for 57.6 kev and $Z = 72$ ($\alpha_{1L} = 0.23$, $\alpha_{2L} = 10$, $\alpha_{3L} = 500$; $\beta_{1L} = 3.3$; $\beta_{2L} = 90$; $\beta_{3L} = 1600$) leads to the conclusion that the 57.6 kev transition is E-1 and the level with 1142.9 kev total excitation energy has spin 9−. Comparison of the preliminary experimental value of the relative L-subshell conversion coefficients (see Fig. 1) with calculated values according to the tables [3] also indicates an E-1 transition.

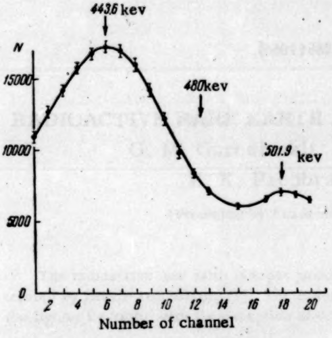

Fig. 3. Gamma spectrum of Hf^{180m} from 400 to 550 kev obtained by subtracting the gamma spectrum of Ta^{181} from the combined spectra of Ta^{181} and Hf^{180m}.

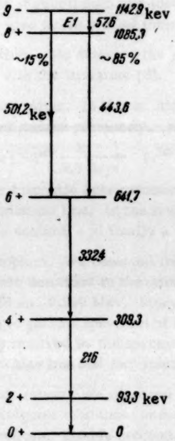

Fig. 4. Hf^{180m} decay scheme.

The lifetime calculated from formulas for single-particle transitions [6] for 57.6 kev electric dipole radiation must be of the order of 10^{-12} sec. It should be noted that this value differs by a factor of $\sim 10^{16}$ from the observed experimental lifetime of Hf^{180m}. For the 501.2 kev electric octupole transition the calculated lifetime is of the order 10^{-4} sec; this differs from the experimental value by the factor $\sim 10^{9}$.

It can be assumed that such a large divergence of the experimental lifetimes resulted from an inadequate investigation of the Hf^{180m} decay scheme. For example, above the 1142.9 kev excited level a weakly excited level may be found with a 5.5 hr halflife, in succession with the 57.6 kev E-1 transition.

The transition from the weakly excited level must be strongly converted. We made preliminary attempts to find this level in the electron range from 5 to 50 kev but the corresponding conversion lines could not be found.

A comparison of $\tau_{\gamma\,\mathrm{exp}}$ and $\tau_{\gamma\,\mathrm{theor}}$ for a large number of isomeric nuclei gives a value of not more than 10^{3} for the ratio $\tau_{\gamma\,\mathrm{exp}}$ to $\tau_{\gamma\,\mathrm{theor}}$ [7]. For Hf^{180m} there is an unusually large value of the ratio of $\tau_{\gamma\,\mathrm{exp}}$ to $\tau_{\gamma\,\mathrm{theor}}$, which indicates additional forbiddenness for the probability of the 57.6 and 501.2 kev isomeric transitions. The existence of such additional forbiddenness (K forbiddenness) is indicated in [3]. This secondary forbiddenness is associated with the fact that the 9−level with 1142.9-kev excitation energy is evidently the first level of a new system of rotational levels.

The transition from this level ($K = 9$) to levels with 8+ and 6+ spins ($K = 0$) is associated with a large change of the quantum number K which results in a long lifetime for E-1 and E-3 transitions in Hf^{180m}.

We wish to thank L. A. Sliv for a discussion of the results and I. A. Kondurov, E. P. Mazets, Iu. I. Filimonov and Iu. L. Khazov for assistance.

Physico-Technical Institute
USSR Academy of Sciences

Received
November 15, 1956

LITERATURE CITED

[1] I. W. Mihelich, G. Scharff-Goldhaber and M. McKeown, Phys. Rev. 94, 794 (1954).

[2] A. Bohr and B. Mottleson, Kgl. Danske Videnskab Selskab Mat fys. Medd. 27, 16 (1953).

[3] K. Siegbahn, Beta- and Gamma-Ray Spectroscopy (Amsterdam, 1955).

[4] L. A. Sliv and I. M. Band, Tables of Internal Conversion Coefficients I, K-Shell (Moscow-Leningrad, 1956).

[5] F. K. McGowan, Phys. Rev. 93, 163(1954).

[6] S. A. Moszkowsky, Phys. Rev. 89, 474(1953).

[7] E. P. Mazets and L. I. Rusinov, Doklady Akad. Nauk SSSR 101, 253(1955).

RADIOACTIVE RARE EARTH ISOTOPES PRODUCED BY SPALLATION

G. M. Gorodinskii, A. N. Murin, V. N. Pokrovskii,
B. K. Preobrazhenskii and N. E. Titov

(Presented by Academician L. A. Artsimovich October 27, 1956)

The radioactive rare earth isotopes produced by irradiating tantalum with 340-Mev protons have been studied by Nervik and Seaborg [1]. The isotopes of erbium, thulium, ytterbium and lutetium were separated; the lighter fractions, with the exception of cerium were not investigated.

We have separated chromatographically [2] the long-lived rare earth radioisotopes produced by irradiating tantalum with 680-Mev protons in the synchrocyclotron of the United Institute for Nuclear Studies.

The determination of the half-lives, types and energies of the radiation, and numerous gamma spectrum measurements with a scintillation spectrometer[using NaI(Tl) and CsI(Tl) crystals] enabled us to identify a number of previously known radioisotopes, improve the determination of a few genetic relationships, discover new isotopes of gadolinium and identify a number of new lines in the gamma spectra of the investigated nuclides. We give below a brief summary of the results for the individual fractions.

1. Cerium. We detected the isotopes Ce^{134} and Ce^{139}, whose radioactive characteristics are in complete agreement with the literature [3].

2. Neodymium. In this fraction we found the single radioisotope Nd^{140} ($T = 3.3$ days), whose gamma spectrum was not studied previously. According to our data, in addition to the intense 0.51 Mev annihilation gamma line ($Nd^{140} \xrightarrow[3.3\text{ days}]{k} Pr^{140} \xrightarrow[3.5\text{ min}]{k,\ \beta+} Ce^{140}$; the corresponding $\simeq$ 2.3 Mev positrons were observed with the aid of a magnetic beta spectrometer) there is a close 0.5 gamma line which is detectable from the shape of the annihilation line. In the range 0.26-0.32 Mev there is a group of weak lines, there is a 0.19 Mev line (evidently a doublet) and finally a weak line at 0.11 Mev.

3. Europium. We observed the isotopes Eu^{145} ($T = 5$ days) and Eu^{147} ($T = 24$ days), whose gamma spectra have not been described in the literature. The gamma spectrum of Eu^{145} consists of four weak lines: 0.630, 0.660, 0.730 and 0.890 Mev. Study of the gamma spectrum in the 0.080-0.300 Mev range is difficult because of the intense gamma spectrum of Eu^{147}; in the 0.30-0.45 Mev region there are a number of weak lines which were poorly resolved by the spectrometer. The Eu^{147} spectrum consists of a weak and evidently strongly converted 0.080 Mev line and two intense lines of 0.124 and 0.200 Mev.

4. Gadolinium. We observed activities with half lives of 1.5 days, 9 days (Gd^{149}) and 70 ± 5 days. In the separated daughter substances accumulated in the gadolinium fraction we detected Eu^{147} with its characteristic gamma spectrum. Doubly precipitated Eu leads us to believe that the parent substance of Eu^{147} is a Gd isotope, 1.5 day half life, mass number 147. The other radioisotope mass number ($T = 70$ days) has not been found, but is presumed to be 145 from the traces of Eu in the daughter fraction. The Gd^{147} spectrum showed three gamma lines of 0.232, 0.373 and 0.385 Mev in order of diminishing intensity; in the previously unknown spectrum of Gd^{149} there are 4 lines (which in order of decreasing intensity are): 0.154, 0.292, 0.350 and 0.505 Mev. The $Gd^{145(?)}$ spectrum consists of three lines: 0.115 (weak), 0.638 and 0.750 Mev.

5. Terbium. Activities were observed with half lives of 20 hrs (Tb^{151} or Tb^{154}), 4.5 days (Tb^{153} or Tb^{156}; Tb^{157} according to [4] has a halflife of less than 10 min or greater than 25 yrs). The gamma spectrum of the

Tb fraction is very complex and poorly resolved. The 0.345 and 0.465 Mev lines belong to a Tb isotope with ≈ 20 hr halflife. In the daughter fraction Gd was observed with ≈70 day halflife and 0.100 and 0.150 Mev gamma lines. Further study of the Tb fraction is absolutely necessary.

6. Dysprosium. In the Dy fraction (separated from Y) we detected activity with an ≈8 hr halflife, which we ascribed to Dy^{157}. In the gamma spectrum of this isotope we observed 0.233 and 0.325 Mev gamma lines, of which the latter is in agreement with the literature [5].

7. Holmium, erbium and thulium fractions. The data are mainly in agreement with the results of Nervik and Seaborg and other authors [1, 3, 6, 7].

The Ho^{160} radioisotope (T = 5 hrs) has in addition to the gamma lines given in [1] two weak lines of 0.29 and 0.51 Mev. The structure of the Tu^{166} spectrum is indicated below.

8. Ytterbium. We detected activity with a 60-hr halflife (Yb^{166}) and a 31-day halflife (Yb^{169}). In [1] the gamma spectrum is given for the equilibrium mixture $Yb^{166} \xrightarrow[60\ hr]{k} Tu^{166} \xrightarrow[7.7\ hr]{k,\ +\beta} Eu^{166}$. Separation of the daughter fraction (Tu^{166} enabled us to distinguish the gamma spectra of Yb^{166} and Tu^{166}. The Tu^{166} spectrum consists of 0.080, 0.180, 0.690 and 0.780 Mev lines. The 0.112 and 0.140 Mev lines must be ascribed to Yb^{166}. The 0.260 Mev line in the Yb^{169} spectrum, which was indicated in [8], is confirmed.

9. Lutetium. We detected activities with halflives of ≈2 days, 7-8 days, about 35 days and longer periods. The suggestion of Nervik and Seaborg that the Lu radioisotope with the 1.7 day halflife (2 days according to our measurements) is the parent of Yb^{169} with the 32-day halflife, is confirmed because the spectrum of Yb separated from the Lu fraction is in full agreement with the well-studied spectrum of Yb^{169}. The 32-day activity observed in the Lu fraction belongs to this daughter isotope. Thus the 1.7-day halflife corresponds to Lu^{169}, which does not exclude the possibility of the formation of Lu^{170} with a halflife close to the indicated value (≈2 days). The long-lived Lu spectrum (evidently Lu^{174}) consists of 0.265 Mev gamma lines. We note also that we observed 0.6 Mev electrons from the transformation $Lu^{174} \xrightarrow{\beta^-} Hf^{174}$.

A detailed description of the methods used and a discussion of the results will be published.

The authors are deeply grateful to the synchrocyclotron crew and especially to V. P. Dzhelepov for their cooperation.

V. G. Khlopin Radium Institute,
USSR Academy of Sciences

Received October 17, 1956

LITERATURE CITED

[1] W. E. Nervik and G. T. Seaborg, Phys. Rev. 97, 1092 (1955).

[2] B. K. Preobrazhenskii, O. Lilova, et. al., J. Inorg. Chem. (U.S.S.R.) 1955 No. 9.

[3] I. M. Mollander, I. Perlman and G. T. Seaborg, Rev. Mod. Phys. 25, 469 (1953).

[4] T. H. Handley and W. S. Lyon, Phys. Rev. 99, 1415 (1955).

[5] T. H. Handley and E. L. Olson, Phys. Rev. 90, 500 (1953).

[6] T. H. Handley and E. L. Olson, Phys. Rev. 92, 1260 (1953).

[7] T. H. Handley, Phys. Rev. 94, 945 (1954).

[8] S. A. E. Johansson, Phys. Rev. 100, 835 (1955).

A THEORY OF THE INTERACTION BETWEEN EVAPORATING OR GROWING DROPLETS AT LARGE DISTANCES

S. S. Dukhin and Associate Academician B. V. Deriagin

An isothermal study of the problem of droplet motion in a diffusion field [1] enabled us to establish the attractive or repulsive forces, which acts between fog droplets or between droplets and an extended liquid surface and exert considerable effect on their motion with respect to the medium. But in this study the diffusion forces were compensated in first approximation by the Stefanov current so that the velocity of a droplet with respect to the surface of a phase transition was zero. However, in the present article it will be shown that by taking account of the heat transfer which occurs at the same time as diffusion such balancing is in general destroyed in first approximation, so that the diffusion forces can have considerable effect on the condensation and coagulation of an aerosol.

1. For the solution of this problem we use the simplifications discussed in [1]. We confine ourselves to the most important case of small partial vapor density, which enables us to use a linearized set of equations for the hydrodynamics of the mixture. We calculate the interaction of the droplets at a distance so large that each droplet can be regarded as existing in given homogeneous diffusion and temperature fields caused by a phase transition on the surface of another droplet. All processes will be regarded as quasistationary, since the thermal and diffusion relaxation times of droplets measuring a few microns, for which the effect of the forces under consideration is most appreciable, is quite negligible. In order to find the boundary conditions on the surface of the droplet with allowance for the evolved heat of condensation, it is necessary to consider the temperature fields outside of the droplet $T_1(r_2, \theta_2)$ and inside $T_2(r_2, \theta_2)$, which satisfy the Laplace equation subject to the given simplifications. From the above considerations, using the boundary conditions for the velocity field which were discussed in [1] and introducing spherical coordinates with the origin at the center of droplet 2 of radius R_2 and the axis ($\theta_2 = 0$) in the direction of increasing vapor concentration, we obtain the following set of equations and boundary conditions:

$$\operatorname{grad} p = \eta \Delta \mathbf{v}, \quad \operatorname{div} \mathbf{v} = 0; \tag{1}$$

$$\Delta \rho' = 0, \quad \Delta T_1 = 0, \quad \Delta T_2 = 0; \tag{2}$$

$$v_\theta (R_2, \theta_2) = 0, \quad \rho'' v_r (R_2, \theta_2) + D \frac{\partial \rho'}{\partial r_2} (R_2, \theta_2) = 0; \tag{3}$$

$$v \big|_{r \to \infty} = - D \frac{\nabla \rho'_{\mathrm{ext}}}{\rho''}; \tag{4}$$

$$\begin{gathered} \rho' \Big|_{r \to \infty} = \rho'_\infty + A r_2 \cos \theta_2 \quad \left(A = \frac{\partial \rho'}{\partial (r_2 \cos \theta_2)} \Big|_{\substack{\theta_2 = \pm 90^\circ \\ r_2 \to \infty}} \right), \\ T_1 \Big|_{r \to \infty} = T_\infty + B r_2 \cos \theta_2 \quad \left(B = \frac{\partial T}{\partial (r_2 \cos \theta_2)} \Big|_{\substack{\theta_2 = \pm 90^\circ \\ r_2 \to \infty}} \right); \end{gathered} \tag{5}$$

$$T_1 (R_2, \theta_2) = T_2 (R_2, \theta_2); \tag{6}$$

$$\rho' (R_2, \theta_2) = \rho'_s [T_1 (R_2, \theta_2)] \simeq \rho'_s (T^*) [1 + (T_1 (R_2, \theta_2) - T^*) / \Omega]; \tag{7}$$

$$LD \frac{\partial \rho'}{\partial r_2} (R_2, \theta_2) = - k_1 \frac{\partial T_1}{\partial r_2} (R_2, \theta_2) + k_2 \frac{\partial T_2}{\partial r_2} (R_2, \theta_2). \tag{8}$$

where p is the pressure; $\overline{v}$ is mixture particle velocity; ρ' and ρ'' are the partial vapor and air densities; η is the air viscosity coefficient; D is the diffusion coefficient of vapor in the air; L is the specific heat of vaporization; k_1 and k_2 are the heat conductivities of air and water; $\rho'_s(T)$ is the density of saturated vapor at temperature T. The boundary Condition (7) takes into account that the quantity of heat q which is liberated on the surface of the droplet is partly transfered to the outside (q_1), and partly to the inside of the droplet (q_2), with $q = q_1 + q_2$. Expressing the temperature depdence of saturated water vapor density by Magnus' empirical formula $\rho'_s(T) = C \exp\left(\frac{aT}{b+T}\right)$, where a = 17.2, b = 235, and assuming that in fogs the deviation of the droplet temperature from the pyschrometric wet bulb T^* is small and usually satisfies the condition $T - T^* \ll \Omega = (b + T^*)/a$ we simplified (7) by expanding $\rho'_s(T)$ in a series with respect to $T = T^*$ and kept only the first two terms.

2. Solving Equations (2) with the boundary Conditions (5—8) we obtain

$$\rho'(r_2, \theta_2) = \rho'_\infty + (\rho'_s(T^*) - \rho'_\infty)\frac{R_2}{r_2} + Ar_2\cos\theta_2 - \tag{9}$$

$$-\left(A - 3\frac{LDA + k_1B}{k_2 + 2k_1 + 2\,LD\rho'_s(T^*)/\Omega}\,\frac{\rho'_s(T^*)}{\Omega}\right)\frac{R_2^3}{r_2^2}\cos\theta_2;$$

$$T_1(r_2, \theta_2) = T_\infty + (T^* - T_\infty)\frac{R_2}{r_2} + Br_2\cos\theta_2 - \tag{10}$$

$$-\left(B - 3\frac{LDB + k_1B}{k_2 + 2k_1 + 2\,LD\rho'_s(T^*)/\Omega}\right)\frac{R_2^3}{r_2^2}\cos\theta_2;$$

$$T_2(r_2, \theta_2) = T^* + 3\frac{LDA + k_1B}{k_2 + 2k_1 + 2\,LD\rho'_s(T^*)/\Omega}\,r_2\cos\theta_2. \tag{11}$$

As can be seen from (11), upon the average temperature of the droplet, which coincides with the psychrometric temperature, an additional polarization temperature is superimposed. In the homogeneous external temperature and diffusion fields the droplet is subject to heat and diffusion polarization.

3. Using (9) and (3) we obtain

$$v_r(R_2, \theta_2) = u\cos\theta_2 + V, \tag{12}$$

where

$$u = \frac{3D}{\rho''}\left(A - 2\frac{LDA + k_1B}{k_2 + 2k_1 + 2\,LD\rho'_s(T^*)/\Omega}\,\frac{\rho'_s(T^*)}{\Omega}\right), \tag{13}$$

$$V = D[\rho'_s(T^*) - \rho'_\infty]/R\rho''.$$

The boundary Condition (12) which takes account of the heat and diffusion polarization, differs from the corresponding boundary condition in pure diffusion polarization [1] with respect to the magnitude of the coefficient u, which for the special case of diffusion polarization can be obtained from (13) by equating the second

---

• As we know, the psychrometric temperature for evaporation is determined from the condition of complete compensation of the heat absorbed in evaporation $LD(\rho'_s(T^*) - \rho'_\infty) = k(T_\infty - T^*)$. This term can also conveniently be applied to the temperature obtained from this condition for condensation.

term to zero. Therefore, the velocity field which results from heat and diffusion polarization $v_1(r_2, \theta_2)$ and which satisfies (3) and the boundary condition of vanishing at infinity can be obtained by substituting (13) into the equations obtained for diffusion polarization; and the force F_1 of heat and diffusion polarization which corresponds to $v_1(r_2, \theta_2)$ can be obtained from the diffusion polarization force by substituting (13), to give

$$F_1 = \frac{6\pi\eta DR_2}{\rho''}\left(A - 2\frac{LDA + k_1 B}{k_2 + 2k_1 + 2LD\rho'_s(T^*)/\Omega}\frac{\rho'_s(T^*)}{\Omega}\right). \tag{14}$$

The total velocity field which satisfies Equations (1) and the boundary Conditions (3) and (4) is expressed by the superposition of $v_1(r_2, \theta_2)$ and the Stokes velocity field $v_2(r_2, \theta_2)$ resulting from the external Stefanov current, which satisfies (4) and the boundary condition of vanishing on the droplet surface. Correspondingly, the total diffusion force is expressed by the sum of (14) and the force of the external Stefanov current calculated from the Stokes formula $F_2 = -6\pi\eta R_2 DA/\rho''$

$$\mathbf{F} = \mathbf{F}_1 + \mathbf{F}_2 = -2\frac{12\pi\eta DR_2\rho'_s(T^*)(LD\nabla\rho'_{ext} + k_1\nabla T_{int})}{(k_2 + 2k_1 + 2LD\rho'_s(T^*)/\Omega)\,\Omega\rho''}, \tag{15}$$

where by taking (5) into account we have gone over to vector form.

The sign of the diffusion force is determined by the expression in brackets, which represents the resultant heat transfer to the surface by means of molecular heat conduction and vapor diffusion. When emitting heat the surface repels droplets and when absorbing heat it attracts them.

4. When a turbulent current flows past the surface, the diffusion force is localized in a thin boundary layer of thickness δ and in accordance with (15) is expressed by

$$F = \frac{12\pi\eta DR_2\rho'_s(T^*)}{\Omega\rho''\delta(k_2 + 2k_1 + 2LD\rho'_s(T^*)/\Omega)}\left[LD(\rho'_\infty - \rho'_s(T_{st})) + k_1(T_\infty - T_{st})\right], \tag{16}$$

where T_{st} is the surface temperature. When the surface temperature is below the psychrometric temperature it attracts droplets and when it is above the psychrometric temperature it repels them. For example, when a mist moves along a refrigerator coil the diffusion forces assist the condensation of droplets. The diffusion forces must impede the icing-over of surfaces in supercooled clouds because the freezing of droplets there is accompanied by the evolution of heat. Since this usually occurs under conditions of turbulent flow, as during icing of an airplane or cables in a strong wind, the contribution of the diffusion forces to this important effect can be evaluated by the use of (16); the force calculated in this way for droplets of micron size and temperature fall of a few degrees exceeds by a factor of hundreds the force of gravity when $\delta \sim 100\,\mu$.

5. From droplet 1 of radius R_1 to droplet 2 of radius R_2 at the distance $r_{12} \gg R_1, R_2$, there acts according to (15) the diffusion force

$$\mathbf{F}_{12} = \frac{12\pi\eta DR_1R_2\rho'_s(T^*)}{\Omega\rho''(k_2 + 2k_1 + 2LD\rho'_s(T^*)/\Omega)}\left[LD(\rho'_s[T_1(R_1)] - \rho'_\infty) + k_1(T_1(R_1) - T_\infty)\right]\frac{\mathbf{r}_{12}}{r_{12}^3}. \tag{17}$$

The force exerted by droplet 2 on droplet 1 is obtained from (17) by exchanging the subscripts.

A special study shows that the temperature of the droplets for any distance between them coincides with the psychrometric temperature when the droplets neither absorb nor emit heat so that the diffusion interaction force vanishes in this important case.

Solar radiation hinders coagulation processes in clouds and fogs because the droplet temperature during the absorption of radiant energy is established above the psychrometric level. Radioactive droplets are above the psychrometric temperature because of the heat evolved in radioactive decay, so that radioactive fogs must have greater stability.

A freezing droplet, which emits heat, must be a center of repulsion for other droplets and a melting hailstone, which absorbs heat, must be a center of attraction.

Considering the identical character of the distance dependence of diffusion and electrical forces it is easy by substituting into L. M. Levin's [2] formula for the efficiency with which a falling drop captures smaller fog droplets (because of electrical forces) a quantity which in the diffusion interaction corresponds to the production of electric charges, to obtain expressions for the efficiency of droplet capture by a falling melting hailstone:

$$E = \frac{36\,\pi\eta D\rho_s'(T^*)\,[LD\,(\rho_\infty' - \rho_s'[T_1(R_1)] + k_1\,(T_\infty - T_1(R_1))]}{\Omega\rho'\rho\;g\,(k_2 + 2k_1 + 2\,LD\rho_s'(T^*)\,/\,\Omega)\,R_1^3\,(1 - R_2^2\,/\,R_1^2)}, \qquad (18)$$

where ρ_W is the density of water and g is the acceleration of gravity.

A calculation made with this formula shows that the growth of cloud elements by fusion in the 2-15μ range can occur not only through electrical [2], but also through diffusion forces.

In bubble formation the absorption efficiency of an aerosol decreases as the temperature rises and vanishes at the boiling point [3]; this can apparently be attributed to diffusive repulsion of particles from the surface of a bubble whose temperature is higher than that of the air.

Diffusion forces deserve attention in connection with the depositing of dust in the respiratory passages because the small diameter of the lower respiratory passages must make the diffusion forces very large there. The wall temperature of the respiratory pasages must be above the psychrometric temperature so that the forces under consideration must serve to protect the lungs from dust.

It can thus be stated that this first study of the forces acting between aerosol particles during evaporation and condensation, whose importance is obvious in the mechanics of aerosols, is of considerable practical interest for the study and solution of many problems concerning aerosols in various branches of science and technology.

Institute of Physical Chemistry,
USSR Academy of Sciences

Received January 3, 1957

LITERATURE CITED

[1] B. V. Deriagin and S. S. Dukhin, Doklady Akad. Nauk SSSR 106, 851 (1956).

[2] L. M. Levin, Doklady Akad. Nauk SSSR 95, 467 (1954).

[3] H. Remy, H. Finnern, Z. anorg. Chem. 159, 241 (1926).

ON THE INTERACTION OF ANTIPROTONS AND NUCLEI

P. E. Nemirovskii

(Presented by Academician I. V. Kurchatov November 3, 1956)

In a number of articles the Segre group has shown [1, 2] that the cross section for inelastic interactions between antiprotons and nuclei for 300-500 Mev antiprotons considerably exceeds the cross section for the interaction of nucleons with nuclei. Thus for Cu an experiment at 450 Mev gives $\frac{\sigma_a}{\sigma_H} = 1.5 \pm 0.5$ or 1.2 barns [1], and according to other data $\frac{\sigma_a}{\sigma_p} = 2.02$ [2].

For lower energies and lighter nuclei this ratio is possibly larger (the effect has been observed for Be and glass). If the nucleus is regarded as having a sharp edge the effect cannot be explained, since the Cu nucleus is almost black even for nucleons. Therefore, the explanation requires that the nucleus be regarded as having a diffuse boundary.

The potential at the boundary of the nucleus must decrease gradually for two reasons. First, the nucleon-antinucleon interaction has a finite radius. The distance dependence of the elementary interaction is unknown but in any event must vanish rapidly for $r < 1.5 \times 10^{-13}$ cm (if we assume that the interaction is transmitted by particles not lighter than pions). This is clearly insufficient to explain the antinucleon cross sections (especially if there is a Gaussian interaction potential). But there is a second effect which requires a diffuse nuclear boundary. According to some experimental results (scattering of high-energy electrons, mesic atoms, etc.) the density of nuclear matter does not vanish abruptly at the nuclear boundary but decreases gradually. Williams has shown [3] that this hypothesis is in good agreement with data on nuclear scattering of fast neutrons.

Data on nuclear scattering of electrons [4] show that the density of protons decreases from 0.9 to 0.1 in a distance of the order $2.4+0.3 \times 10^{-13}$ cm. In the present note it will be shown that a reasonable explanation of the antiproton cross sections can be given on the basis of the density variation shown above.

It will hereinafter be assumed that the antinucleon-nucleon interaction can be described by a δ-function and we shall consider only the effect of nucleon density variation (the density variation of neutrons and protons will be assumed to be identical). For example, the density ρ can be represented in the following three ways:

$$1)\ \rho = \rho_0 \text{ for } r \leqslant r_0^{(1)},\quad \rho = \rho_0 e^{-\frac{r-r_0}{a_1}} \text{ for } r \geqslant r_0^{(1)}; \qquad (1)$$

$$2)\ \rho = \frac{\rho_0}{1 + e^{\frac{r-r_0^{(2)}}{a_2}}}; \qquad (2)$$

$$3)\ \rho = \rho_0 \text{ for } r \leqslant r_0^{(3)},\quad \rho = \rho_0 e^{-\frac{(r-r_0)^2}{a_3^2}} \text{ for } r \geqslant r_0^{(3)}. \qquad (3)$$

For copper we take

$$a_1 = 0.7 \cdot 10^{-13}\ \text{cm}\ r_0^{(1)} = 4.1 \cdot 10^{-13}\ \text{cm}$$

or

$$a_2 = 0.5 \cdot 10^{-13}\ \text{cm}\ r_0^{(2)} = 4{,}3 \cdot 10^{-13}\ \text{cm}$$

and, finally,

$$a_3 = 2 \cdot 10^{-13}\ \text{cm}\ r_0^{(3)} = 2.8 \cdot 10^{-13}\ \text{cm}$$

All of these values of the parameters are consistent with data on electron scattering.

We must also obtain the absorption coefficient of nuclear matter $K = \rho_0 \bar{\sigma}$ which corresponds to the experimental absorption cross section.

$\bar{\sigma}$ is the nucleon-antinucleon interaction cross section averaged over the protons and neutrons in the nucleus. The Pauli exclusion principle may possibly be unobserved in this interaction, especially at E = 300-500 Mev (since it does not impose limits on annihilation and the limitations on scattering are twice as weak as for nucleon-nucleon collisions). Therefore, $\bar{\sigma}$ must not differ greatly from the cross section for free particle interactions.

In the terminology of geometric optics $2\int_{\infty}^{\infty} \rho\bar{\sigma}\, ds$ gives the attenuation of an antiproton beam passing its target at a distance r and the cross section is expressed as

$$\sigma_a = 2\pi \int_0^\infty r\left(1 - \exp\left[-2\int_0^\infty \rho(\varkappa)\bar{\sigma}\, ds\right]\right) dr, \tag{4}$$

where $\varkappa = \sqrt{r^2 + s^2}$

We shall use the expressions given for the density variation in order to calculate for collisions of nucleons and nuclei. In this case the absorption coefficient is easily determined. The proton-nucleon cross section averaged over neutrons and protons is 28 mb at E ~ 300-500 Mev. If the Pauli principle is observed for an incident nucleon of 450 Mev the interaction cross section of intranuclear and incident nucleons must be 24 mb. The density of nuclear matter at the center of the nucleus ρ_0 in case (1) is 1.30×10^{38}, in case (2) 1.25×10^{38} and in case (3) 1.43×10^{38}. The absorption coefficient K (0) is 3.12×10^{12}; 3×10^{12} and 3.4×10^{12} respectively. With such absorption coefficients a nucleus with a rectangular edge is almost black (absorption cross section $\sim 0.82\pi R^2$). The calculated absorption cross sections for the three potentials with different K (0) are given in Table 1. They are in satisfactory agreement with each other and with experiment. The calculations for Be are considerably less reliable, but for $K(0) = 25 \times 10^{12}$ the cross section exceeds the nucleonic cross section by a factor larger than 2.

TABLE 1

(1)		(2)		(3)	
$K(0) \cdot 10^{-12}$	σ_a, barns	$K(0) \cdot 10^{-12}$	σ_a, barns	$K(0) \cdot 10^{-12}$	σ_a, barns
3.12	0.7	3.0	0.66	3.4	0.68
6.2	0.91	6.2	0.84	6.2	0.85
12.4	1.103	12.4	1.0	12.4	1.03
24.8	1.28	24.8	1.16	24.8	1.20

As can be seen from the table $\sigma_a = 1.20$ b is obtained in case (1) for $\bar{\sigma} = 150$ mb, in case (3) for $\bar{\sigma} = 175$ mb and in case (2) for $\bar{\sigma} = 200$ mb. Thus the cross sections for the collisions of free antiprotons and nucleons in this energy range is about 0.15-0.20 b. But the existence of such large cross sections does not require essential increase of the interaction range between nucleons and antinucleons compared with the range of ordinary nuclear forces.

Let us consider the effect of the range of nuclear forces on the absorption potential at the edge of the nucleus. A finite range can be introduced into the absorption coefficient by the formula:

$$K(x) = \int_V L(|x - x'|)\,\rho(x')\,\bar{\sigma}\,dx'. \qquad (5)$$

If we take $L(\xi) = \text{const}$ for $\xi << \xi_0$ and $L(\xi) = 0$ for $\xi > \xi_0$, the integrals are easily calculated. For a rectangular well of radius 1×10^{-13} cm the dependence of the absorption coefficient on $\underline{r}$ changes very little. When the density at the nuclear center and the cross section of the elementary act remain unchanged, the nuclear absorption cross section (for $\bar{\sigma} = 200$ mb) changes by only 3%. When $\xi_0 = 2 \cdot 10^{-13}$ cm, the absorption cross section for the density Functions (1) and (2) with $\bar{\sigma} = 200$ mb increases by 15%. Thus the effect of a finite range of nuclear forces is very small in the case of a diffuse boundary.

It should be noted that at low energies there are other causes for stronger interaction between antinucleons and nuclei. First among these is the Coulomb attraction, as a result of which the wave phases with $l > kR$ do not vanish within the range of nuclear forces. Furthermore, if the real part of the nuclear potential for antinucleons is considerably larger than for nucleons the refraction of antinucleonic waves is increased, which however, cannot strongly affect the cross section when the absorption coefficient is large. These effects can somewhat reduce the cross sections obtained for the elementary acts. Since the cross sections for antiproton interaction with neutrons and protons can differ considerably a comparison can be carried through only after measurements on the deuteron.

Received October 16, 1956

LITERATURE CITED

[1] O. Chamberlain, E. Segre, et. al., Phys. Rev. 102, 1659 (1956).

[2] J. M. Brabant, B. Cork, et al., Phys. Rev. 102, 1622 (1956).

[3] R. W. Williams, Phys. Rev. 98, 1387 (1955).

[4] B. Hahn, D. G. Ravenhall and R. Hofstadter, Phys. Rev. 101, 1131 (1956).

α-DECAY FINE STRUCTURE OF EVEN-EVEN NUCLEI

V. G. Nosov

(Presented by Academician M. A. Leontovich November 3, 1956)

It is known [1, 2] that in the α-decay of nonspherical heavy nuclei, excited rotational levels of the daughter nucleus are observed. The behavior of the daughter nucleus + α-particle system is described by the Schroedinger equation

$$\frac{\hbar^2}{2I}\mathbf{J}^2\Psi - \frac{\hbar^2}{2m}\nabla^2\Psi + U(\xi,\eta,\zeta)\Psi = E\Psi, \tag{1}$$

where **J** is the anglular momentum operator of the daughter nucleus, **I** is its moment of inertia, m is the reduced mass, U is the potential energy of the electrostatic interaction between the α-particle and the nucleus and E is the total energy of the system. The angular momentum of the daughter nucleus is expressed through the total angular momentum of the system **K** and the orbital angular momentum **l** of the α-particle, by $\mathbf{J} = \mathbf{K} - \mathbf{l}$. Since for even-even nuclei (hereinafter only such nuclei will be considered) $\mathbf{K} = 0, \mathbf{J}^2 = \mathbf{l}^2$, and thus

$$\frac{\hbar^2}{2I}\mathbf{l}^2\Psi - \frac{\hbar^2}{2m}\nabla^2\Psi + U(\xi,\eta,\zeta)\Psi = E\Psi. \tag{2}$$

This equation was first obtained by Strutinskii [3].

The potential energy depends only on the coordinates ξ, η, ζ of the α-particle with respect to the nucleus, i. e., on the Cartesian coordinates in the reference system which rotates with the nucleus and is independent of the Eulerian angles Ω which determine the orientation of the rotating axes with respect to the fixed axes. Therefore, (2) can conveniently be solved in the variables ξ, η, ζ, Ω.

In the transition from the fixed coordinate system to the rotating system the operators $\mathbf{l}^2$ and ∇^2 keep the same form. The wave function of the state with $\mathbf{K} = 0$ is independent of Ω; by transforming from the Cartesian coordinates ξ, η, ζ to the spherical coordinates, r, $\mu = \cos\vartheta$, φ, it can also easily be shown that the wave function cannot depend on φ. We finally obtain

$$\frac{1}{r}\frac{\partial^2}{\partial r^2}(r\Psi) + \left(\frac{m}{I} + \frac{1}{r^2}\right)\frac{\partial}{\partial\mu}\left[(1-\mu^2)\frac{\partial\Psi}{\partial\mu}\right] + \frac{2m}{\hbar^2}[E - U(r,\mu)]\Psi = 0. \tag{3}$$

The special solution which describes an α-particle with momentum l departing from the nucleus is

$$\Psi_l(r,\mu) = \frac{\sqrt{2l+1}}{2}P_l(\mu)\psi_l(r,\mu), \tag{4}$$

where ψ is no longer dependent on μ for large r (the factor $\sqrt{\frac{2l+1}{2}}$ is introduced for convenience). Substitution in (3) leads to the equation

$$P_l\left\{\frac{1}{r}\frac{\partial^2}{\partial r^2}(r\psi_l)+\left[\frac{2m}{\hbar^2}(E-U)-l(l+1)\left(\frac{m}{I}+\frac{1}{r^2}\right)\right]\psi_l\right\}+ \\ +\left(\frac{m}{I}+\frac{1}{r^2}\right)\left\{P_l\left[(1-\mu^2)\frac{\partial^2\psi_l}{\partial\mu^2}-2\mu\frac{\partial\psi_l}{\partial\mu}\right]+2(1-\mu^2)\frac{dP_l}{d\mu}\frac{\partial\psi_l}{\partial\mu}\right\}=0, \qquad (5)$$

which can conveniently be solved in the quasiclassical approximation:

$$\psi_l=e^{\sigma},$$

$$P_l\left\{\left(\frac{\partial\sigma}{\partial r}\right)^2+\frac{2}{r}\frac{\partial\sigma}{\partial r}+\frac{\partial^2\sigma}{\partial r^2}+\frac{2m}{\hbar^2}(E-U)-l(l+1)\left(\frac{m}{I}+\frac{1}{r^2}\right)\right\}+ \\ +\left(\frac{m}{I}+\frac{1}{r^2}\right)\left\{P_l\left[(1-\mu^2)\left(\frac{\partial\sigma}{\partial\mu}\right)^2-2\mu\frac{\partial\sigma}{\partial\mu}+(1-\mu^2)\frac{\partial^2\sigma}{\partial\mu^2}\right]+ \\ +2(1-\mu^2)\frac{dP_l}{d\mu}\frac{\partial\sigma}{\partial\mu}\right\}=0. \qquad (6)$$

The corresponding expansion for $\sigma(r,\mu)$ is given by $\sigma=\sigma_{-1}+\sigma_0+\sigma_1+\ldots$; for the successive approximations σ_k we have the infinite sequence of equations

$$\left(\frac{\partial\sigma_{-1}}{\partial r}\right)^2+\left(\frac{m}{I}+\frac{1}{r^2}\right)(1-\mu^2)\left(\frac{\partial\sigma_{-1}}{\partial\mu}\right)^2=-\frac{2m}{\hbar^2}(E-U)+l(l+1)\left(\frac{m}{I}+\frac{1}{r^2}\right); \\ P_l\left[2\frac{\partial\sigma_{-1}}{\partial r}\frac{\partial\sigma_0}{\partial r}+\frac{2}{r}\frac{\partial\sigma_{-1}}{\partial r}+\frac{\partial^2\sigma_{-1}}{\partial r^2}\right]+\left(\frac{m}{I}+\frac{1}{r^2}\right)\left\{P_l\left[2(1-\mu^2)\frac{\partial\sigma_{-1}}{\partial\mu}\frac{\partial\sigma_0}{\partial\mu}-\right.\right. \\ \left.\left.-2\mu\frac{\partial\sigma_{-1}}{\partial\mu}+(1-\mu^2)\frac{\partial^2\sigma_{-1}}{\partial\mu^2}\right]+2(1-\mu^2)\frac{dP_l}{d\mu}\frac{\partial\sigma_{-1}}{\partial\mu}\right\}=0, \qquad (7) \\ \cdots\cdots\cdots\cdots\cdots\cdots\cdots\cdots$$

The solution of Equations (7) is easier for a slightly nonspherical daughter nucleus. In this case the equation of the nuclear surface can conveniently be represented as

$$R(\mu)=R_0+\xi(\mu)=R_0\left\{1+\sum_n\alpha_nP_n(\mu)\right\}. \qquad (8)$$

The values of σ_k are then sought as power series of ξ: $\sigma_k=\sigma_k^{(0)}+\sigma_k^{(1)}+\sigma_k^{(2)}+\ldots$. The electrostatic potential created by the daughter nucleus is easily calculated in a similar series (it is assumed that the nuclear charge is uniformly distributed throughout its volume). By simple calculations we obtain

$$\sigma_{-1}^{(0)}=i\int_{a_l}^{r}k_l\,dr,\quad \sigma_0^{(0)}=-\ln\sqrt{-ik_lr}, \\ \sigma_{-1}^{(1)}=\frac{3}{2}i\varkappa_b^2\sum_n\frac{\alpha_n}{2n+1}P_n(\mu)\int_r^{\infty}\left(\frac{R_0}{r}\right)^{n+1}\frac{dr}{k_l}. \qquad (9)$$

Here

$$k_l = \sqrt{k_\varepsilon^2 - \varkappa_b^2 \frac{R_0}{r} - \frac{l(l+1)}{r^2}}, \qquad \varkappa_b^2 = \frac{4mZe^2}{\hbar^2 R_0},$$
$$k_\varepsilon^2 = \frac{2m\varepsilon}{\hbar^2}, \quad \varepsilon \equiv \varepsilon_l = E - \frac{\hbar^2}{2I} l(l+1).$$

The classical distance a_l of closest proximity is defined by the equation

$$k_l^2(a_l) = k_\varepsilon^2 - \varkappa_b^2 \frac{R_0}{a_l} - \frac{l(l+1)}{a_l^2} = 0.$$

Equations (9) are also valid for $r < a_l$ if it is remembered that in this region

$$k_l = i\varkappa_l = i\sqrt{\frac{l(l+1)}{r^2} + \varkappa_b^2 \frac{R_0}{r} - k_\varepsilon^2}.$$

Further terms of the double series $\sigma = \sum_{k,m} \sigma_k^{(m)}$ are negligibly small.

Substituting (9) in (6) and (4) and passing to the limit $r \to \infty$, we obtain

$$\Psi_l \to \frac{\sqrt{2l+1}}{2} \frac{1}{\sqrt{-ik_\varepsilon r}} \left[\exp i\left(k_\varepsilon r - \frac{\varkappa_o^2 R_0}{2k_\varepsilon} \ln 2k_\varepsilon r + \delta_\varepsilon\right)\right] P_l(\mu),$$

that is, the corresponding current through a closed sphere is independent of l. Therefore, when the wave function of the system is represented as $\Psi = \sum_l c_l \Psi_l$, the relative excitation probability of a rotational level with orbital angular momentum l will be $w_l = |c_l|^2$.

It is easy to express the coefficients c_l through the value of the wave function on the nuclear surface $\psi(S)$. Indeed, since the values of l in question are small we obtain in the required approximation:

$$\sigma_{-1}^{(0)}(S) = \sigma_{-1}^{(0)}(R_0)\,|_{l=0} - \varkappa_0(R_0)\cdot\xi + \frac{\gamma}{2} l(l+1),$$
$$\sigma_{-1}^{(1)}(S) = \sigma_{-1}^{(1)}(R_0)\,|_{l=0}, \quad \sigma_0^{(0)}(S) = \sigma_0^{(0)}(R_0)\,|_{l=0}, \tag{10}$$

where $\gamma = 2\dfrac{\partial\sigma_{-1}^{(0)}}{\partial l(l+1)}(R_0)\,|_{l=0}$. Simple calculation leads to

$$\gamma = \frac{2\varkappa}{\varkappa_0^2 R_0} + \frac{m/I}{k^2}\left(\frac{\varkappa_0^2 R_0}{k}\operatorname{arctan}\frac{\varkappa}{k} + \varkappa R_0\right), \tag{11}$$

where $k \equiv k_E = \sqrt{\frac{2mE}{\hbar^2}}$, $\varkappa \equiv \varkappa_0(R_0) = \sqrt{\varkappa_0^2 - k^2}$.

Substituting (10) in (6) and (4) we obtain

$$\begin{aligned}\Psi(S) &= \sum_l c_l \Psi_l(S) = \\ &= \sum_l c_l \frac{\sqrt{2l+1}}{2} \frac{1}{\sqrt{\varkappa}\, R_0}\left[\exp\left(\sigma_{-1}^{(0)}\Big| - \varkappa\xi + \frac{\gamma}{2} l(l+1) + \sigma_{-1}^{(1)}\Big|\right)\right] P_l(\mu).\end{aligned} \tag{12}$$

In the last sum we everywhere take $r = R_0$. The vertical stroke to the right of the corresponding expression denotes that it must be taken for $l = 0$. The factor $\frac{1}{\sqrt{\varkappa}\, R_0} e^{\sigma_{-1}^{(0)}| - \varkappa\xi + \sigma_{1}^{(1)}|}$ which is independent of l can be taken outside the summation sign and transferred to a different part of the equation. Use of the completeness theorem gives

$$\begin{aligned}c_l &= \sqrt{\varkappa}\, R_0 e^{-\sigma_{-1}^{(0)}|} \sqrt{2l+1}\, e^{-\frac{\gamma}{2} l(l+1)} \int_{-1}^{1} \Psi(S)\, e^{\varkappa\xi - \sigma_{-1}^{(1)}|} P_l(\mu)\, d\mu, \\ w_l &= \varkappa R_0^2 e^{-2\sigma_{-1}^{(0)}|} (2l+1)\, e^{-\gamma l(l-1)} \left|\int_{-1}^{1} \Psi(S)\, e^{\varkappa\xi - \sigma_{-1}^{(1)}|} P_l(\mu)\, d\mu\right|^2.\end{aligned} \tag{13}$$

For slightly nonspherical nuclei it is most reasonable to assume $\psi(S) = \text{const}$. Normalizing the relative probability w_l by the condition $w_0 = 1$ we finally obtain

$$w_l = (2l+1)\, e^{-\gamma l(l+1)} \left| \frac{\int_{-1}^{1} e^{\varkappa\xi - \sigma_{-1}^{(1)}|} P_l(\mu)\, d\mu}{\int_{-1}^{1} e^{\varkappa\xi - \sigma_{-1}^{(1)}|}\, d\mu} \right|^2. \tag{14}$$

We know [4] that in heavy nuclei the quadrupole deformation of the form $\xi = R_0 \alpha_2 P_2(\mu)$ is the most important. Substitution into (9) and (14) gives

$$w_l = (2l+1)\, e^{-\gamma l(l+1)} \left| \frac{\int_{0}^{1} e^{\beta P_2(\mu)} P_l(\mu)\, d\mu}{\int_{0}^{1} e^{\beta P_2(\mu)}\, d\mu} \right|^2, \tag{15}$$

where

$$\beta = \left[\frac{4}{5} \varkappa R_0 \left(1 - \frac{k^2}{2\varkappa_b^2} \right) - i \frac{2}{5} \frac{k^3 R_0}{\varkappa_b^2} \right] \alpha_2. \tag{16}$$

The physical meaning of (15) is simple. The exponential factor represents the dependence of penetration of the Coulomb barrier on the energy and angular momentum of the α-particle. In particular, it takes into account the fact that the process is nonadiabatic, i. e., while the α-particle is passing through the region below the barrier the nucleus can be rotated through an appreciable angle. Therefore, previous results obtained in an adiabatic approximation [5, 6] are not entirely reliable. The integral within the square of the modulus describes the direct effect of the deformation of the nuclear surface $\varepsilon(\mu)$ added to the effect of the quadrupole potential $\sigma_{1}^{(1)}$ |. We note that this integral can easily be calculated by using tables [7] of the function

$$w(z) = e^{-z^2} \int_0^z e^{x^2} dx.$$

TABLE 1

Nucleus	α_2		$Q_0 = \frac{6}{5} Z R_0^2 \alpha_2 \cdot 10^{24}$		Nucleus	α_2		$Q_0 = \frac{6}{5} Z R_0^2 \alpha_2 \cdot 10^{24}$	
	(I)	(II)	(I)	(II)		(I)	(II)	(I)	(II)
Em^{220}	0.26	0.21	10	16	U^{230}	0.13	0.11	5	9
Em^{222}	0.29	0.23	11	17	U^{232}	0.15	0.13	6	11
Ra^{222}	0.24	0.20	9	15	U^{234}	0.20	0.16	8	13
Ra^{224}	0.30	0.24	12	18	U^{236}	0.18	0.15	8	12
Ra^{226}	0.26	0.21	10	16	U^{238}	0.16	0.14	7	12
Ra^{228}	0.30	0.24	12	19	Pu^{238}	0.18	0.15	8	13
Th^{226}	0.27	0.22	11	17	Pu^{240}	0.17	0.15	7	13
Th^{228}	0.26	0.21	10	17	Cm^{242}	0.15	0.13	7	11
Th^{230}	0.21	0.17	9	14	Cm^{246}	0.13	0.11	6	10
Th^{232}	0.23	0.19	9	15	Cm^{248}	0.12	0.10	5	9
Th^{234}	0.21	0.17	9	14	Cf^{250}	0.12	0.10	6	9

It is possible from experimental data [1, 8, 9] to use (11), (15) and (16) to calculate the deformation α_2 for some nuclei. k, I and w_2 are determined experimentally; two alternate values can be taken for the nuclear radius: $R_0 = 1.0 A^{1/3} \cdot 10^{-13}$ cm (I) and $R_0 = 1.4 A^{1/3} \cdot 10^{-13}$ cm (II). The results obtained from such use of experimental findings are given in Table 1. The calculated variation of the quadrupole moment Q_0 of the daughter nucleus can be verified by measuring the cross section of Coulomb excitation $O_+ \longrightarrow 2_+$ or the probability of gamma emission $2_+ \xrightarrow{\gamma} O_+$ [4].

Received August 29, 1956

LITERATURE CITED

[1] Ann. Rev. Nucl. Sci. 1954.

[2] A. Bohr, P. Froman and B. Mottelson, Kgl. Danske Videnskab Selskab Mat. fys. Medd. 29, 10 (1955).

[3] V. Strutinskii, J. Exptl. Theoret. Phys. (U.S.S.R.) 30, 2, 411 (1956).

[4] A. Bohr, Rotational States in Atomic Nuclei (1954).

[5] V. Nosov, Doklady Akad. Nauk SSSR 103, 1, 65 (1955).

[6] V. Strutinskii, Doklady Akad. Nauk SSSR 104, 4, 524 (1955).

[7] K. Karpov, Tables of the Function $w(z) = e^{-z^2}\int_0^z e^{x^2}dx$ in the Complex Region (1954).

[8] F. Asaro, F. Stephens, B. Harvey and I. Perlman, Phys. Rev. 100, 1, 137 (1955).

[9] F. Asaro, F. Stephens, S. Thompson and I. Perlman, Phys. Rev. 98, 1, 19 (1955).

ON CRYSTALLIZATION IN STATISTICAL PHYSICS

E. A. Arinshtein

(Presented by Academician N. N. Bogoliubov October 25, 1956)

The problem of crystallization in statistical physics has still not been solved. The method of A. A. Vlasov [1] always leads to continuous crystallization. It is difficult to determine the accuracy of his equations and the form of the kernel. Similar results were obtained by S. V. Tiablikov [2]. He starts with an arbitrary representation of a binary function in terms of ordinary ones. Kirkwood [3] begins with a similar representation. The kernel of Kirkwood's equation cannot be determined either theoretically or experimentally. The problem is also unsolved in articles which consider either only the liquid phase [4] or only the crystalline phase [5, 6] and in articles which are based on models [7, 8].

In the present article crystallization is investigated by the method of N. N. Bogoliubov [9], which enables us to relate thermodynamical functions to structure.

The distribution of s particles is defined in terms of the generating functional:

$$F_s(1\dots s) = V^s\int D_N dq_{s+1}\dots dq_N = \left[\frac{\delta^s L(u)}{\delta u(1)\dots\delta u(s)}\right]_{u=0}; \qquad (1)$$

$$L(u) = \int D_N \prod_{i=1}^{N}(1 + vu(i))\,dq_i.$$

The functional W(u) = ln L determines the correlation functions:

$$q_s = \left[\frac{\delta^s W(u)}{\delta u(1)\dots\delta u(s)}\right]_{u=0}; \quad F_1 = g_1; \quad F_2(1, 2) = F_1(1)F_1(2) + g_2(1, 2); \dots \qquad (2)$$

We make use of Bogoliubov's functional equation:

$$\frac{\delta^s L(u)}{\delta u(1)\dots\delta u(s)} = (zv)^s \exp\left(-\frac{U_s}{\vartheta}\right) L\Big(u(i)(\varphi_{1\dots s}(i) + 1) + \frac{1}{v}\varphi_{1\dots s}(i)\Big), \qquad (3)$$

where $\varphi_{1\dots s}(i) = \prod_{j=1}^{s}(1 + f_{ij}) - 1 \; (i > s)$; $f_{ij} = \exp\left(-\frac{U_{ij}}{\vartheta}\right) - 1$ and z is the activity. Taking the logarithm and then the functional derivative of (3) we obtain with s = 1:

$$\frac{\delta^2 W(u)}{\delta u(1)\,\delta u(2)} = \frac{\delta W(u)}{\delta u(1)}\left\{\frac{\delta W\left(u(i)(1+f_{1i})+\frac{1}{v}f_{1i}\right)}{\delta u(2)} - \frac{\delta W(u)}{\delta u(2)}\right\}. \tag{4}$$

By further functional differentiation and substitutions we can express all g_s in terms of F_1 in any correlation approximation, that is, accurate to any term in the expansion of the functional W(u).

For the distribution function F_1 we obtain by this method:

$$\ln\frac{F_1(1)}{zv} = \sum_{s=1}^{\infty}\frac{1}{v^s s!}\int K_{s+1}(1,\ldots,s+1)\,F_1(2)\ldots$$
$$\ldots F_1(s+1)\,dq_2\ldots dq_{s+1} = W\left(\frac{1}{v}f_{1i}\right), \tag{5}$$

where

$$K_2(1,2) = f_{12};\quad K_3(1,2,3) = f_{12}f_{13}f_{23};\ \ldots$$

For $F_1 \equiv 1$ the system of correlation approximations agrees with the expansion in powers of the density. But (5) still has a periodic solution which cannot be obtained by expansion in powers of the density. Equation (5) together with the additional normalization condition $\langle F_1\rangle_{av} = 1$ is equivalent to the problem of obtaining the arbitrary extremum of the functional

$$A(F_1, v, \vartheta) = \vartheta\left\langle F_1(1)\ln F_1(1) - \sum_{s=1}^{\infty}\frac{F_1(1)}{v^s(s+1)!}\int K_{s+1}(1,\ldots,s+1)\;F_1(2)\ldots\right.$$
$$\left.\ldots F_1(s+1)\,dq_2\ldots dq_{s+1}\right\rangle_{av} - \vartheta\ln\frac{v(2\pi m\vartheta)^{3/2}}{h^3}, \tag{6}$$

which can be determined from (5) with accuracy up to terms and factors that are independent of F_1. These are selected so as to make $A(F_1)$ equal to the specific free energy. At constant temperature and density the equilibrium distribution corresponds to the minimum free energy. We shall also show that the pressure and internal energy can be expressed in terms of the derivatives of the functional A with respect to v and ϑ. The pressure according to [9] is

$$p = \frac{\vartheta}{v}\left\{1 - \frac{1}{6\vartheta v}\left\langle\int\frac{du(\lambda r_{12})}{d\lambda}\bigg|_{\lambda=1}F_2(1,2)\,dq_2\right\rangle_{av}\right\}. \tag{7}$$

F_2 will be expressed with the aid of (4). For this purpose f_{1i} in (5) is replaced by $f_{1i} + vu(i)(1+f_{1i})$, where f_{ij} which do not contain the coordinates of (1) are not transformed, and we take the functional derivative. After some transformations we obtain

$$F_2(1, 2) = F_1(1) F_1(2)(1 + f_{12}) \sum_{s=1}^{\infty} \frac{1}{v^{s-1}(s-1)!} \int \frac{\partial K_{s+1}(1, \ldots, s+1)}{\partial f_{12}} F_1(3) \ldots \ldots F_1(s+1)\, dq_3 \ldots dq_{s+1}, \tag{8}$$

$$p = \frac{\vartheta}{v} \left\{ 1 - \sum_{s=1}^{\infty} \frac{1}{v^s (s+1)!} \left\langle \int K_{s+1}(1, \ldots, s+1) \left[\left(s - \frac{1}{3} \frac{d}{d\lambda} \right) F_1\left(\frac{r_1}{\lambda}\right) \ldots \ldots F_1\left(\frac{r_{s+1}}{\lambda}\right) \right]_{\lambda=1} dq_2 \ldots dq_{s+1} \right\rangle_{\text{av}} \right\}. \tag{9}$$

$F_1 = \sum a_l \exp[i(\mathbf{k}_l \mathbf{r})]$, where $\mathbf{k}_l = 2\pi \mathbf{b}_l$, $\mathbf{b}_l$ are the vectors of the reciprocal lattice and $\partial A / \partial a_l = 0$. Under isotropic compression

$$k_l \sim v^{-1/3}; \quad \frac{1}{3} \frac{d}{d\lambda} F_1\left(\frac{\mathbf{r}}{\lambda}\right)\Big|_{\lambda=1} = -\frac{1}{3} \sum \left(k_l \frac{\partial F_1}{\partial k_l} \right)_{a_l} = \left(v \frac{dF_1}{\partial v} \right)_{a_l} \text{av}$$

and $p = - \partial A / \partial v$.

The expression for the internal energy (see [9]) can with the aid of (8) easily be brought into the form $\vartheta^2 \partial(A/\vartheta)/\partial\vartheta$. The constants in the last term of (6) are determined by comparison with the power series in the density and are in general unimportant. Thus, the Functional (6) expresses the relation between the structure and thermodynamical functions.

The departure of the particles from their equilibrium positions in the crystal is the sum of a large number of random quantities and is therefore distributed according to a normal curve. For a highly symmetrical structure, this distribution is spherically symmetrical and the function F_1 can be given in the form

$$F_1 = \frac{v}{(2\pi)^{3/2} r_0^3} \sum_l \exp\left\{ -\frac{(\mathbf{r} - \mathbf{r}_l)^2}{2r_0^2} \right\} = \sum_l \exp\left\{ -\frac{r_0^2 k_l^2}{2} + i(\mathbf{k}_l \mathbf{r}) \right\}. \tag{10}$$

The standard deviation r_0 is the only variational parameter and is determined from the condition $\partial A(r_0) / \partial r_0 = 0$.

For small values of r_0 the function $(2\pi)^{-3/2} r_0^{-3} \exp(-r^2/2r_0^2)$ is δ-like, and expanding the kernel K near lattice sites we obtain:

$$A = -\frac{3}{2} \vartheta - \vartheta \ln \frac{(m\vartheta)^{3/2} r_0^3}{h^3} - \vartheta \sum_{s=1}^{\infty} \frac{1}{s!} \sum_{l_1 \ldots l_s} K_{s+1}(0, r_{l_1}, \ldots, r_{l_s}) + O(r_0^2), \tag{11}$$

whence it follows that $\partial A / \partial r_0 = -3\vartheta / r_0 + O(r_0) < 0$.

For large r_0 we use the Fourier Expansion (10) of F_1. When for large r_0 we have $\partial A / \partial r_0 > 0$, the functional $A(F_1)$ has a minimum for a finite value of r_0; otherwise, there may be no periodic structure. The direct insertion of (10) in (6) gives

$$A(r_0, \vartheta, v) = -\vartheta \ln \frac{v(2\pi m\vartheta)^{3/2}}{h^3} - \vartheta \sum_{s=1}^{\infty} \frac{K_{s+1}}{v^s (s+1)!} -$$

$$- \frac{\vartheta}{2!} \sum{}' \exp[-k_l^2 r_0^2] \{\sigma(\mathbf{k}_l) - 1\} -$$

$$- \frac{\vartheta}{3!} \sum_{\mathbf{k}_{l_1}+\mathbf{k}_{l_2} \neq 0}{}' \exp\left[-\frac{(\mathbf{k}_{l_1} + \mathbf{k}_{l_2})^2 + k_{l_1}^2 + k_{l_2}^2}{2} r_0^2\right] \{\sigma(\mathbf{k}_{l_1}, \mathbf{k}_{l_2}) - 1\} - \ldots, \tag{12}$$

$$\frac{\partial A}{\partial r_0} = \vartheta r_0 \Big\{ \sum{}' k_l^2 \exp[-k_l^2 r_0^2] \{\sigma(\mathbf{k}_l) - 1\} +$$

$$+ \frac{1}{3} \sum_{\mathbf{k}_{l_1}+\mathbf{k}_{l_2} \neq 0}{}' \frac{(\mathbf{k}_{l_1} + \mathbf{k}_{l_2})^2 + k_{l_1}^2 + k_{l_2}^2}{2} \exp\left[-\frac{(\mathbf{k}_{l_1} + \mathbf{k}_{l_2})^2 + k_{l_1}^2 + k_{l_2}^2}{2} r_0^2\right] \times$$

$$\times \{\sigma(\mathbf{k}_{l_1}, \mathbf{k}_{l_2}) + 1\} + \ldots \Big\}, \tag{13}$$

where

$$K_{s+1} = \int K_{s+1}(1, \ldots, s+1)\, dq_2 \ldots dq_{s+1}; \quad \sigma(\mathbf{k}_l) = \frac{1}{v} \int \exp[i(\mathbf{k}_l \mathbf{r})] K(r)\, dq_2;$$

$$K(r) = \sum_{s=1}^{\infty} \frac{1}{v^{s-1}(s-1)!} \int K_{s+1}(1, \ldots, s+1)\, dq_3 \ldots dq_{s+1};$$

$$\sigma(\mathbf{k}_{l_1}, \mathbf{k}_{l_2}) = \frac{1}{v^2} \exp[i(\mathbf{k}_{l_1} \mathbf{r}_{12}) + i(\mathbf{k}_{l_2} \mathbf{r}_{13})] K(r_1, r_2, r_3)\, dq_2\, dq_3;$$

$$K(r_1, r_2, r_3) = \sum_{s=2}^{\infty} \frac{1}{v^{s-2}(s-2)!} \int K_{s+1}(1, \ldots, s+1)\, dq_4 \ldots dq_{s+1}.$$

The sign of $\partial A/\partial r_0$ for large r_0 is determined by the sign of the principal term and the condition for the existence of a periodic structure becomes:

$$\sigma(\mathbf{k}) = \frac{4\pi}{v} \int_0^{\infty} K(r) \frac{\sin kr}{kr} r^2 dr > 1. \tag{14}$$

The region of thermodynamically stable crystalline states is defined by the conditions

$$\frac{\partial A}{\partial r_0} = 0; \quad p\,(v\;, \vartheta) = p\,(v\;, \vartheta); \quad \mu\,(v\;, \vartheta) \geqslant \mu\,(v\;, \vartheta). \tag{15}$$

For given v_s and ϑ the first of Conditions (15) determines the magnitude of r_0 and the second determines v_l. For small $\Delta v = v_l - v_s$, Δv can be eliminated, and taking account of the first of Equations (15) and the Expansion (13) we obtain the stability condition in the form

$$\sum{}' \exp[-k_l^2 r_0^2]\{\sigma(\mathbf{k}_l) - 1\} +$$
$$+\frac{1}{3}\sum_{\mathbf{k}_{l_1}+\mathbf{k}_{l_2}\neq 0}{}' \exp\left[-\frac{(\mathbf{k}_{l_1}+\mathbf{k}_{l_2})^2 + k_{l_1}^2 + k_{l_2}^2}{2} r_0^2\right]\{\sigma(\mathbf{k}_{l_1}, \mathbf{k}_{l_2}) + 1\} + \ldots \geqslant 0. \tag{16}$$

For example, for a face-centered cubic lattice the region of stability and the parameter r_0 are determined by the following conditions:

$$\sigma(\mathbf{k}) - 1 + \exp\left[-\frac{k^2 r_0^2}{3}\right]\left[\sigma\left(\frac{2\mathbf{k}}{\sqrt{3}}\right) - 1\right] + 5\exp\left[-2\frac{k^2 r_0^2}{3}\right][\sigma(\mathbf{k}, \mathbf{k}) + 1] + \ldots = 0, \tag{17}$$

$$\left[\sigma\left(\frac{2\mathbf{k}}{\sqrt{3}}\right) - 1\right] + 8\exp\left[-\frac{k^2 r_0^2}{3}\right][\sigma(\mathbf{k}, \mathbf{k}) + 1] + \ldots \leqslant 0, \tag{18}$$

where $\mathbf{k}$ is the basic vector of the reciprocal lattice (multiplied by 2π) and $v = 6\sqrt{3}\pi^3/k^3$. In order to determine all properties of the crystal, Equations (17) and (18) must be supplemented by the equation of state (9).

From (17) and (18) there follows the possibility of continuous crystallization. The continuous transition curve is defined by

$$\sigma(\mathbf{k}) \equiv \frac{4\pi}{v}\int_0^\infty K(r)\frac{\sin kr}{kr} r^2 dr = 1 \tag{19}$$

subject to the condition $\sigma(2\mathbf{k}/\sqrt{3}) < 1$. For $\sigma(2\mathbf{k}/\sqrt{3}) > 1$ crystallization will be a first-order transition with a density discontinuity; the transition curve is defined by (17) and (18) when in (18) the sign $\leq$ is replaced by the equality sign.

Calculations based on the simplest interaction model (an infinitely high barrier and a narrow well) in the first and second correlation approximations showed that at high temperatures there are no periodic solutions; a continuous crystallization region follows, and only at lower temperatures does crystallization become a first-order transition.

Landau states [10] that crystallization can be continuous only at isolated points. This follows from the assumption that the Fourier series of F_1 contains only one harmonic. But the Expansion (10) contains all harmonics with coefficients which are of higher orders of smallness. The continuous crystallization region was also obtained by Lennard-Jones and Devonshire [8] by the free volume method.

In the first correlation Approximation (5) agrees with the equations of A. A. Vlasov and S. V. Tiablikov. In the following approximations the kernel determined in [2] is incorrect.

Tomsk Structural Engineering Institute

Received July 9, 1956

LITERATURE CITED

[1] A. A. Vlasov, Theory of Many Particles (1950)

[2] S. V. Tiablikov, J. Exptl.-Theoret. Phys. (U.S.S.R.) 17, 5, 386 (1947).

[3] J. G. Kirkwood and E. Monroe, J. Chem. Phys. 9, 7, 515 (1941).

[4] I. Z. Fisher, J. Exptl.-Theoret. Phys. (U.S.S.R.) 23, 2, 171; 4, 437, 447 (1955).

[5] K. F. Herzfeld and M. Goeppert-Mayer, Phys. Rev. 46, 995 (1935).

[6] M. Born, J. Chem. Phys. 7, 591 (1939).

[7] Ia. I. Frenkel', Kinetic Theory of Liquids (Acad. Sci. USSR Press, 1948).

[8] J. E. Lennard-Jones and A. F. Devonshire, Proc. Roy. Soc. (London) A169, 317 (1939); 170, 464 (1939).

[9] N. N. Bogliubov, Problems of Dynamical Theory and Statistical Physics (1946).

[10] L. D. Landau, J. Exptl.-Theoret. Phys. (U.S.S.R.) 7, 1, 19; 5, 627 (1937).

ON THE CAUSES OF RETROGRADE ARC CATHODE SPOT MOTION IN A MAGNETIC FIELD

I. G. Kesaev

(Presented by Academician L. A. Artsimovich November 15, 1956)

The orderly motion of a cathode spot in a magnetic field has long attracted the attention of physicists because of the unusual direction of the motion at low pressures of the ambient [1-10]. In a homogeneous field this direction is diametrically opposed to the direction in which charges should move when subjected to an electromagnetic force. This type of motion has been called "retrograde."

The study of "retrograde" motion during many years [3-9] has not cleared up the nature of the mechanism of the arc spot motion. It was a serious omission that in connection with this problem until recently no attention has been paid to the proper magnetic field of the cathode part of the arc, whose strength near the boundaries of the spot can reach 600 oersteds according to an approximate estimate. As a result of the superposition of the outside field and the proper field of the arc there must be strong asymmetry in the field distribution at the spot boundary. As will be shown below, this type of asymmetry can be the dominant cause of the motion of the cathode spot at low pressures.

If there is asymmetry of the conditions near the cathode spot boundary we must consider the possibility that the spot will move in the direction in which the emission conditions are more favorable. In order to determine the role of magnetic field asymmetry in spot motion two questions must first be answered:

1. Does the magnetic field affect the operating conditions of the spot ?

2. Is there any correspondence between the direction of motion and the direction in which the change of the combined magnetic field in the region of the spot can be considered most favorable with regard to influence on the arc ?

Experiment shows that the application of a magnetic field with any orientation leads to considerably increased stability of the mercury arc cathode spot at low pressures, and that the stabilizing effect of the field increases with higher field strength. This effect reveals itself in the fact that under the conditions for an unstable arc near the critical value of the arc current (0.5-3 amp) the imposed field stabilizes the cathode fall and increases the average time of arcing. Therefore, asymmetry of the field around the cathode spot can cause shifting of the spot because of the formation of new and more stable emission centers near an edge. The motion of the spot which results from field asymmetry must be in the direction of increasing field. This conclusion results from an analysis of the asymmetry of charged particle concentration around a spot which is produced by the electron-optical action of the magnetic field. The principal characteristic of the concentration distribution is that the concentration maximum must correspond to the field maximum. However, considerable asymmetry in the concentration distribution can arise only at low pressures, for which the mean free electron path λ remains greater than the mean Larmor radius R.

Thus, for such pressures the direction of motion of the mercury arc cathode spot must coincide with the direction of the strongest increase of the combined magnetic field near the edge of the spot. As follows from the discussion given below, this principle of a maximum field without any additional hypotheses regarding the mechanism and shape of the spot enables us to predict the direction of motion for the general case of an inhomogeneous field. The field strength of the current $\underline{i}$ which moves with the spot can be given by the simple relation

$$H_i = \frac{0{,}2i}{r}, \tag{1}$$

which holds true for any shape of a spot at distances r which exceed its radius.

In Fig. 1 the field of an arc on a circle of radius r from the center O of the spot is represented by a vector that is tangent to the circle. Because of the symmetry of the arc field with respect to the spot this field alone cannot cause the spot to select a direction of motion φ. The required asymmetry results from the application of an external field H. For further deductions it is of interest to consider a strong field in which random motion is reduced to a minimum and the trajectory of the spot is regular. In a strong field the directions φ_m in which the combined field on the circle has extremal values can be determined with sufficient accuracy from the equation

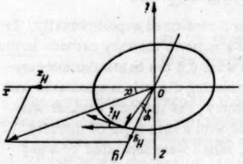

Fig. 1. Graph showing the superposition of the proper field of the arc H_i and the external field with components H_x and H_y.

$$\tan\varphi_m = \frac{\dfrac{\partial H}{\partial x} - \dfrac{H_y}{H}\dfrac{0.2i}{r^2}}{\dfrac{\partial H}{\partial y} + \dfrac{H_x}{H}\dfrac{0.\ 2i}{r^2}}. \tag{2}$$

The x and y axes are in the plane of the cathode and the angle φ is reckoned from the positive y axis in the direction of positive x. The components H_x and H_y of the external field are considered positive when the corresponding vectors are in the positive directions of the axes. Each value of the fraction in the right-hand side of the equation corresponds to two directions φ_m, of which one is the direction of the field maximum and the other in the direction of the field minimum. Because these are diametrically opposed the direction of the maximum is the direction of spot motion if r denotes the effective range of interaction between the cathode spot and the magnetic field. According to the formulation of the problem r must somewhat exceed the actual radius of the spot since the direction of motion depends on the field distribution in the neighborhood of the spot. When the coordinate axes are placed in such a position that the denominator of the right-hand side of the equation remains positive the field maximum will correspond to acute angles and we can transform (2) into a differential equation for the trajectory by replacing tan φ_m with the derivative $\partial x/\partial y$. In a homogeneous field

$$\tan\varphi_m = -\frac{H_y}{H_x} = -\tan\alpha,$$

and, consequently, the spot must move perpendicularly to the tangential component of the field H since the angles φ and α are measured from mutually perpendicular axes. It is easily seen that the direction of this motion is opposite to the deflection of electrons emitted by the cathode in a field H, that is, the motion is "retrograde." In an inhomogeneous field $\tan\varphi_m \neq -\tan\alpha$ and the direction of motion must be determined by the more complex law (2).

The equation of the cathode spot trajectory becomes simple in a field which depends only on the coordinates x and z, with its tangential component along the x axis:

$$\frac{dx}{dy} = \frac{r^2}{0.2i}\,\frac{H}{H}\cdot\frac{dH}{dx}. \tag{3}$$

Such a field is found at the poles of an electromagnet which are separated by a parallel gap along the y axis. It is characteristic of the trajectory that the slope of the tangent to the direction of "retrograde" motion which coincides with the y axis must be approximately proportional to the inhomogeneity of the field. This property of the trajectory is easily understood on the basis of the relation which exists between the "retrograde" motion of the spot and its motion in the direction of a stronger field. Both of these motions have a common cause, which is the field asymmetry in the region of the spot. The asymmetry of the combined external and proper fields gives rise to the "retrograde" motion, while the asymmetry of the external field alone causes deflection of the spot along the x axis.

This property of the trajectory has been confirmed experimentally. In the initial experiments the spot moved on a uniform mercury cathode in the field of an electromagnet whose pole tips were 0.6 cm below the mercury level. Thereafter, for the purpose of eliminating distortions associated with the excitation of surface waves in the mercury, the mercury cathode was replaced by a smooth copper plate covered with a thin layer of mercury. The plate was fastened over the pole tips, which were separated by a gap 1 cm wide and 6 cm long. The equilibrium pressure of the mercury vapor in the space corresponded to a temperature of 20-22°.

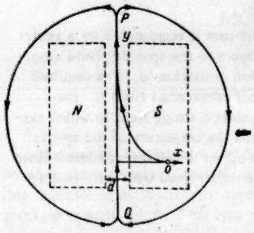

Fig. 2. Arrangement of magnet poles and the trajectory of the cathode spot.

The usual path of the spot is represented schematically in Fig. 2. From its point of origin O the spot moved in the direction of the symmetry axis of the field, approaching it continuously. When it reached the point P of the cathode boundary, the spot moved around the cathode in a semicircle to the right or left until it reached the axis of symmetry at the point Q; it then moved along this axis, making it clearly distinguishable in the photographs.

Figure 3 is a (3x) photograph showing the spot trajectory with a current of 3 amperes and field $H_0 = 1300$ oersteds at the axis of symmetry. Study of many of these photographs showed that within a distrance $x = 0.7$ cm from the field symmetry y axis the spot trajectory can be represented by the simple equation:

$$\ln\frac{x_0}{x} = Ay. \tag{4}$$

Within these limits the field distribution used in the experiments can be approximated by the expression

$$H = H_0(1 - ax^2),$$
$$H_x = H_0(1 - bx^2)$$

with the constants $a = 0.28$ cm^{-2} and $b = 0.76$ cm^{-2}, while Eq.(4) is a quite accurate representation of the trajectory obtained by solving the differential Equation (3). The constant A is connected with r by the relation:

$$A = \frac{2.8H_0}{i} r^2.$$

The numerical value of A was found to be 1.1 cm^{-1} for a current of 3 amperes and 1.65 cm^{-1} for 15 amperes, so that for the effective radius r we obtain 3.3×10^{-2} cm and 9×10^{-2} cm, respectively. The actual size of the spot for the currents indicated varies according to Froome's data [11] between 0.3×10^{-2} cm and 1.5×10^{-2} cm.

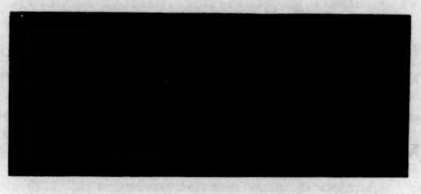

Fig. 3. Photograph of the trajectory of a cathode spot in an inhomogeneous field (3×).

The agreement between the theoretical and actual trajectories of the spot in an inhomogeneous field and the reasonable order of magnitude of the radius r obtained by comparing theory and experiment are evidence of the correctness of the hypotheses concerning the dominant role of magnetic field asymmetry around the cathode spot in the mechanism of orderly retrograde spot motion at low pressures.

V. I. Lenin All-Union Electrotechnical Institute

Received November 9, 1956

LITERATURE CITED

[1] N. Minorsky, J. Phys. Rad 9, 127 (1928).

[2] C. G. Smith, Phys. Rev. 62, 48 (1942); 69, 96 (1946); 73, 543 (1948); 83, 194 (1951); 84, 1075 (1951).

[3] R. L. Longini, Phys. Rev. 71, 642 (1947); 72, 184 (1947).

[4] G. J. Himler and G. I. Cohn, Elec. Eng. 67, 1148 (1948).

[5] C. J. Gallagher and J. D. Cobine, Phys. Rev. 71, 481 (1947); Elec. Eng. 68, 469 (1949).

[6] C. J. Gallagher, J. Appl. Phys. 21, 768 (1950).

[7] J. Rothstein, Phys. Rev. 78, 331 (1950).

[8] S. Iamamura, J. Appl. Phys. 21, 193 (1950).

[9] R. S. John and J. G. Winans, Phys. Rev. 93, 653 (1954); 94, 5 (1954); 98, 562 (1955).

[10] C. G. Miller and N. L. Sanders, Phys. Rev. 93, 654 (1954).

[11] K. D. Froome, Proc. Phys. Soc. B 62, 805 (1949).

PARAMAGNETIC RESONANCE HYPERFINE STRUCTURE, NUCLEAR SPIN AND THE MAGNETIC MOMENT OF THE 5.3-YEAR RADIOACTIVE ISOTOPE Eu^{152}

A. A. Manenkov, A. M. Prokhorov, P. S. Trukhliaev and G. N. Iakovlev

(Presented by Academician L. A. Artsimovich November 13, 1956)

From the paramagnetic resonance hyperfine structure the nuclear spin and magnetic moment of the 5.3-year radioactive isotope Eu^{152} have been determined: $I(\mathrm{Eu}^{152}) = 3$, $|(\mu_{152})| = 2.03$ nuclear magnetons.

In [1, 2] the paramagnetic resonance hyperfine structure of Eu^{2+} was investigated, which was due to the nuclei of the stable isotopes Eu^{151} and Eu^{153}.

In the present work we have investigated paramagnetic resonance in the powdered phosphor SrS activated by europium which contained the 5.3-year radioactive isotope Eu^{152}. The latter was prepared by irradiating a natural mixture of the isotopes Eu^{151} (47.77%) and Eu^{153} (52.23%) with pile neutrons. Such irradiation produces an appreciable yield of radioactive Eu^{152} formed from Eu^{151} through the reaction Eu^{151}(n, γ) Eu^{153}.

There is no appreciable production of the other radioactive isotopes Eu^{154} and Eu^{155} in the pile through the reactions Eu^{153}(n, γ) Eu^{154} and Eu^{154}(n, γ) Eu^{155}, because of unsuitable neutron cross sections for Eu^{153}, Eu^{154} and Eu^{155} [3, 4]. The original mixture of Eu^{151} and Eu^{153} was irradiated with 4×10^{13} neutron flux for 39 days.

The irradiation produced a mixture of Eu^{151}, Eu^{152} and Eu^{153}, whose relative abundance as shown by our experiments on paramagnetic resonance, which are described below, was 29%, 17% and 54%, respectively.

The sample of the SrS phosphor that was activated by this mixture of europium isotopes was prepared by a method developed by Z. A. Trapeznikova. The method is the following: into a mixture of 2 g SrCO$_3$, 1.5 g S and 0.35 g SrCl$_2$ a solution of EuCl$_2$ was introduced, after which the mixture was dried and annealed in air at 1150°C for 20 min. The relative europium content in the phosphor was $\sim 10^{-4}$.

Paramagnetic resonance in this sample was investigated at 9343 Mc with the superheterodyne radiospectroscope described in [5]. The observed spectrum is shown in Fig. 1. It consists of three series of components of the hyperfine structure due to Eu^{151}, Eu^{152} and Eu^{153}; the spectrum belongs to the single electron transition $M = \frac{1}{2} \leftrightarrow -\frac{1}{2}$ (lines belonging to other electron transitions are not observed because of their anisotropic broadening in the powder).

Series I consists of the most intense lines which belong to Eu^{153}; series II, which is less intense, belongs to Eu^{151}; and series III, which is least intense, belongs to the radioactive isotope Eu^{152}.

The solid lines in the figure represent well-resolved components of the spectrum; the dotted lines represent components belonging to Eu^{152}, which in the observed spectrum overlap components of Eu^{151}. The magnetic field was measured through the use of proton resonance. The line positions in Fig. 1 are given in proton resonance frequencies (in Mc).

Figure 1 shows that the number of components in each of series I and II is 6, which corresponds to nuclear spin $I = {}^{5}/_{2}$ for Eu^{151} and Eu^{153}, and the total splittings in these series, as has already been reported [1, 2] gives for the ratio of the magnetic moments of Eu^{151} and Eu^{153} the value $\mu_{151}/\mu_{153} = 2.24$.

In series III, which belongs to the radioactive isotope Eu^{152}, not all components are resolved because they overlap lines of the stable isotope Eu^{151}. Complete resolution is obtained for the lines 14.096; 14.160; 14.290 and 14.416 Mc. The relative spacings between these lines shows that the nuclear spin of Eu^{152} is $I = 3$. The remaining 3 lines, which should be observed at 14.225, 14.354 and 14.480 Mc overlap the lines 14.218, 14.353

and 14.488 Mc of Eu^{151}, since the separations between these respective lines is smaller than the line widths (12 kc in the proton resonance frequency scale). This overlapping is confirmed by the fact that the intensities of the lines at 14.218, 14.354 and 14.488 Mc in the observed spectrum are greater than the intensities of other lines of Eu^{151}.

All values of the nuclear spin of Eu^{152} except $I = 3$ are excluded because we would otherwise have to observe additional lines which would be quite well resolved from the lines of the stable isotopes. A likely value would have been $I = 6$ since the additional lines would have to be close to the Eu^{153} lines and could be hidden by the latter.

However, a detailed analysis of the observed spectrum shows that $I = 6$ is also excluded. This is confirmed by two circumstances.

For $I = 6$ the line 14.128 Mc would have to exist. This hypothetical line would be quite well resolved from the 14.139 Mc line of Eu^{153} with a separation of 11 kc, which is almost equal to the line width. We can point to the lines 14.083 and 14.096 Mc, which are separated by 13 kc. Careful study showed that the hypothetical line 14.139 Mc is absent. A comparison of the relative intensities of the spectral lines also indicated the absence of additional lines besides those corresponding to $I = 3$.

Thus it can be considered established that the nuclear spin of Eu^{152} is 3.

The observed frequencies are described by the formula [2]:

$$h\nu = g\beta H + Am + \frac{1}{2}\frac{A^2}{g\beta H_0}\{I(I+1) - m^2\}. \qquad (1)$$

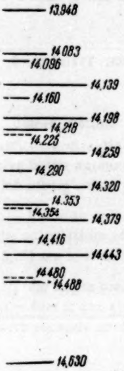

Fig. 1. Paramagnetic resonance hyperfine structure in $SrS \cdot Eu^{151, 152, 153}$ in the electron transition $M = = 1/2 \leftrightarrow -1/2$

Comparison of the observed frequencies and this formula gives for the g factor and the hyperfine structure constant A_{152} the following values: $g = 1.992 \pm 0.001$; $A^{*}_{152} = 0.064 \pm 0.002$ Mc (on the proton resonance frequency scale); $A_{152} = (13.9 \pm 0.1) \cdot 10^{-4}\ cm^{-1}$. It should be noted that for the hyperfine structure constants A_{152} and A_{153} we obtain the values $A_{151} = (29.4 \pm 0.1) \cdot 10^{-4}\ cm^{-1}$; $A_{153} = (13.1 \pm 0.1) \cdot 10^{-4}\ cm^{-1}$, which are somewhat smaller than the values determined for $SrS \cdot Eu$ in [1, 2]. Since the hyperfine splitting depends on the electric field of the crystal this discrepancy is probably associated with some difference in the crystal structures of these samples.

A considerable difference in the values of the hyperfine structure constant (about 15%) was previously found [2] for $SrS \cdot Eu$ and $CaF_2 \cdot Eu$. But in all instances the ratio A_{151}/A_{153} was identical, that is, independent of the crystal structure.

The total hyperfine splitting for a given isotope is 2AI and since the constant A is proportional to the ratio of the nuclear magnetic moment μ and spin I, the total splitting is proportional to μ. Therefore, we can determine directly from the observed spectrum the ratio of the magnetic moments of Eu^{151} (or Eu^{153}) and Eu^{152}. This ratio is

$$\mu_{152}/\mu_{151} = 1.77 \pm 0.02.$$

Using for μ_{151} the known value 3.6 nuclear magnetons [6] we obtain for the magnetic moment of Eu^{152}:

$$\mu_{152} = 2.03 \text{ nuclear magnetons.}$$

The relative signs of the moments μ_{151} and μ_{152} remains undetermined. They can be determined by comparing the hyperfine splitting in different electron transitions [2].

Received November 2, 1956

LITERATURE CITED

[1] B. Bleaney and W. Low, Proc. Phys. Soc. A 68, 55(1955).

[2] A. A. Manenkov and A. M. Prokhorov, Doklady Akad. Nauk SSSR 107, 402(1956).*

[3] D. Hughes, Neutron Investigations in Nuclear Reactors, (Foreign Lit. Press, 1954) (Russian Translation).

[4] R. Hayden, J. H. Reynolds and M. G. Inghram, Phys. Rev. 75, 1500(1949).

[5] A. A. Manenkov and A. M. Prokhorov, Radiotekh. i Elektronika(Radio Engr. and Electronics) 1, 4, 469 (1956).

[6] P. F. A. Klinkenberg, Rev. Mod. Phys. 25, 63(1952).

---

* [Soviet Physics-Doklady, p. 196].

ON THE THEORY OF MAGNETOSTRICTION OF NICKEL SINGLE CRYSTALS

W. F. Brown, Jr.

(Presented by Academician L. A. Artsimovich December 14, 1956)

Recently Akulov [1] compared his theory [2] of the variation of longitudinal elongation in nickel crystals with magnetization and Heisenberg's theory [3]. For magnetization along the [111] axis he found that his curves give better agreement with experiment than the curves calculated by Gans and Harlem [4] on the basis of Heisenberg's theory. This result apparently refutes Heisenberg's theory.

I wish to call attention to an article [5] in which it was shown that this discrepancy results from errors in the calculations of Gans and Harlem. Curves which are correctly calculated according to Heisenberg's theory [5, 6] are in satisfactory agreement with experiment.

No single theory accurately describes the process of magnetization, but Heisenberg's theory has the advantage that it can easily be applied to different problems. Thus, this theory and its subsequent modifications were recently used [7] to interpret the reversible behavior of ferrites. It was also once used by Akulov [8].

St. Paul, Minnesota, USA

Received November 12, 1956

LITERATURE CITED

[1] N. S. Akulov, Doklady Akad. Nauk SSSR 106, 31 (1956).

[2] N. S. Akulov, Z. Physik 69, 78 (1931).

[3] W. Heisenberg, Z. Physik 69, 287 (1931).

[4] R. Gans and J. v. Harlem, Ann. Physik 15, 516 (1932); 16, 162 (1933).

[5] W. F. Brown, Jr., Phys. Rev. 52, 325 (1937).

[6] R. H. Fowler, Statistical Mechanics, 2nd ed. (New York, 1936) p. 520.

[7] D. M. Grimes, Bull. Am. Phys. Soc. 1, (2), 25 (1956).

[8] N. Akulov and E. Kondorsky, Z. Physik 78, 801 (1932); 85, 661 (1933).

CONCERNING THE NOTE OF W. F. BROWN, Jr., REGARDING THE THEORY OF MAGNETOSTRICTION OF NICKEL SINGLE CRYSTALS

Academician N. S. Akulov of the Academy of Sciences, Byelorussian SSR

The calculations of Gans and Harlem do indeed, contain an error, and we are thankful to Brown for pointing it out. But this error has no connection with our theory and our calculations, and the arguments against the formal method employed by Heisenberg remain valid even on the basis of the calculations which were corrected by Brown.

In the work of Gans and Harlem our basic equations for magnetostriction are used correctly; their error is associated with an incorrect application of Heisenberg's method, thus showing that this method cannot always be applied simply. Although Brown's formula, based on a more accurate application of Heisenberg's method, is in better agreement with experiment than the curve of Gans and Harlem, it is still true that the theoretical curve based on our energy method is a better description of experimental findings than Brown's equation.

We believe that the agreement between our curve and experiment can hardly be attributed to experimental errors. Yet, even aside from a comparison of theory and experiment a certain shortcoming of Heisenberg's method must be pointed out, resulting from the fact that real crystals always have internal elastic stresses. Heisenberg's method is not well-founded physically and ignores the role of these stresses.

During magnetization work is done against the internal stresses. Neglecting hysteresis this work for the domain transitions

$$I_s \parallel [\bar{1}\,\bar{1}\,\bar{1}] \rightarrow I_s \parallel [111]. \tag{1}$$

has the value zero unlike the transitions

$$I_s \parallel [11\bar{1}] \rightarrow I_s \parallel [111], \tag{2}$$

where this work is not zero. Therefore, the transitions (1) and (2) are not statistically equivalent as is assumed in Heisenberg's method. The resulting error is to a certain extent similar to the error of Gans and Harlem when they assume statistical equivalence for the $[\bar{1}11]$ direction on the one hand, the $[1\bar{1}\bar{1}]$ direction on the other. As is shown by experiment, the resulting error in some cases can be relatively small; nevertheless, there exists a fundamental inadequacy in the formal statistical method for explaining some specific characteristics of the magnetostriction curves and other effects. Therefore, in some cases the energy method of calculating the distribution function of domains in the easy direction of magnetization (which has been further developed in various versions by other authors) gives better agreement with experiment and has a better physical basis.

After the publication of these two methods (the energy and the formal statistical methods), as early as 1932 it was suggested that they be combined. This was done to first approximation in the energy-statistical method in which the role of the internal stresses was taken into account (although not entirely) by introducing the magnetic susceptibility ($\chi_0 = I/H$) into the theory for $I \ll I_s$, which is very sensitive to the magnitude of the internal elastic stresses. The theory of elastically-stressed domains based on this method, which was developed by Akulov and Kondorsky [6] and analogously by Brown [3] makes it possible to give a satisfactory description of a large number of different effects associated with the action of external and internal elastic stresses σ on single crystals and polycrystals (see also [9]). In particular, pretty good agreement with experiment is given by the formulas obtained by Akulov and Kondorsky for different mechano-magnetic effects. Unlike Heisenberg's theory these formulas contain the suceptibility χ_0. An example is the formula for ΔE of the effect

$$\left(\frac{\Delta E}{E}\right)_s = c\chi_0\lambda_s E_0 / I_s^2 , \tag{3}$$

where the coefficient $\underline{c}$ averaged by the Rauss method is $^3/_5$. In the literature our formula is sometimes used with larger values for this coefficient (up to $^4/_5$). The experiments of Jamamoto and Taniguchi [8] confirm this Formula (3) although they call it semi-empirical. In actuality it was derived purely from theory in the articles [6, 3, 9].

For the coefficient $\underline{c}$ these authors gave the value 0.7 as an average from different experimental data, which within the limits of experimental error agrees with the theoretical value. Akulov and Kondorsky took the Rauss average. If the Fokht average is taken we obtain a different value for $\underline{c}$, which of course, does not alter the theoretical essence of our formula. The question as to the kind of averaging is naturally interesting independently and can only be answered eventually by accumulating sufficiently reliable experimental data.

It should be noted that the basis for the theory of mechano-magnetic phenomena mentioned in Brown's note lies in the equations for magnetostriction:

$$\begin{aligned}\lambda = {}^3/_2\,\lambda_{100}\,(\alpha_1^2\beta_1^2 + \alpha_2^2\beta_2^2 + \alpha_3^2\beta_3^2 - {}^1/_3) + \\ + 3\lambda_{111}\,(\alpha_1\alpha_2\beta_1\beta_2 + \alpha_2\alpha_3\beta_2\beta_3 + \alpha_3\alpha_1\beta_3\beta_1\end{aligned} \tag{4}$$

and for the energy of the elastic stresses σ:

$$\begin{aligned}E_\sigma = -{}^3/_2\sigma\,[\lambda_{100}\,(\alpha_1^2\gamma_1^2 + \alpha_2^2\gamma_2^2 + \alpha_3^2\gamma_3^2) + \\ + 3\lambda_{111}\,(\alpha_1\alpha_2\gamma_1\gamma_2 + \alpha_2\alpha_3\gamma_2\gamma_3 + \alpha_3\alpha_1\gamma_3\gamma_1)].\end{aligned} \tag{5}$$

These equations are sometimes given without proper reference to the original sources [7, 5] and are sometimes erroneously attributed to Becker and Doering (see, for example, [10]).

Heisenberg's work is based on relations such as (4), as Heisenberg duly states. In some articles use is also made of our relation for the thermodynamical potential of elastic stresses with additional terms suggested by Gans and his collaborators and also by Becker and Doering.

We mention in conclusion that despite individual exceptions and the need for further verification, the statistical theory of elastically stressed domains based on the relations given above as a rule gives more universal and exact results than other methods of calculation. In this respect we are in full agreement with Brown. For a final decision and for perfecting of the theory it would be very desirable to obtain new and more exact experimental information.

Received December 14, 1956

LITERATURE CITED

[1] R. Gans and J. v. Harlem, Ann. Phys. 15, 516(1932); 16, 162(1933).

[2] W. Heisenberg, Z. Physik 69, 287(1931).

[3] W. F. Brown, Jr., Phys. Rev. 52, 325(1937).

[4] N. S. Akulov, Doklady Akad. Nauk SSSR 106, 31(1956).*

[5] N. S. Akulov, Z. Physik 69, 78(1931).

[6] N. Akulov and E. Kondorsky, Z. Physik 78, 801(1932); 85, 661(1933).

[7] N. S. Akulov, Z. Physik 52, 389(1928).

[8] M. Jamamoto and S. Taniguchi, Sci. Repts Research Inst., Tohoku Univ. 8, 3(1956); Sci. Repts Research Insts. Tohoku Univ. 7, 1(1956).

[9] N. S. Akulov, Ferromagnetism (Moscow, 1939).

[10] R. M. Bozorth, Ferromagnetism (Toronto-New York-London, 1951). [Russian Translation (Moscow, 1956) p. 642].

---

* [Soviet Physics-Doklady, p. 1].

THE INVARIANCE PRINCIPLE FOR A HOMOGENEOUS MEDIUM OF ANY GEOMETRIC FORM

B. B. Kadomtsev

(Presented by Academician M. A. Leontovich November 27, 1956)

1. An invariance principle in the theory of light scattering was first formulated by V. A. Ambartsumian for a semi-infinite medium [1]. It was extended to the case of a plane layer by S. Chandrasekhar [2]. In the present article the invariance principle is applied to a medium of any geometric shape; this is of interest both for the theory of light scattering and for some problems in neutron physics.

In order to avoid excessive complications we assume that the scattering takes place without change of frequency (as will be seen subsequently, there are no special difficulties in making the extension to scattering with change of frequency). We shall also assume that the medium under consideration is homogeneous and bounded by a convex surface S. Because of the homogeneous medium the transfer equation contains no explicit dependence on $\mathbf{r}$ and is thus invariant with respect to an infinitely small movement of space. Therefore, the effect of such a transformation can be entirely taken into account by a change of the boundary conditions. This statement represents the content of the invariance principle for the general case.

Taking as the unit of length the mean free path of a quantum we write the transfer equation for the Green's function [3] in the form

$$\{(\boldsymbol{\omega}\nabla) + \rho(\mathbf{r})\} G(\boldsymbol{\omega}, \mathbf{r}; \boldsymbol{\omega}_0, \mathbf{r}_0) =$$

$$= \lambda\rho(\mathbf{r}) \int p(\boldsymbol{\omega}\cdot\boldsymbol{\omega}') G(\boldsymbol{\omega}', \mathbf{r}; \boldsymbol{\omega}_0, \mathbf{r}_0)\, d\omega' + \delta(\boldsymbol{\omega} - \boldsymbol{\omega}_0)\,\delta\,(\mathbf{r} - \mathbf{r}_0). \qquad (1)$$

Here $G(\boldsymbol{\omega}, \mathbf{r}; \boldsymbol{\omega}_0, \mathbf{r}_0)$ is the Green's function representing the intensity of radiation at the point $\mathbf{r}$ in the direction $\boldsymbol{\omega}$ from a point source located at the point $\mathbf{r}_0$ and emitting radiation in the direction $\boldsymbol{\omega}_0$; λ is the absorption coefficient; $p(\cos\theta)$ is the scattering characteristic function; $\rho(\mathbf{r})$ is the "density of matter," which has the value 1 inside of S and 0 outside of S.

We displace the medium by the infinitely small amount ϵ in the direction of the unit vector $\mathbf{e}$ leaving the point of the source and observed point fixed. The Green's function $G(\boldsymbol{\omega}, \mathbf{r}; \boldsymbol{\omega}_0, \mathbf{r}_0)$ becomes the new function $G'(\boldsymbol{\omega}, \mathbf{r}; \boldsymbol{\omega}_0, \mathbf{r}_0)$, which is clearly equal to the old function but with displaced source and observed point

$$G'(\boldsymbol{\omega}, \mathbf{r}; \boldsymbol{\omega}_0, \mathbf{r}_0) = G(\boldsymbol{\omega}, \mathbf{r} - \varepsilon\mathbf{e};\ \boldsymbol{\omega}_0, \boldsymbol{\omega}_0 - \varepsilon\mathbf{e}).$$

Thus we have the variation

$$\delta G = G' - G = -\varepsilon\mathbf{e}\,(\nabla + \nabla_0)\, G(\boldsymbol{\omega}, \mathbf{r}; \boldsymbol{\omega}_0, \mathbf{r}_0). \qquad (2)$$

On the other hand this shift is equivalent to a certain variation of the density in which matter is removed on one side and added on the other (this is also equivalent to a change of the boundary conditions). Varying (1) we obtain

$$\{(\omega\nabla)+\rho(\mathbf{r})\}\,\delta G(\omega,\mathbf{r};\omega_0,\mathbf{r}_0)-\rho(\mathbf{r})\cdot\lambda\int p(\omega\omega')\,\delta G(\omega',\mathbf{r};\omega_0,\mathbf{r}_0)\,d\omega'=$$
$$=-\delta\rho(\mathbf{r})\,\{G(\omega,\mathbf{r};\omega_0,\mathbf{r}_0)-\lambda\int p(\omega\omega')\,G(\omega',\mathbf{r};\omega_0,\mathbf{r}_0)\,d\omega'\}. \tag{3}$$

We see that the variation δG satisfies the transfer equation and can thus be represented in terms of the Green's function:

$$\delta G(\omega,\mathbf{r};\omega_0,\mathbf{r}_0)=-\int G(\omega,\mathbf{r};\omega',\mathbf{r}')\cdot\delta\rho(\mathbf{r}')\,\{G(\omega',\mathbf{r}';\omega_0,\mathbf{r}_0)-$$
$$-\lambda\int p(\omega'\omega'')\,G(\omega'',\mathbf{r}';\omega_0,\mathbf{r}_0)\,d\omega''\}\,d\omega'\,d\mathbf{r}',$$

where $d\mathbf{r}'$ denotes a volume element. Inserting (2) and assuming that the density variation is $\delta\rho=\varepsilon$ and is nonvanishing only on the surface S where it is δ-like, we obtain

$$-\varepsilon\mathbf{e}\,(\nabla+\nabla_0)\,G(\omega,\mathbf{r};\omega_0,\mathbf{r}_0)=$$
$$=-\varepsilon\mathbf{e}\oint_S\int G(\omega,\mathbf{r};\omega',\mathbf{r}_s)\,G(\omega',\mathbf{r}_s;\omega_0,\mathbf{r}_0)\,d\omega'\,dS+$$
$$+\varepsilon\mathbf{e}\lambda\oint_S\int G(\omega,\mathbf{r};\omega',\mathbf{r}_s)\,p(\omega'\omega'')\,G(\omega'',\mathbf{r}_s;\omega_0,\mathbf{r}_0)\,d\omega'\,d\omega''\,dS,$$

where $\mathbf{r}_s$ is the running radius-vector over which we integrate. The first integral on the right-hand side of this equation vanishes because of the boundary conditions obeyed by the Green's function:

$$G(\omega,\mathbf{r};\omega_0,\mathbf{r}_0)=0\quad\text{for}\quad\mathbf{r}\in S,\ \omega\cdot\mathbf{n}<0\quad\text{or}\quad\mathbf{r}_0\in S,\ \omega_0\cdot\mathbf{n}_0>0,$$

where $\mathbf{n}$ is the exterior normal to S at the point $\mathbf{r}$ and $\mathbf{n}_0$ at the point $\mathbf{r}_0$. With arbitrary vector $\mathbf{e}$ we finally obtain:

$$(\nabla+\nabla_0)\,G(\omega,\mathbf{r};\omega_0,\mathbf{r}_0)=$$
$$=-\lambda\oint_S\int G(\omega,\mathbf{r};\omega',\mathbf{r}_s)\,p(\omega'\omega'')\,G(\omega'',\mathbf{r}_s;\omega_0,\mathbf{r}_0)\,d\omega'\,d\omega''\,dS. \tag{4}$$

We now rotate space through the infinitely small angle ξ around some point $\mathbf{R}$. Then G becomes

$$G'(\omega,\mathbf{r};\omega_0,\mathbf{r}_0)=$$
$$=G(\omega-[\xi\omega],\ \ \mathbf{r}-[\xi(\mathbf{r}-\mathbf{R})];\ \omega_0-[\xi\omega_0],\ \mathbf{r}_0-[\xi(\mathbf{r}_0-\mathbf{R})]).$$

On the other hand, a change of the Green's function can be regarded as a variation of density $\delta\rho = -[\boldsymbol{\xi}(\mathbf{r}-\mathbf{R})]\cdot\nabla\rho(\mathbf{r})$. By a calculation similar to that above we easily obtain :

$$\left\{[(\mathbf{r}-\mathbf{R})\ \nabla] + [(\mathbf{r}_0-\mathbf{R})\,\nabla_0] + \left[\boldsymbol{\omega}\frac{\partial}{\partial\boldsymbol{\omega}}\right] + \left[\boldsymbol{\omega}_0\frac{\partial}{\partial\boldsymbol{\omega}_0}\right]\right\} G(\boldsymbol{\omega},\mathbf{r};\boldsymbol{\omega}_0,\mathbf{r}_0) =$$
$$= -\lambda \oint_S\!\int G(\boldsymbol{\omega},\mathbf{r};\boldsymbol{\omega}',\mathbf{r}_s)\,p(\boldsymbol{\omega}'\boldsymbol{\omega}'')\,G(\boldsymbol{\omega}'',\mathbf{r}_s;\boldsymbol{\omega}_0,\mathbf{r}_0)\,d\boldsymbol{\omega}'\,d\boldsymbol{\omega}''\,[(\mathbf{r}_s-\mathbf{R})\,dS]. \qquad (5)$$

Six scalar equations corresponding to the two vector Equations (4) and (5) are the mathematical formulation of the invariance principle. In order to derive these equations it is very essential that the optical properties be homogeneous : otherwise, the variation $\delta\rho$ would be different from zero throughout the space inside S and the integrals could not be transformed into surface integrals.

We apply the derived equations to diffusive reflection of light by a homogeneous medium. This problem reduces to that of obtaining the action function $G(\boldsymbol{\omega},\mathbf{r};\ \boldsymbol{\omega}_0,\mathbf{r}_0)$ subject to the condition that the points $\mathbf{r}$ and $\mathbf{r}_0$ are on the surface S. We denote by ∇' the gradient along the surface S defined by the equation $\nabla' = \nabla - \mathbf{n}(\mathbf{n}\nabla)$, where $\mathbf{n}$ is the exterior normal to S at the point $\mathbf{r}$. Taking into accoun the identity $\nabla \equiv \nabla' - \frac{\mathbf{n}}{\boldsymbol{\omega}\mathbf{n}}(\boldsymbol{\omega}\nabla') + \frac{\mathbf{n}}{\boldsymbol{\omega}\mathbf{n}}(\boldsymbol{\omega}\nabla)$ and using Equation (1) and its adjoint [3] Equations (4) and (5) can easily be transformed into

$$\left\{\nabla' - \frac{\mathbf{n}}{\boldsymbol{\omega}\mathbf{n}}(\boldsymbol{\omega}\nabla') - \frac{\mathbf{n}}{\boldsymbol{\omega}\mathbf{n}} + \nabla_0' - \frac{\mathbf{n}_0}{\boldsymbol{\omega}_0\mathbf{n}_0}(\boldsymbol{\omega}_0\nabla_0') + \frac{\mathbf{n}_0}{\boldsymbol{\omega}_0\mathbf{n}_0}\right\} G(\boldsymbol{\omega},\mathbf{r};\boldsymbol{\omega}_0,\mathbf{r}_0) =$$
$$= -\frac{\mathbf{n}}{\boldsymbol{\omega}\mathbf{n}}\lambda\int p(\boldsymbol{\omega}\boldsymbol{\omega}')\,G(\boldsymbol{\omega}',\mathbf{r};\boldsymbol{\omega}_0,\mathbf{r}_0)\,d\boldsymbol{\omega}' +$$
$$+ \frac{\mathbf{n}_0}{\boldsymbol{\omega}_0\mathbf{n}_0}\lambda\int G(\boldsymbol{\omega},\mathbf{r};\boldsymbol{\omega}',\mathbf{r}_0)\,p(\boldsymbol{\omega}'\boldsymbol{\omega}_0)\,d\boldsymbol{\omega}' -$$
$$-\lambda\oint_S G(\boldsymbol{\omega},\mathbf{r};\boldsymbol{\omega}',\mathbf{r}_s)\,p(\boldsymbol{\omega}'\boldsymbol{\omega}'')\,G(\boldsymbol{\omega}'',\mathbf{r}_s;\boldsymbol{\omega}_0,\mathbf{r}_0)\,d\boldsymbol{\omega}'\,d\boldsymbol{\omega}''\,dS; \qquad (6)$$

$$\left\{\left[(\mathbf{r}-\mathbf{R})\left(\nabla' - \frac{\mathbf{n}}{\boldsymbol{\omega}\mathbf{n}}(\boldsymbol{\omega}\nabla') - \frac{\mathbf{n}}{\boldsymbol{\omega}\mathbf{n}}\right)\right] +\right.$$
$$+\left[(\mathbf{r}_0-\mathbf{R})\Big(\nabla_0' - \frac{\mathbf{n}_0}{\boldsymbol{\omega}_0\mathbf{n}_0}(\boldsymbol{\omega}_0\nabla_0') + \frac{\mathbf{n}_0}{\boldsymbol{\omega}_0\mathbf{n}_0}\right] +$$
$$\left. + \left[\boldsymbol{\omega}\frac{\partial}{\partial\boldsymbol{\omega}}\right] + \left[\boldsymbol{\omega}_0\frac{\partial}{\partial\boldsymbol{\omega}_0}\right]\right\} G(\boldsymbol{\omega},\mathbf{r};\boldsymbol{\omega}_0,\mathbf{r}_0) =$$
$$= -\frac{[(\mathbf{r}-\mathbf{R})\,\mathbf{n}]}{\boldsymbol{\omega}\mathbf{n}}\lambda\int p(\boldsymbol{\omega}\boldsymbol{\omega}')\,G(\boldsymbol{\omega}',\mathbf{r};\boldsymbol{\omega}_0,\mathbf{r}_0)\,d\boldsymbol{\omega}' +$$
$$+ \frac{[(\mathbf{r}_0-\mathbf{R})\,\mathbf{n}_0]}{\boldsymbol{\omega}_0\mathbf{n}_0}\lambda\int G(\boldsymbol{\omega},\mathbf{r};\boldsymbol{\omega}',\mathbf{r}_0)\,p(\boldsymbol{\omega}'\boldsymbol{\omega}_0)\,d\boldsymbol{\omega}' -$$
$$-\lambda\oint_S\!\int G(\boldsymbol{\omega},\mathbf{r};\boldsymbol{\omega}',\mathbf{r}_s)\,p(\boldsymbol{\omega}'\boldsymbol{\omega}'')\,G(\boldsymbol{\omega}'',\mathbf{r}_s;\boldsymbol{\omega}_0,\mathbf{r}_0)\,d\boldsymbol{\omega}'\,d\boldsymbol{\omega}''\,[(\mathbf{r}_s-\mathbf{R})\,dS]. \qquad (7)$$

These equations contain no dependence on interior points because $\mathbf{r}$ and $\mathbf{r}_0$ lie on the surface and all derivatives are taken along the surface. Thus in this case, as in the one-dimensional case, the invariance principle leads to a closed set of equations. These equations are in general, only the necessary conditions which must be obeyed by the Green's function for a homogeneous medium. Whether these equations are sufficient for a solution, in other words, the question of the uniqueness of the solution, requires further study.

In the practical use of the derived equations the δ-singularity must first be removed from G, which is caused by light quanta that are not scattered. We do not here remove this singularity in order to avoid complicating the equations.

2. When the scattering is isotropic, i. e., $p(\cos\theta) = \frac{1}{4\pi}$, then from (4) - (7) we can derive simpler equations. For example, we integrate (4) and (5) over $\boldsymbol{\omega}_0$ and express ∇ again in terms of the gradient along the surface.

Introducing the Green's function G_0 with the isotropic source $G_0(\boldsymbol{\omega}, \mathbf{r} : \mathbf{r}_0) = \frac{1}{4\pi}\int G(\omega, \mathbf{r}; \omega_0, \mathbf{r}_0)\, d\omega_0$, we obtain the following equations:

$$\left\{\nabla' - \frac{\mathbf{n}}{\boldsymbol{\omega}\mathbf{n}}(\boldsymbol{\omega}\nabla') - \frac{\mathbf{n}}{\boldsymbol{\omega}\mathbf{n}} + \nabla_0\right\} G_0(\boldsymbol{\omega}, \mathbf{r}; \mathbf{r}_0) =$$

$$= -\frac{\mathbf{n}}{\boldsymbol{\omega}\mathbf{n}}\,\frac{\lambda}{4\pi}\int G_0\,(\boldsymbol{\omega}', \mathbf{r}; \mathbf{r}_0)\, d\boldsymbol{\omega}' - \lambda \oint_S G_0(\boldsymbol{\omega}, \mathbf{r}; \mathbf{r}_s) \int G_0(\boldsymbol{\omega}', \mathbf{r}_s; \mathbf{r}_0)\, d\boldsymbol{\omega}' dS \tag{8}$$

$$\left\{\left[(\mathbf{r} - \mathbf{R})\left(\nabla' - \frac{\mathbf{n}}{\boldsymbol{\omega}\mathbf{n}}(\boldsymbol{\omega}\nabla') - \frac{\mathbf{n}}{(\boldsymbol{\omega}\mathbf{n})}\right)\right] + [(\mathbf{r}_0 - \mathbf{R})\,\nabla_0] + \left[\boldsymbol{\omega}\frac{\partial}{\partial\boldsymbol{\omega}}\right]\right\} G_0(\boldsymbol{\omega}, \mathbf{r}; \mathbf{r}_0) =$$

$$= -\frac{[(\mathbf{r} - \mathbf{R})\,\mathbf{n}]}{\boldsymbol{\omega}\mathbf{n}}\frac{\lambda}{4\pi}\int G_0(\boldsymbol{\omega}', \mathbf{r}; \mathbf{r}_0)\, d\boldsymbol{\omega}' -$$

$$-\lambda \oint_S G_0(\boldsymbol{\omega}', \mathbf{r}; \mathbf{r}_s) \int G_0(\boldsymbol{\omega}', \mathbf{r}_s; \mathbf{r}_0)\, d\boldsymbol{\omega}'\, [(\mathbf{r}_s - \mathbf{R})\, d\mathbf{S}]. \tag{9}$$

It is easily seen that in the one-dimensional plane case Equation (8) coincides with Equation (23) of [4] for the probability $p(\mu, x)$ that a quantum absorbed at the depth $\underline{x}$ will leave the medium at the angle arc cos μ, since this probability differs from G_0 only by a constant factor. Therefore (8) and (9) can be regarded as the extension of V. V. Sobolev's method to a medium of arbitrary shape. We thus see that these equations are a simple result of the invariance principle.

When (4) and (5) are integrated with respect to $\boldsymbol{\omega}$ and $\boldsymbol{\omega}_0$ still simpler equations can be obtained:

$$(\nabla + \nabla_0)\, I(\mathbf{r}, \mathbf{r}_0) = -\lambda \oint_S I(\mathbf{r}, \mathbf{r}_s)\, I(\mathbf{r}_s, \mathbf{r}_0)\, d\mathbf{S}, \tag{10}$$

$$\{[(\mathbf{r} - \mathbf{R})\,\nabla] + [(\mathbf{r}_0' - \mathbf{R})\,\nabla_0]\}\, I(\mathbf{r}, \mathbf{r}_0) = -\lambda \oint_S I(\mathbf{r}, \mathbf{r}_s)\, I(\mathbf{r}_s, \mathbf{r}_0)\, [(\mathbf{r}_s - \mathbf{R})\, d\mathbf{S}], \tag{11}$$

where $I(\mathbf{r}, \mathbf{r}_0)$ is defined by $I(\mathbf{r}, \mathbf{r}_0) = \frac{1}{4\pi}\int G(\boldsymbol{\omega}, \mathbf{r}; \boldsymbol{\omega}_0, \mathbf{r}_0)\, d\boldsymbol{\omega} d\boldsymbol{\omega}_0$ and represents the radiation density at the point $\mathbf{r}$ resulting from the presence of an isotropic point source at the point $\mathbf{r}_0$.

Equations (10) and (11) are also only the necessary conditions which must be obeyed by $I(\mathbf{r}, \mathbf{r}_0)$; therefore, we cannot depend on them to lead us to the complete solution. Nevertheless, in some instances they can be useful.

For example, for an isotropic plane source in a semi-infinite medium, Equation (10) subject to the symmetry condition $I(x, x_0) = I(x_0, x)$ can be transformed into

$$I(x, x_0) = I_0(|x - x_0|) + \frac{\lambda}{2}\int_{|x - x_0|}^{x} I(x', 0)\, I(x' - x + x_0, 0)\, dx' +$$

$$+ \frac{\lambda}{2}\int_{|x - x_0|}^{x_0} I(x', 0)\, I(x' - x_0 + x, 0)\, dx', \tag{12}$$

where $I(x, x_0)$ denotes the radiation density from the plane source, the distances $\underline{x}$ and x_0 are taken from the boundary of the medium and I_0 is an arbitrary function. But from the form of (12) it follows that I_0 is a solution for a plane source in an infinite medium. If I_0 is assumed to be known [5, 6] then (12) enables us to determine $I(x, x_0)$.

I am grateful to Professor D. I. Blokhintsev for discussions.

Received November 26, 1956

LITERATURE CITED

[1] V. A. Ambartsumian et al., Theoretical Astrophysics (1952).

[2] S. Chandrasekar, The Transfer of Radiant Energy (Foreign Lit. Press, 1953) (Russian Translation).

[3] B. B. Kadomtsev, Doklady Akad. Nauk SSSR 113, 541 (1957).

[4] V. V. Sobolev, Astron. Zhur. 28, 355 (1951).

[5] W. Bothe, Z. Physik 122, 648 (1944).

[6] R. Marshak, H. Brooks and H. Hurwitz, Nucleonics 4, 10 (1949).

DEPOLARIZATION AND INTENSITIES IN THE RAMAN SPECTRA OF BENZENE AND HEXADEUTEROBENZENE

M. A. Kovner and B. N. Snegirev

(Presented by Academician G. S. Landsberg November 27, 1956)

In the present article we use the method of calculating depolarization and intensities which was developed in [1] and given in detail in [2]. The method is being applied to unsaturated compounds for the first time.

1. Fully Symmetrical Vibrations (A_{1g})

The CH bonds in benzene are formed by carbon atoms with trigonal hybridization and cannot possess cylindrical symmetry; it can be assumed that $\alpha_{q1} \neq \alpha_{q2} \neq \alpha_{q3}$ and $\alpha'_{q1} \neq \alpha'_{q2} \neq \alpha'_{q3}$. The derivatives of the polarization tensor of the molecule with respect to the normal coordinates K_i are:

$$\frac{\partial a_{\xi\xi}}{\partial K_i} = \frac{\partial a_{\eta\eta}}{\partial K_i} = \frac{3}{\sqrt{6}} N_i \left[C_{1i}(\alpha'_{Q1} + \alpha'_{Q2}) + C_{2i}(\alpha'_{q1} + \alpha'_{q2})\right];$$

$$\frac{\partial a_{\xi\xi}}{\partial K_i} = \sqrt{6} N_i (C_{1i}\alpha'_{Q3} + C_{2i}\alpha'_{q3}) \quad (i = 1, 2, 3, 4). \tag{1}$$

The coefficients C_{1i} and C_{2i} and the normalization factors N_i are known from the solution of the mechanical problem [3]:

$$\begin{aligned} C_6H_6&: \nu_1 = 992 \text{ cm}^{-1}; \; N_1^2 = 0.083; \; C_{11} = 1; \; C_{21} = 0.037; \\ &\nu_2 = 3062 \text{ cm}^{-1}; \; N_2^2 = 1.091; \; C_{12} = -0.085; \; C_{22} = 1; \\ C_6D_6&: \nu_3 = 945 \text{ cm}^{-1}; \; N_3^2 = 0.074; \; C_{13} = 1 \; C_{23} = 0.151; \\ &\nu_4 = 2292 \text{ cm}^{-1}; \; N_4^2 = 0.601; \; C_{14} = -0.168; \; C_{24} = 1. \end{aligned} \tag{2}$$

Introducing the notation:

$$\begin{aligned} &\alpha'_{Q1} + \alpha'_{Q2} + \alpha'_{Q3} = v; \; \alpha'_{Q1} + \alpha'_{Q2} - 2\alpha'_{Q3} = u; \\ &\alpha'_{q1} + \alpha'_{q2} + \alpha'_{q3} = d; \; \alpha'_{q1} + \alpha'_{q2} - 2\alpha'_{q3} = c, \end{aligned} \tag{3}$$

we represent the squares of the traces $b_i'^2$ and of the anisotropy $g_i'^2$ of the tensor polarization derivatives as follows:

$$\begin{aligned} b_i'^2 &= 6N_i^2 (C_{1i} v + C_{2i} d)^2, \\ g_i'^2 &= \frac{3}{2} N_i^2 (C_{1i} u + C_{2i} c)^2. \end{aligned} \tag{4}$$

Reference [4] gives the experimental values of the quantities

$$S_i = \frac{5b_i'^2 + 7g_i'^2}{(5b'^2 + 7g'^2)_{458}}, \tag{5}$$

where the denominator refers to the 458 cm^{-1} line of CCl_4 and its numerical value is not indicated in [4]. Therefore, only the ratios u: v: d: c are determined on the basis of the experimental values of

$$\rho_i = \frac{6g_i'^2}{5b_i'^2 + 7g_i'^2} \quad (i = 1, 2, 3, 4) \tag{6}$$

and the ratios S_1/S_2, S_3/S_2, S_4/S_2, for example. Inserting (2) in (4), (5) and (6) and assuming, in accordance with [4], $\rho_1 = 0.11$; $\rho_2 = 0.21$; $S_1/S_2 = 0.267$, we obtain

$$d = 1.090c;\ u = 1.180c;\ v = 1.837c, \tag{7}$$

while in paraffins [1] d = 1.95 c. The signs in the solutions of the equations are chosen so that u, v, c, d will have the same sign, since all of the quantities are positive according to their physical meaning. Insertion of (7) into (4), (5) and (6) enables us to obtain ρ_3, ρ_4 and S_3/S_2, S_4/S_2 (see Table 1).

TABLE 1

	Observed[1]	Calc.
ρ_3	0.11	0.11
ρ_4	0.21	0.23
S_3/S_2	0.24	0.27
S_4/S_2	0.47	0.40

The values in (2) differ a little from those obtained in reference [3]. They are improved so that the quantities in (4) exactly satisfy the sum rule [5].

2. Degenerate Nonplanar Vibrations (E_g^-)

A calculation of the projection of the angular momentum M in Jacobian coordinates [1] leads to the equations:

$$M_\xi = \sqrt{3}\,[m_{H(D)}(a + b)^2 \dot{\varphi}_{H(D)} + m_C a^2 \dot{\varphi}_C]; \quad \cancel{M}_\xi = 0; \tag{8}$$

$$\varphi_{H(D)} = \frac{1}{\sqrt{3}}\left(-\varphi_1 - \frac{\varphi_2}{2} + \frac{\varphi_3}{2} + \varphi_4 + \frac{\varphi_5}{2} - \frac{\varphi_6}{2}\right); \tag{9}$$

$$\varphi_C = \frac{1}{\sqrt{3}}\left(-\varphi_7 - \frac{\varphi_8}{2} + \frac{\varphi_9}{2} + \varphi_{10} + \frac{\varphi_{11}}{2} - \frac{\varphi_{12}}{2}\right), \tag{10}$$

where a, b are the CC and CH(D) bond lengths; a = 1.39 A; b = 1.08 A; $\varphi_1 \ldots, \varphi_6$; $\varphi_7, \ldots, \varphi_{12}$ are angles which characterize the departure of H and C atoms from the plane of the ring. From the geometric picture of nonplanar vibrations [1] it follows that

$$\varphi_{H(D)} = \frac{b}{a+b}\Phi_{H(D)} + \frac{a}{a+b}\Phi_C; \quad \varphi_C = \Phi_C; \tag{11}$$

$$\Phi_{H(D)} = \frac{1}{\sqrt{3}}\left(-\Phi_1 - \frac{\Phi_2}{2} + \frac{\Phi_3}{2} + \Phi_4 + \frac{\Phi_5}{2} - \frac{\Phi_6}{2}\right), \tag{12}$$

$$\Phi_C = \frac{1}{\sqrt{3}}\left(-\frac{\Phi_7}{2} - \Phi_8 - \frac{\Phi_9}{2} + \frac{\Phi_{10}}{2} + \Phi_{11} - \frac{\Phi_{12}}{2}\right), \tag{13}$$

where $\Phi_1, \ldots, \Phi_6$; $\Phi_7, \ldots, \Phi_{12}$ are angles which characterize the departure of the CH(D) and CC bonds from the plane of the ring. The symmetry coordinate of the nonplanar vibrations is

$$\rho = \rho_{E_g^- \mathrm{II}} = \frac{1}{\sqrt{3}}\left(-\rho_1 - \frac{\rho_2}{2} + \frac{\rho_3}{2} + \rho_4 + \frac{\rho_5}{2} - \frac{\rho_6}{2}\right) = \Phi_{\mathrm{H}} - \Phi_{\mathrm{C}}, \qquad (14)$$

where ρ_i are the natural vibrational coordinates. Assuming $\rho = NK$, $\varphi_H = E_1K$, $\varphi_C = E_2K$, where K is the normal coordinate, and using (8)-(14) we obtain:

$$E_{1\mathrm{H(D)}} = \frac{b}{a+b} N_{\mathrm{H(D)}} \frac{I_{\mathrm{C}}}{I_{\mathrm{C}} + I_{\mathrm{H(D)}}}, \quad E_{2\mathrm{H(D)}} = -\frac{b}{a+b} N_{\mathrm{H(D)}} \frac{I_{\mathrm{H(D)}}}{I_{\mathrm{C}} + I_{\mathrm{H(D)}}}; \qquad (15)$$

$$I_{\mathrm{C}} = 3m_{\mathrm{C}}a^2; \quad I_{\mathrm{H(D)}} = 3m_{\mathrm{H(D)}}(a+b)^2. \qquad (16)$$

Here N_H and N_D are the normalizing factors for C_6H_6 and C_6D_6.

The derivative of the polarization tensor with respect to the normal coordinate is

$$\left(\frac{\partial a_{\eta\zeta}}{\partial K}\right)_{\mathrm{H(D)}} = \frac{\partial a_{\eta\zeta}}{\partial \varphi_{\mathrm{H(D)}}} E_{1\mathrm{H(D)}} + \frac{\partial a_{\eta\zeta}}{\partial \varphi_{\mathrm{C}}} E_{2\mathrm{H(D)}} = g'_{\mathrm{H(D)}}. \qquad (17)$$

From the theory of Vol'kenshtein and El'iashevich we can obtain [1]

$$\frac{\partial a_{\eta\zeta}}{\partial \Phi_{\mathrm{H(D)}}} = \sqrt{3}x; \quad \frac{\partial a_{\eta\zeta}}{\partial \Phi_{\mathrm{C}}} = \sqrt{3}y, \qquad (18)$$

where

$$x = \alpha_{q1} + \alpha_{q2} - 2\alpha_{q3}; \quad y = \alpha_{Q1} + \alpha_{Q2} - 2\alpha_{Q3}. \qquad (19)$$

The anisotropy of the polarization tensor of the molecule [7] is

$$g = 3(x+y) = 5.96\ \mathrm{A}^3. \qquad (20)$$

Substitution of (11), (15), (18) and (19) into (17) gives

$$g'_{\mathrm{H(D)}} = N_{\mathrm{H(D)}} z_{\mathrm{H(D)}}; \quad z_{\mathrm{H(D)}} = \sqrt{3}x - \frac{b}{a+b} \frac{g}{\sqrt{3}} \frac{I_{\mathrm{H(D)}}}{I_{\mathrm{C}} + I_{\mathrm{H(D)}}}. \qquad (21)$$

The theoretical ratio of the intensities J of the lines E_g^- C_6D_6 and C_6H_6 is

$$\tau = \frac{J_{\mathrm{D}}}{J_{\mathrm{H}}} = \frac{\nu_{\mathrm{D}}}{\nu_{\mathrm{H}}} \frac{z_{\mathrm{D}}^2}{z_{\mathrm{H}}^2} \frac{1 - \exp(-h\nu_{\mathrm{H}}/kT)}{1 - \exp(-h\nu_{\mathrm{D}}/kT)} \left(\frac{\nu_0 - \nu_{\mathrm{D}}}{\nu_0 - \nu_{\mathrm{H}}}\right)^4,$$

where ν_0 is the frequency of the unshifted line, $\nu_D = 661\ \text{cm}^{-1}$ and $\nu_H = 849\ \text{cm}^{-1}$. Formula (22) was obtained by using relations

$$\frac{\nu_H}{\nu_D} = \sqrt{\frac{\mu_D}{\mu_H}} = \frac{N_H}{N_D} = \sqrt{\frac{A_H}{A_D}}, \tag{23}$$

where A_H, A_D are the kinematical coefficients of C_6H_6 and C_6D_6 and the μ are the reduced moments of inertia:

$$\mu_{H(D)} = \frac{I_{H(D)} I_C}{I_C + I_{H(D)}}. \tag{24}$$

Equation (22) agrees with Equation (10) of reference [6] if we set $(1-\delta)^2 = z_D^2/z_H^2$. From (21) it follows that

$$\delta = \frac{1}{\sqrt{3}} \frac{b}{a+b} \frac{g\mu_H}{(I_C + I_D) z_H}. \tag{25}$$

The sign of δ depdends on the sign of z_H. The equation for δ in the reference mentioned is easily transformed into (25). Inserting (20), (23), (24) into (21) and assuming, in accordance with [4], that $g'^2_D/g'^2_H = 0.204/0.105$, we find that

$$x = 0.22\ \text{A}^3, \quad y = 1.76\ \text{A}^3. \tag{26}$$

In paraffins [1] $x = 0.21\ \text{A}^3$ and the values in (26) can be considered reasonable. The value of y includes the increased polarizability of π-electrons, so that $y \gg x$. By also inserting (20) and (26) into (21) and (21) into (25) we find that $\delta = +2.79$ instead of the value -0.676 in [6]. Thus the ratio of the intensity of the unshifted line J_0 to J_H which was used in [6] is in need of correction. We note that for $\nu_0 = 22938\ \text{cm}^{-1}$, $T = 300°\text{K}$ [4] and by inserting (20), (26) and (21) into (22) we obtain $\tau = 2.66$. The true value of J_D/J_H can be considerably different from τ, as is seen from Equation (1) of reference [4].

3. Degenerate Plane Vibrations (E_g^+)

A simple calculation gives the valence part of each component of the tensor of the polarization derivatives with respect to the normal coordinates. In order to calculate the deformation part we use Equation (25) of reference [2]. Although the latter was derived for bonds with axial symmetry it can be applied to the E_g^+ vibrations of benzene because in these vibrations the angles formed by the perpendiculars to the bonds and the plane of the molecule with the coordinate axes do not change and the tensors are independent of α_{Q_3}, α_{q_3} [1].

The tensors are

$$E_g^{+\text{I}}: \begin{pmatrix} T_l & 0 & 0 \\ 0 & -T_l & 0 \\ 0 & 0 & 0 \end{pmatrix}, \quad E_g^{+\text{II}}: \begin{pmatrix} 0 & T_l & 0 \\ -T_l & 0 & 0 \\ 0 & 0 & 0 \end{pmatrix}. \tag{27}$$

Here

$$T_l = N_l \left\{ \frac{\sqrt{3}}{2} \left[(\alpha'_{Q2} - \alpha'_{Q1}) C_{Ql} + (\alpha'_{q2} - \alpha'_{q1}) C_{ql} \right] + \right.$$
$$\left. + \left(\alpha_{Q1} - \alpha_{Q2} - \frac{\alpha_{q1}}{2} + \frac{\alpha_{q2}}{2} \right) C_{\gamma l} - \sqrt{\frac{3}{2}} (\alpha_{q1} - \alpha_{q2}) C_{\beta_b l} \right\}, \qquad (28)$$

where l is the frequency number of E_g^+ and the C's are the coefficients which define the form of the vibrations in the symmetry coordinates of E_g^+: Q, q, γ, β_b [3].

Similarly to the case for A_{1g} from the experimental values in [4] we can obtain the ratio of the electron optical parameters in (28). But such a calculation is not entirely justfied since for the frequency 1600 cm^{-1} of benzene Fermi resonance splitting occurs and the influence of the latter on the intensity is not reflected in the theory under consideration.

After the present work had been concluded we learned of article [8] concerning the same problem. In this article $\underline{x}$ and $\underline{y}$ are not determined, but by comparing the equations of the article with (21) it follows that $\underline{x} = \frac{b}{\sqrt{3}} \frac{\partial \alpha_{x^* z^*}}{\partial S_{10}} = 0.03$ A. It is obvious that (26) is closer to the true value.

In conclusion the authors wish to express their sincere thanks to Academician G. S. Landsberg for his interest and valuable suggestions.

N. G. Chernyshevskii Saratov State University

Received November 14, 1956

LITERATURE CITED

[1] M. V. Vol'kenshtein, M. A. El'iashevich and B. I. Stepanov, Molecular Vibrations (Foreign Lit. Press, 1949).

[2] S. M. Ferigle and A. Weber, Can. J. Phys. 32, 799 (1954).

[3] M. A. Kovner, J. Exptl.-Theoret. Phys. (U.S.S.R.) 26, 598 (1954).

[4] G. Allen and H. J. Bernstein, Can. J. Phys. 33, 1137 (1955).

[5] B. Crawford, J. Chem. Phys. 20, 977 (1952).

[6] R. C. Lord and E. Teller, J. Chem. Soc. 1937, 1728.

[7] M. V. Vol'kenshtein, Molecular Optics (1951) p. 431.

[8] D. H. Whiffen, Proc. Phys. Soc. (London) 69, 437A, 375 (1956).

A UNIVERSAL RELATION BETWEEN THE ABSORPTION AND LUMINESCENCE SPECTRA OF COMPLEX MOLECULES

Academician B. I. Stepanov of the Byelorussian Academy of Sciences

Hundreds of articles have been devoted to a comparison of absorption and luminescence spectra. Especially significant for the theory of luminescence was the discovery of mirror symmetry of the absorption and emission spectra [1-6]. In the present article it is shown that the absorption and luminescence spectra of many complex systems are connected by a universal relation which enables us to calculate the shape of the luminescence spectrum from knowledge of the shape of the long-wave absorption band and vice versa.

Let us consider, for example, the luminescence of some dye solution. Numerous experiments have shown that between the act of light absorption and the act of luminescence there takes place a process of redistribution of vibrational energy over the various vibrational degrees of freedom of the excited molecule, as well as energy exchange between the excited molecule and molecules of the solvent. This process is extremely rapid so that within a time of the order of 10^{-10} - 10^{-12} sec, which is considerably less than the duration of the excited electronic state, an equilibrium distribution is established for the vibrational energy over the degrees of freedom and vibrational levels of the excited molecule. The form of this distribution is given completely by the temperature of the solvent. A criterion of the actual establishment of an equilibrium distribution in any specific system is provided especially by the fact that the quantum yield and spectrum are independent of the frequency exciting light (in Stokes line excitation).

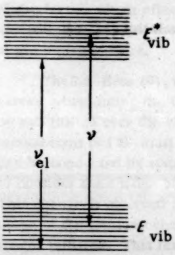

Fig. 1.

The frequency dependence of the luminescent power of complex molecules was defined in general form by the equation [7]:

$$W_\nu^{lum} = h\nu \cdot n^* \int \rho^*(E^*_{vib})\, A(E^*_{vib}\ \nu)\, dE^*_{vib} \tag{1}$$

Here n^* is the total number of molecules in an excited electronic state, $A(E^*_{vib}, \nu)$ is the probability of a spontaneous transition from vibrational level E^*_{vib} to vibration level E_{vib} of a lower electronic state. The values of E^*_{vib}, E_{vib} and the emission frequency ν are related by (Fig. 1):

$$E^*_{vib} + h\nu_{el} = E_{vib} + h\nu. \tag{2}$$

The distribution function over the vibrational levels is defined by the usual expression

$$\rho^*(E^*_{vib}) = C^* g^*(E^*_{vib})\, e^{-E^*_{vib}/kT}, \tag{3}$$

where $g^*(E^*_{\text{vib}})$ is the statistical weight of the level E^*_{vib} and T is the temperature of the surrounding medium. Equations (1) and (2) are always valid but Equation (3) is valid only when thermal equilibrium is established between the excited molecules and the surrounding medium.

The absorbed power for frequency ν

$$W_\nu^{\text{abs}} = h\nu \cdot n \int \rho(E_{\text{vib}})\, B(E_{\text{vib}}, \nu)\, u_\nu\, dE_{\text{vib}} + \\ + h\nu \cdot n \int \rho(E_{\text{vib}})\, B'(E_{\text{vib}}, \nu)\, u_\nu\, dE_{\text{vib}} \tag{4}$$

generally has two components. The first determines the absorption associated with a molecular transition to an excited electronic state; the second is the absorption associated with transitions between the vibrational levels of the normal electronic state (nonexciting absorption). The second term is usually small and began to be taken into account only in connection with the problem of anti-Stokes fluorescence [7, 8]. In (4) n is the total number of molecules, $\rho(E_{\text{vib}}) = Cg(E_{\text{vib}})\, e^{-E_{\text{vib}}/kT}$ is the distribution function over the vibrational levels of the lower electronic state, $g(E_{\text{vib}})$ is the statistical weight of the level E_{vib}, u_ν is the density of incident radiation, $B(E_{\text{vib}}, \nu)\, u_\nu$ and $B'(E_{\text{vib}}, \nu')\, u_\nu$ are the probabilities of transitions with and without excitation of the higher electronic state.

When we neglect the second term of (4) and take into account Equation (2) and the relation between the Einstein coefficients

$$\frac{A(E^*_{\text{vib}}, \nu)}{B(E_{\text{vib}}, \nu)} = \frac{g(E_{\text{vib}})}{g^*(E^*_{\text{vib}})} \frac{8\pi h\nu^3}{c^3}, \tag{5}$$

we obtain

$$\frac{W_\nu^{\text{lum}}}{W_\nu^{\text{abs}}/u_\nu} = \frac{n^* \int\limits_{h\nu - h\nu_{\text{el}}}^{\infty} C^* g^*(E^*_{\text{vib}})\, e^{-E^*_{\text{vib}}/kT} A(E^*_{\text{vib}}, \nu)\, dE^*_{\text{vib}}}{n \int\limits_0^{\infty} Cg(E_{\text{vib}})\, e^{-E_{\text{vib}}/kT} B(E_{\text{vib}}, \nu)\, dE} = \\ = \frac{n^* C^* e^{h\nu_{\text{el}}/kT}}{nC} \frac{8\pi h\nu^3}{c^3} e^{-h\nu/kT} = D \frac{8\pi h\nu^3}{c^3} e^{-h\nu/kT}. \tag{6}$$

The limits of integration in (6) correspond to $\nu > \nu_{\text{el}}$. When $\nu < \nu_{\text{el}}$ the intergral in the numerator must be taken from $E^*_{\text{vib}} = 0$ to $E^*_{\text{vib}} = \infty$, and the denominator intergral from $E_{\text{vib}} = h\nu_{\text{el}}$ to $E_{\text{vib}} = \infty$.

Since W_ν^{abs}/u_ν is proportional to the absorption coefficient κ_ν we have

$$\frac{W_\nu^{\text{lum}}}{\kappa_\nu} = D(T) \frac{8\pi h\nu^3}{c^2} e^{-h\nu/kT} = d(T)\, \nu^3 e^{-h\nu/kT}. \tag{7}$$

It is appropriate to compare (6) with Kirchhoff's law for the thermal emission of the same system. Neglecting the induced emission, i. e., for $h\nu \gg kT$, Kirchhoff's law is

$$\frac{W_\nu^{\text{therm. emis}}}{W_\nu^{\text{abs}}/u_\nu} = \frac{8\pi h\nu^3}{c^3} e^{-h\nu/kT}. \tag{8}$$

The denominators of the left-hand sides of (6) and (8) contain the same quantity $\frac{W_\nu^{\text{abs}}}{u_\nu}$, which is the absorptive ability of the investigated system at temperature T. Thus

$$W_\nu^{\text{lum}} = D(T)\, W_\nu^{\text{therm. emis.}} \tag{9}$$

and thus the luminescent power (at frequency ν) is proportional to the thermal emissive power of the system. The proportionality factor D (T) for a given molecule depends only on the temperature and on the conditions for luminescence excitation (on n^*) but is independent of ν. At a given temperature the shape of the luminescence band coincides with the shape of the thermal emission band. Thus according to (6) - (9) from experimental knowledge of the shape of the absorption band it is easy to obtain the shape of the luminescence band. This can enable us to investigate the observation of the laws of mirror symmetry, to determine the frequency of a pure electronic transition without measuring the luminescence spectrum, and to obtain a better understanding of the factors which effect the formation of absorption and emission bands. In some instances it is difficult to measure the shape of the absorption band. In such cases it can be found by a careful measurement of the shape of the emission band.

The Relations (6), (7) and (9) are universal to a very high degree. They can be violated in only two cases: when during the time that the molecules are in an excited electronic state thermal equilibrium cannot be established over the vibrational sublevels of the excited state, or when unexcited absorption is large and the second term of (4) must be taken into account. A study of these two factors is of considerable interest and can be conducted by systematically investigating the violation of (6), (7) and (9). Here it is only necessary to consider the change of the luminescence band shape in the transition from Stokes to anti-Stokes excitation. This change is observed not only in vapors [9] but also in solutions [10]. When under Stokes excitation the shape of the luminescence band corresponds to (6), then in the transition to anti-Stokes excitation (6) is no longer fulfilled. This result shows unambiguously that in the anti-Stokes excitation of complex molecules equilibrium distribution of the excited molecules cannot be established (see [7]).

The Relations (6), (7) and (9) cannot be verified from existing experimental data, which are usually confined to measurements of W_ν^{lum} and W_ν^{abs} near the center of the band and do not include careful measurements at the band edge where W_ν^{lum} and W_ν^{abs} are quite small. In addition, before comparing with theory it is necessary to account for reabsorption and secondary luminescence.

Equations (6), (7) and (9) are strictly applicable only to a condensed phase. In the vapors of complex molecules they can be satisfied only approximately because there is no exchange of vibrational energy with the medium and an equilibrium distribution of the excited molecules over the vibrational energy levels is not established.

V. I. Lenin Byelorussian State University

Received June 4, 1956

LITERATURE CITED

[1] V. L. Levshin, Photoluminescence of Liquids and Solids (1951)

[2] V. L. Levshin, J. Phys. Chem. (U.S.S.R.) 2, 641 (1931); 6, 1 (1935); 9, 1 (1937).

[3] B. S. Neporent and B. I. Stepanov, Progr. Phys. Sci. (USSR) 43, 380 (1951).

[4] B. S. Neporent, J. Exptl.-Theoret. Phys. (U.S.S.R.) 21, 172 (1951).

[5] B. S. Neporent, V. V. Zelinskii and V. P. Klochkov, Doklady Akad. Nauk SSSR 92, 927 (1953).

[6] B. P. Klochkov, J. Phys. Chem. (U.S.S.R.) 29, 1432 (1955).

[7] B. I. Stepanov, Luminescence of Complex Molecules (Acad. Sci. Byelorussian SSR Press, 1955).

[8] B. I. Stepanov, Progr. Phys. Sci. USSR 108, 3(1956).

[9] B. S. Neporent and N. A. Borisevich, Doklady Akad. Nauk SSSR 94, 447 (1954).

[10] L. A. Tumerman, Trans. Phys. Inst. Acad. Sci. USSR 1938, No. 4.

TIME CORRELATION IN CLASSICAL STATISTICAL SYSTEMS CONSISTING OF A LARGE NUMBER OF INTERACTING PARTICLES

V. V. Tolmachev

(Presented by Academician N. N. Bogoliubov November 19, 1956)

In some problems of the statistical physics of classical systems consisting of a large number of interacting particles it is necessary to know the correlation function $\Phi_1(t, x_1 | x_0)$, which gives the probability for the transition of a particle of the system in time t into the infinitely small neighborhood dx_1 of the dynamical state x_1 from the dynamical state x_0. For the determination of this function it is entirely reasonable to use the idea of a Markovian process. The equation for $\Phi_1(t, x_1 | x_0)$ which is obtained thus will, of course, be of the Fokker-Planck type. The problem of determining the coefficients which are associated with physical concepts of dynamical friction and diffusion in velocity space can be solved by special methods [1, 2]. But this approach, aside from the fact that it is excessively phenomenological because it avoids the deduction of the Fokker-Planck equation,* fails entirely when the concept of a Markovian process is inapplicable, as in the case of a real gas. In the present article we give the results obtained by a different method using a chain of linked distribution functions [3], which from a single point of view gives both a deduction of the Fokker-Planck equation for $\Phi_1(t, x_1 | x_0)$ for systems with long-range interaction (systems of the plasma type) and the deduction of the equation for systems with short-range interaction (real gases) where the concept of the Fokker-Planck mechanism cannot be applied.

We shall be concerned with a system of N identical classical particles interacting in pairs with the potential $\Phi(|q|)$ within a macroscopic volume V.

We introduce the following chain of correlation functions with single, double, etc., arguments:

$$\Phi_s(t, x_1, \ldots, x_s \mid x_0) = V^{s-1} \frac{\langle \delta(x_1(0) - x_0) \prod\limits_{(1<i\leq s)} \delta(x_i(t) - x_i)\rangle}{\langle \delta(x_1(0) - x_0)\rangle}, \qquad (1)$$

which give the formal probability of finding a complex of s particles of the system at time t in the respective infinitely small neighborhoods $dx_1, \ldots, dx_s$ of the dynamical states $x_1, \ldots, x_s$, when at initial time the particle of this complex with subscript 1 was in the dynamical state x_0. The symbol $\langle \ldots \rangle$ denotes the usual statistical average over the initial states of the system; $x_1(0)$ and $x_i(t)$ are respectively the dynamical state of the first particle of the complex at initial time and the i-th particle of the complex at time t. The factor V^{s-1} was introduced to provide the correct possibility for the limiting transition $N \to \infty$, $V \to \infty$, $V/N = v = \text{const}$. The first of the functions $\Phi_1(t, x_1 | x_0)$ is just the probability for the transition of a particle of the system in time t into the infinitely small neighborhood dx_1 of the dynamical state x_1 when this particle was at first in the dynamical state x_0. In order to obtain the other important correlation function $\Psi_1(t, x_1 | x_0)$ giving the probability of finding a particle of the system at time t in the infinitely small vicinity dx_1 of the dynamical state x_1, when at $t = 0$ some other particle was in the state x_0 (this function is a direct extension of the usual two-particle distribution function and coincides with it at $t = 0$), it is necessary to know the function $\Phi_2(t, x_1, x_2 | x_0)$; the integral of this function over the first argument equals the function Ψ_1:

---

* A deduction is known [4] for a Fokker-Planck equation in the case of a special model of coupled harmonic oscillators.

$$\Psi_1(t, x_1 \mid x_0) = \int \Phi_2(t, x, x_1 \mid x_0)\, dx. \tag{2}$$

By differentiating (1) we easily establish the following chain of equations for the functions $\Phi_s(t, x_1, \ldots, x_s \mid x_0)$:

$$\frac{\partial \Phi_s(t, x_1, \ldots, x_s \mid x_0)}{\partial t} = [H_s;\ \Phi_s(t, x_1, \ldots, x_s \mid x_0)] + \\ + \frac{1}{v} \int \Big[\sum_{(1 \leqslant i \leqslant s)} \Phi(|q_i - q|);\ \Phi_{s+1}(t, x_1, \ldots, x_s, x \mid x_0) \Big]\, dx, \tag{3}$$

where [;] denotes Poisson brackets for the variables $x_1, \ldots, x_s$; H_s is the Hamiltonian of the s-particle complex. The equation chain (3) coincides with the chain of equations for the ordinary distribution functions $F_s(t, x_1, \ldots, x_s)$, given in [3]:

$$\frac{\partial F_s(t, x_1, \ldots, x_s)}{\partial t} = [H_s;\ F_s(t, x_1, \ldots, x_s)] + \\ + \frac{1}{v} \int \Big[\sum_{(1 \leqslant i \leqslant s)} \Phi(|q_i - q|);\ F_{s+1}(t, x_1, \ldots, x_s, x) \Big]\, dx. \tag{4}$$

Unlike (4) the chain (3) must be solved with the following initial conditions:

$$\Phi_s(t, x_1, \ldots, x_s \mid x_0)\big|_{t=0} = \delta(x_1 - x_0)\, \frac{F_s(0, x_1, \ldots, x_s)}{F_1(0, x_1)}, \tag{5}$$

where $F_s(0, x_1, \ldots, x_s)$ gives the initial conditions for the chain (4).

The methods of solving the chain (4) were developed by N. N. Bogoliubov [3]. In our case, because of the intimate relation between the functions $\Phi_s(t, x_1, \ldots, x_s \mid x_0)$ and the ordinary correlation functions $F_s(t, x_1, \ldots, x_s)$ (3) and (4) must be solved simultaneously. In doing this it is possible to use the majority of the ideas of [3].

The solution of (3) and (4) which is valid for times much longer than the mean free time will be sought in a form in which the time enters through functional dependence on the first correlation functions:

$$\Phi_s(t, x_1, \ldots, x_s \mid x_0) = \Phi_s(x_1, \ldots, x_s \mid x_0;\ F_1, \Phi_1), \tag{6}$$

$$F_s(t, x_1, \ldots, x_s) = F_s(x_1, \ldots, x_s;\ F_1) \tag{7}$$

for the correlation functions for s = 2, 3, etc. The very first correlation functions are assumed to satisfy the equations

$$\frac{\partial \Phi_1(t, x_1 \mid x_0)}{\partial t} = B(x_1 \mid x_0;\ F_1, \Phi_1), \tag{8}$$

$$\frac{\partial F_1(t, x_1)}{\partial t} = A(x_1; F_1), \tag{9}$$

where $A(x_1; F_1)$ and $B(x_1 \mid x_0; F_1, \Phi_1)$ are functionals of F_1 and F_1, Φ_1 respectively; these functionals are defined by means of the functionals $F_2(x_1, x_2; F_1)$ and $\Phi_2(x_1, x_2; F_1, \Phi_1)$ in the first equations of chains (3) and (4) respectively. From the following equations of chains (3) and (4) we obtain equations which relate the functionals $F_s(x_1, \ldots, x_s; F_1)$ and $\Phi_s(x_1, \ldots, x_s \mid x_0; F_1, \Phi_1)$ with the following functionals $F_{s+1}(x_1, \ldots, x_{s+1}; F_1)$ and $\Phi_{s+1}(x_1, \ldots, x_{s+1} \mid x_0; F_1, \Phi_1)$ respectively $(s \geq 2)$.

In order to produce a unique solution of the problem it is necessary to impose on the functionals $F_s(x_1, \ldots, x_s; F_1)$ and $\Phi_s(x_1, \ldots, x_s \mid x_0; F_1, \Phi_1)$ the following supplementary conditions, which mean physically a weakening of correlation:

$$S_{-t}^{(s)}\Big\{F_s(x_1, \ldots, x_s; S_t^{(1)}F_1) - \prod_{(1 \leqslant i \leqslant s)} S_t^{(1)}F_1\Big\} \to 0 \quad \text{for } t \to +\infty \quad (s \geqslant 2), \tag{10}$$

$$S_{-t}^{(s)}\Big\{\Phi_s(x_1, \ldots, x_s \mid x_0; S_t^{(1)}F_1, S_t^{(1)}\Phi_1) - S_t^{(1)}\Phi_1 \prod_{(2 \leqslant i \leqslant s)} S_t^{(1)}F_1\Big\} \to 0$$
$$\text{for } t \to +\infty \quad (s \geqslant 2), \tag{11}$$

in which the operator $S_{-t}^{(s)}$ is defined as follows: it transforms the arbitrary function $\varphi(x_1, \ldots, x_s)$ into the function $\varphi(t, x_1, \ldots, x_s)$ which is a solution of the equation

$$\frac{\partial \varphi(t, x_1, \ldots, x_s)}{\partial t} = [H_s; \varphi(t, x_1, \ldots, x_s)], \tag{12}$$

that satisfies the initial condition

$$\varphi(t, x_1, \ldots, x_s)\big|_{t=0} = \varphi(x_1, \ldots, x_s); \tag{13}$$

H_s is the Hamiltonian of the s-particle complex.

Having in mind systems with long-range interaction we assume that the potential energy is $\Phi(|q_i - q_j|) = \varepsilon\,\psi(|q_i - q_j|)$, where ε is a small parameter, and expand the desired functionals in powers of ε:

$$B(x_1 \mid x_0; F_1, \Phi_1) = B_0(x_1 \mid x_0; F_1, \Phi_1) + \varepsilon B_1(x_1 \mid x_0; F_1, \Phi_1) + \ldots, \tag{14}$$

$$A(x_1; F_1) = A_0(x_1; F_1) + \varepsilon A_1(x_1; F_1) + \ldots, \tag{15}$$

$$\Phi_s(x_1, \ldots, x_s \mid x_0; F_1, \Phi_1) = \Phi_s^0(x_1, \ldots, x_s \mid x_0; F_1, \Phi_1) + $$
$$+ \varepsilon\Phi_s^1(x_1, \ldots, x_s \mid x_0; F_1, \Phi_1) + \ldots \; (s \geqslant 2), \tag{16}$$

$$F_s(x_1, \ldots, x_s; F_1) = F_s^0(x_1, \ldots, x_s; F_1) + \varepsilon F_s^1(x_1, \ldots, x_s; F_1) + \ldots \; (s \geqslant 2). \tag{17}$$

After some calculation it is possible to obtain the following Fokker-Planck equation for $\Phi_1(t, x_1 \mid x_0)$ in second approximation for the case of statistical equilibrium:

$$\frac{\partial\Phi_1(t, x_1 \mid x_0)}{\partial t} = -\sum_{(1\leqslant\alpha\leqslant 3)} \frac{p_1^\alpha}{m}\frac{\partial\Phi_1(t, x_1 \mid x_0)}{\partial q_1^\alpha} +$$

$$+\frac{1}{2}\sum_{\substack{(1\leqslant\alpha\leqslant 3)\\(1\leqslant\beta\leqslant 3)}} \frac{\partial^2}{\partial p_1^\alpha \partial p_1^\beta}\left(\langle\Delta p_1^\alpha \Delta p_1^\beta\rangle \Phi_1(t, x_1 \mid x_0)\right) -$$

$$-\sum_{(1\leqslant\alpha\leqslant 3)} \frac{\partial}{\partial p_1^\alpha}\left(\langle\Delta p_1^\alpha\rangle \Phi_1(t, x_1 \mid x_0)\right), \tag{18}$$

$$\Phi_1(t, x_1 \mid x_0)_{t=0} = \delta(x_1 - x_0), \tag{19}$$

where

$$\langle\Delta p_1^\alpha\rangle = -\frac{1}{m\theta}\sum_{(1\leqslant\beta\leqslant 3)} \langle\Delta p_1^\alpha \Delta p_1^\beta\rangle, \tag{20}$$

$$\langle\Delta p_1^\alpha \Delta p_1^\beta\rangle = 2K \frac{\partial^2}{\partial p_1^\alpha \partial p_1^\beta}\int_{(p_2)} |p_2 - p_1| \frac{1}{(2\pi m\theta)^{3/2}} e^{-\frac{p_2^2}{2m\theta}} dp_2, \tag{21}$$

$$K = \frac{\pi m}{2v}\int_0^\infty r^3 F^2(r)\,dr, \quad F(r) = \int_{-\infty}^{+\infty} \frac{\Phi'(\sqrt{x^2 + r^2})}{\sqrt{x^2 + r^2}}\,dx. \tag{22}$$

For a pure Coulomb potential the integral for F(r) diverges and we must follow the usual procedure of cutting it below at the particle separation $\underline{d}$ and above at the Debye length λ_D; then for K with a pure Coulomb potential we obtain

$$K = \frac{2\pi m e^4}{v} \ln\frac{\lambda_D}{d}. \tag{23}$$

Thereupon the expressions obtained for the Coefficients (20) and (21) of the Fokker-Planck equation can be compared with those calculated by Chandrasekhar [1] and Gasiorowicz, Neuman and Riddell [2]. Our expressions are in full agreement with those of the other authors.

An interesting equation is obtained for systems with short-range interactions. In this case we consider the parameter 1/v to be small. The functionals are sought in the form of power series of this small parameter:

$$B(x_1 \mid x_0;\ F_1, \Phi_1) = B_0(x_1 \mid x_0;\ F_1, \Phi_1) + \frac{1}{v} B_1(x_1 \mid x_0;\ F_1, \Phi_1) + \ldots, \tag{24}$$

$$A(x_1;\ F_1) = A_0(x_1;\ F_1) + \frac{1}{v} A_1(x_1;\ F_1) + \ldots, \tag{25}$$

$$\Phi_s(x_1, \ldots, x_s \mid x_0;\ F_1, \Phi_1) = \Phi_s^0(x_1, \ldots, x_s \mid x_0;\ F_1, \Phi_1) + \\ + \frac{1}{v}\Phi_s^1(x_1, \ldots, x_s \mid x_0;\ F_1, \Phi_1) + \ldots \quad (s \geqslant 2), \tag{26}$$

$$F_s(x_1, \ldots, x_s;\ F_1) = F_s^0(x_1, \ldots, x_s;\ F_1) + \frac{1}{v} F_s^1(x_1, \ldots, x_s;\ F_1) + \ldots \quad (s \geqslant 2). \tag{27}$$

After some calculation we obtain for statistical equilibrium in the special case of perfectly hard spheres, the equation for $\Phi_1(t, x_1 \mid x_0)$:

$$\frac{\partial\Phi_1(t, q_1, p_1 \mid x_0)}{\partial t} = -\sum_{(1 \leqslant \alpha \leqslant 3)} \frac{p_1^\alpha}{m} \frac{\partial\Phi_1(t, q_1, p_1 \mid x_0)}{\partial q_1^\alpha} +$$

$$+\frac{1}{v}\int_0^{2\pi}\int_0^{\infty}\int_{(p_2)} \frac{|p_1 - p_2|}{m}\left\{\Phi_1(t, q_1, p_1^* \mid x_0)\frac{e^{-\frac{p_2^{*2}}{2m\theta}}}{(2\pi m\theta)^{3/2}} -\right.$$

$$\left. -\Phi_1(t, q_1, p_1 \mid x_0)\frac{e^{-\frac{p_2^2}{2m\theta}}}{(2\pi m\theta)^{3/2}}\right\} dp_2\, a\, da\, d\varphi, \tag{28}$$

$$\Phi_1(t, q_1, p_1 \mid x_0)|_{t=0} = \delta(q_1 - q_0)\,\delta(p_1 - p_0), \tag{29}$$

where p_1^* and p_2^* are the momenta of the particles after collision, and where a is the particle separation and φ is the azimuthal angle; p_1 and p_2 are the momenta of these same particles before collision.

In conclusion the author takes this opportunity to thank Academician N. N. Bogoliubov for valuable discussions of this work.

M. V. Lomonosov Moscow State University

Received November 12, 1956

LITERATURE CITED

[1] S. Chandrasekar, Principles of Stellar Dynamics, (Foreign Lit. Press, 1948) Chapt. 2 (Russian Translation).

[2] S. Gasiorowicz, M. Neuman and R. J. Riddell, Phys. Rev. 101, 922 (1956).

[3] N. N. Bogoliubov, Dynamical Problems in Statistical Physics (Moscow, 1946).

[4] N. M. Krilov and N. N. Bogoliubov, Reports Dept. Math. Phys., Acad. Sci. Ukrainian SSR 4, Kiev (1939) (In Ukrainian).

π^0-PHOTOMESON PRODUCTION ON COMPLEX NUCLEI

A. S. Belousov, E. I. Tamm and E. V. Shitov

(Presented by Academician A. P. Aleksandrov October 10, 1956)

The investigation of the photoproduction of π^0-mesons on nuclei at different gamma energies can supply information which will determine whether mesons are created throughout the entire volume of a nucleus or only on its surface.

In experiments on π^0 photomeson production [1] as well as the photoproduction of charged pions by nuclei [2] with bremstralung possessing 320 Mev maximum energy it was shown that in both instances the cross section for the production of photomesons by a nucleus increases as $A^{2/3}$, where A is the atomic number. This result was attributed to the reabsorption of mesons produced inside the nucleus, so that only the nuclear surface, which is proportional to $A^{2/3}$, is effective in the production of mesons.

Measurements of the cross sections for interactions between charged mesons and nuclei [3] showed that the mean free path of a meson in nuclear matter depends strongly on the meson energy and is increased as the energy is reduced. In the experiments of [1] and [2] mesons with energies from 60 to 100 Mev were recorded, for which the interaction cross section with nuclei is equal to the geometrical cross section. If mesons are recorded with energies below 20 Mev, for which the nuclei should be largely transparent, we should obtain a pion yield whose dependence on A is approximately linear ($\sigma \sim A$ instead of $A^{2/3}$) if mesons are produced throughout the nuclear volume. If meson production occurs only on the nuclear surface the change of the energy spectrum of the recorded mesons should not change the character of the dependence of meson yield per nucleus on atomic number.

The energy spectrum of π^0-mesons can be changed by changing the energy of the gamma rays which are used to produce the mesons.

The experimental scheme is shown in Fig. 1. Measurements were made with the synchrotron of the Physics Institute of the Academy of Sciences USSR. The gamma beam of the synchrotron after collimation entered the target to be investigated. Target thickness was of the order 0.1 radiation unit in order to insure identical gamma attenuation in all samples. Samples were fastened with a special device for remote control of target change.

Gamma rays from the decay of π^0-mesons were recorded by a telescope of scintillation counters forming an angle of 90° with the synchrotron beam. The telescope consisted of four counters, one of which was connected for anticoincidences and three for coincidences. In front of the anticoincidence counter we placed a 7 cm thick carbon block which could absorb gamma rays and low-energy charged particles. Between the anticoincidence and coincidence counters was placed a 5 mm thick lead converter. Between the coincidence counters were aluminum absorbers each 1 cm thick; the resultant energy threshold of the telescope was about 35 Mev. In all counters liquid scintillators were used (a 5 g/l solution of terphenyl in xylene). The scintillator measurements were 5×5×3 cm. Scintillations were recorded by FEU-19 photomultipliers. Pulses from the photomultiplier output were shaped and fed to a coincidence circuit with the resolving time $\tau = 2 \cdot 10^{-8}$ sec.

The dependence of the π^0-yield on atomic number was measured when E_γ^m, the maximum energy of the bremstralung beam, was 265 and 200 Mev.

For the purpose of reducing the background of random coincidences the telescope was surrounded with a lead shield; in addition the duration of the synchrotron gamma pulse was extended to 3000 μ sec at 265 Mev and to 1000 μ sec at 200 Mev.

The intensity of the synchrotron beam was measured by a thin-walled ionization chamber placed in the path of the beam.

Measurements at 265 Mev were made with Li, C, Al, Cu, Cd, Pb targets; at 200 Mev the same targets were used with the exception of Li.

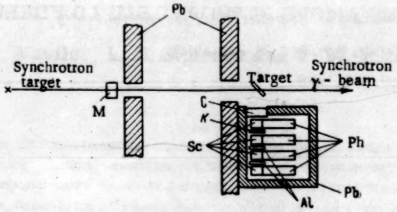

Fig. 1. Diagram of experiment: M – monitor ionization chamber; Sc – scintillators; Ph – photomultipliers; C – 7 cm carbon absorber; Al – 1 cm Al absorber; K – 5 mm Pb converter.

The results are shown in Fig. 2. In the first case (E_{γ}^{m} = 265 Mev) all points coincide with the curve which corresponds to $\sigma \sim A^{2/3}$, with accuracy within the error of measurement, which in this instance was 3%. At E_{γ}^{m} = 200 Mev the law $\sigma \sim A^{2/3}$ remains valid within 10% limit of error with the exception of the point corresponding to Pb, which is above the curve. This discrepancy may be due to a contribution from Thomson scattering of gamma rays by nuclei, whose cross section depends strongly on the atomic number of the nuclear matter.

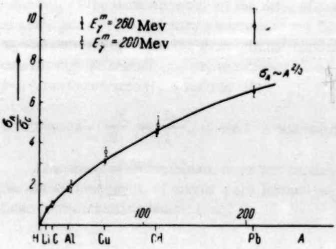

Fig. 2.

For the same reason it was impossible to measure the cross section of π^0-photomeson production at gamma energies close to the photoproduction threshold by the method of recording mesons through one decay quantum.

The results show that the character of the dependence of the π^0-photomeson production cross section on atomic number remains unchanged when E_{γ}^{m} is 310 Mev [1], 265 Mev and 200 Mev, despite the fact that the π^0-energy maximum changes from 100 to 20 Mev.

These results cannot be attributed to the reabsorption of π^0-mesons produced inside nuclei because a change of meson energy should be accompanied by a change of their mean free path in nuclear matter. The fact that the character of the dependence of the π^0-photomeson production cross section on atomic number does not change when the energy spectrum of the produced mesons varies from 100 to 20 Mev can be attributed to the presence of a competing process which suppresses meson production inside nuclei and leads to surface production.

In conclusion we take this opportunity to thank Associate Member of the Academy of Sciences USSR V. I. Veksler and Professor P. A. Cherenkov for their interest in this work, S. Grebenshchikov for his assistance in

preparing the apparatus, S. Rusakov for assistance with the measurements, and the synchrotron crew.

Received November 28, 1956

LITERATURE CITED

[1] W. K. Panofsky, J. W. Steinberg and J. Steller, Phys. Rev. 86, 180 (1952).

[2] R. M. Littaner and D. Walker, Phys. Rev. 86, 838 (1952).

[3] D. H. Stork, Phys. Rev. 93, 868 (1954).

IONIZING ENERGY OF ELECTRONS IN GERMANIUM CRYSTALS

V. S. Vavilov, L. S. Smirnov and V. M. Patskevich

(Presented by Academician D. V. Skobel'tsyn October 27, 1956).

Energy losses by fast electrons traversing crystals are associated with ionization, that is, with the appearance of pairs of extra charge carriers — electrons and holes. The average energy ϵ expended in the production of one pair of carriers depends on the nature of the excitation. On the magnitude of ϵ in ionization by particles, especially fast electrons, depends the efficiency of conversion of β-and γ-radiation into electrical energy by means of semiconductor structures [1, 2] as well as the efficiency of recording radiation with crystalline counters and dosimeters.

For fast electrons in germanium crystals ϵ was evaluated in articles [3, 2], which were concerned with the problem of the direct transformation of β-radiation energy into electrical energy. The direct measurement of ϵ in germanium was carried out by MacKay for ionization by α-particles. MacKay obtained the values 3.0 ± 0.4 ev [4] and 2.94 ± 0.15 ev [5] for ϵ.

Our experiments aimed at determining the mean energy of ionization in germanium excited by electrons of 5-15 kev.

We used n-type crystals with p-n junctions produced by fusing with indium [6]. They were irradiated on the side opposite the indium electrode. The electrons lost all their energy in the n-type region. Our method consisted of the determination of the ratio of the hole flux N_2 through the p-n junction due to the generation of extra pairs by the primary electrons to the flux N_1 of primary electrons.* This ratio will be denoted by β_1. N_2 was determined from the short-circuit current I_2 of the p- and n-regions, which flowed in the outside circuit through an instrument whose resistance was very small compared with the differential resistance R_0 of the p-n junction at zero [6] (See Fig. 1).

Thus $\beta = \frac{N_2}{N_1} = \frac{I_2}{I_1}$, where I_1 is the primary current corresponding to the fast electron flux.

As a result of recombinations on the surface and in the interior the hole flux N_2 was always smaller than the actual number N_0 of carrier pairs formed per unit time but proportional to the latter for very small intensities of the exciting beam, i. e.,

$$N_2 = \alpha N_0.$$

The "multiplication" coefficient β is expressed by

$$\beta = \frac{N_0}{N_1} = \frac{\beta_1}{\alpha} = \frac{I_2}{\alpha I_1}.$$

---

* Measurements of induced conduction in homogeneous blocks do not give sufficiently reliable results because of difficulty in controlling the rate of surface recombination, which varies differently in the irradiated and "dark" portions of the crystal.

The value of ϵ can be written as

$$\varepsilon = \frac{V}{\beta} = \frac{\alpha I_1 V}{I_2},$$

where V is the energy of the primary electrons; α was determined independently from the generation of extra carrier pairs by monochromatic light of known intensity. The reflection coefficient of germanium in the region of 0.6-2 μ wave lengths was measured in our laboratory and practically coincided with values given in the literature [7]. The quantum yield was taken as unity.

In the crystals which we investigated α was independent of the wave length up to lengths for which a considerable portion of the light flux passed through the crystal without absorption. In our experiments for the measurement of α we used light with $\lambda = 1.05\mu$ which was mainly absorbed in a layer of not of not greater than 1.0 μ thickness, i. e., in approximately the region of ionization by electrons.

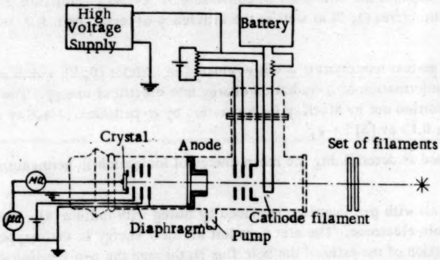

Fig. 1.

α depends strongly on the conditions at the crystal surface and changes during evacuation of the apparatus and bombardment with electrons. For constant control of α during the measurements we simultaneously irradiated the crystals with electrons and with light. For this purpose we constructed an electron gun whose design enabled us to direct the light beam along the electron beam (see Fig. 1).

In front of the irradiated crystal we placed diaphragms for cutting down the beam and collecting secondary electrons. The coefficient of secondary emission at V = 5-15 kev was about 0.3.

A calorimetric control experiment was performed in which we evaluated the energy removed by secondary electrons and by x-rays and we showed that this energy is about 4% of the energy of the incident electron beam.

The experiments were performed at pressures $10^{-4} - 2 \cdot 10^{-6}$ mm Hg. We detected no dependence of ϵ on pressure from $2 \cdot 10^{-6}$ to 10^{-4} mm Hg.

A series of measurements on crystals which had been subjected to different surface treatment (etching in hydrogen peroxide and a SR-4 mixture) [8] gave identical values for ϵ. The average value of ϵ from 4 series of measurements was 3.7±0.4 ev.

From V = 5 to 15 kev, ϵ does not vary. This indicates a small energy loss of the primary electrons in the oxidized surface layer produced by etching germanium.

The near coincidence of the values of ϵ in ionization by electrons and alpha particles evidently results from the fact that in the second case a considerable fraction of the charge carrier pairs are produced by relatively fast δ-electrons. We also cannot exclude the possibility of radiative energy transfer within the crystal from the region of dense ionization by photons produced through the direct recombination of electrons and holes.

The authors wish to thank B. M. Vul for a number of valuable comments.

Received October 24, 1956

LITERATURE CITED

[1] E. Linder, Trans. of the Geneva Conference on the Peaceful Uses of Atomic Energy, 1955.

[2] W. Pfann and W. Roosebroeck, J. Appl. Phys. 25, 1422(1955).

[3] P. Rappaport, Phys. Rev. 93, 246(1954).

[4] K. MacKay, Phys. Rev., 84, 829(1951).

[5] K. MacKay and K. MacAffee, Phys. Rev. 91, 1079(1953).

[6] V. S. Vavilov and L. S. Smirnov, Radio and Electronics I, No. 8, 1147(1956).

[7] H. Y. Fan and M. Becker, Semiconductor Materials, Ed. V. M. Tuchkevich(Foreign Lit. Press, 1954) (Russian Translation).

[8] J. MacKelvey and R. L. Longini, Electrophysical Properties of Germanium and Silicon, Ed. A. V. Rzhanov, Moscow, 1956, p. 350(Russian Translation).

ON THE THEORY OF STATIONARY STRIATIONS IN THE POSITIVE COLUMN OF A GAS DISCHARGE

O. V. Prudkovskaia and M. F. Shirokov

(Presented by Academician N. N. Bogoliubov November 14, 1956)

There have been many investigations of stationary and moving striations in the positive column of a gas discharge. It has been shown [1] that the basis for the theoretical investigation of striations in a gas discharge must be the diffusion equations for the charged particles constituting the plasma.

But it has appeared that the theory as a rule accounts only for moving periodicities and does not explain stationary striations. Watanabe and Oleson [2] on the basis of a set of equations consisting of the diffusion equations for charged particles and the Poisson equation for the electric field obtain expressions for the wave number and velocity of the wave propagated in a plasma and show from an analysis that the wave velocity never vanishes if the wave period is not exceedingly large. In other words, their article gives a theory of moving layers.

The same problem was solved by Druyvesteyn [3] for a quasi-neutral plasma taking into account both thermal diffusion and the dependence of the ionization coefficient on the electron temperature. The initial set of equations here includes the diffusion equation for charged particles, the energy conservation equation for electrons and the equality of the electronic and ionic current gradients, which holds true for a quasi-neutral plasma. As the author noted, this theory is unsatisfactory from the point of view of comparison with experiment, gives a poor physical picture of the phenomenon and does not explain the existence of stationary striations. Among his simplifying assumptions Druyvesteyn uses Schottky's hypothesis of the preservation of ambipolar radial diffusion, which is inherent in a homogeneous positive column, for a layered column also. Thereby, all particles produced by ionization remain in the same section of the tube and can be transported only by the radial flow of ambipolar diffusion. Druyvesteyn also shows that allowance for ambipolar diffusion along the tube axis leads to different results and possibly enables us to explain the dependence of the period of the stationary striations on the radius. However, this was not shown either by Druyvesteyn or by his successors.

In a recent article, Chapnik [4] solved this problem using perturbation theory and departure from quasi-neutrality. He retained the very arbitrary hypothesis of Druyvesteyn that particles resulting from ionization are borne away only by the radial flow of ambipolar diffusion and thus eliminated them from participation in the formation of longitudinal layers. As Chapnik showed, the remaining terms gave a periodic solution for gases in which the collision cross section for electrons is inversely proportional to their velocity. Unlike Druyvesteyn, Chapnik obtained a dispersion equation for stationary periodicity resulting principally from thermal diffusion.

It should be noted that stationary striations in a discharge are observed also in gases in which the cross section for electron collisions is directly proportional to their velocity, and in gases in which the thermal diffusion coefficient is zero. In argon, for example, both where the cross section is increasingly dependent and where it is decreasingly dependent on velocity the strata show no difference in external appearance or in the laws which govern them. Therefore, although thermal diffusion undoubtedly plays a part in a gas discharge (for those gases whose thermal diffusion coefficient is different from zero) Chapnik's explanation of stationary striations is unsatisfactory. Nor is sufficient proof provided by the numerical agreement with experiment of the striation period, based on observation of the Schottky relation in the two instances indicated by Chapnik.

Thus far, no theoretical explanation has been given for a number of well-known laws which govern the period of stationary striations, such as the dependence of the striation period on the radius in a dc discharge or the dependence of the period on the temperature of the electron gas at constant pressure.

Yet on the basis of the indicated diffusion equations it is possible to obtain completely rigorous expressions for the period of stationary strata which agree with experiment in order of magnitude and enable us to explain the dependence of the period on the tube radius, on the strength of the discharge current, etc.

Let us write the initial set of equations for a striated discharge:

$$\frac{\partial n_1}{\partial t} - \frac{\partial (n_1 u_{1\alpha})}{\partial x_\alpha} - D_1 \frac{\partial^2 n_1}{\partial x_\alpha^2} = \beta n_1 - R\,, \tag{1}$$

$$\frac{\partial n_2}{\partial t} + \frac{\partial (n_2 u_{2\alpha})}{\partial x_\alpha} - D_2 \frac{\partial^2 n_2}{\partial x_\alpha^2} = \beta n_1 - R\,, \tag{2}$$

$$\frac{\partial E_\alpha}{\partial x_\alpha} = 4\pi e\,(n_2 - n_1)\,. \tag{3}$$

Here the subscript 1 refers to electrons and the subscript 2 refers to ions; $u_{1\alpha}$ and $u_{2\alpha}$ are the drift velocities of electrons and ions, respectively; D_1 and D_2 are diffusion coefficients; β is the ionization coefficient; R is the volume recombination in the discharge; n_1 and n_2 are the electron and ion concentrations, respectively.

Let the tube axis coincide with the x axis. In the central portion of the tube we can assume slight dependence of particle concentration on the coordinates other than x: $x_\alpha = x$; and for the volume recombination we can take the relation $R = \beta n_0$, where n_0 is the equilibrium concentration of charged particles in the central portion of an unstriated discharge, which is taken as the zero-th approximation.

Setting

$$\begin{aligned} n_1 &= n_0 + \nu_1 e^{i(\omega t + kx)} \qquad (\nu_1 \ll n_0); \\ n_2 &= n_0 + \nu_2 e^{i(wt + kx)} \qquad (\nu_2 \ll n_0) \end{aligned} \tag{4}$$

and considering that $u_1 = \mu_1 E$, where μ_1 and μ_2 are the mobilities of electrons and ions, we obtain:

$$\nu_1 \left(i\omega - i\;k \quad + D_1 k^2 - \beta + \frac{\omega_e^2}{\alpha_1} \right) - \nu_2 \frac{\omega_e^2}{\alpha_1} = 0\,, \tag{5}$$

$$\nu_2 \left(i\omega + u_2 ik + D_2 k^2 + \frac{\omega_i^2}{\alpha_2} \right) - \left(\beta + \frac{\omega_i^2}{\alpha_2} \right) \nu_1 = 0\,, \tag{6}$$

where $\frac{\omega_e^2}{\alpha_1} = 4\pi e n_0 \mu_1 = \frac{D_1}{d_1^2}$; $\frac{\omega_i^2}{\alpha_2} = 4\pi e n_0 \mu_2 = \frac{D_2}{d_2^2}$; d_1 and d_2 are the Debye radii for electrons and ions.

From the condition for the existence of a nontrivial solution we obtain the following dispersion equation:

$$\begin{aligned} (i\omega - u_1 ik + D_1 k^2 + 4\pi e n_0 \mu_1 - \beta)\,(i\omega + u_2 ik + D_2 k^2 + 4\pi e n_0 \mu_2) - \\ - 4\pi e n_0 \mu_1 (\beta + 4\pi e n_0 \mu_2) = 0. \end{aligned} \tag{7}$$

If we take into account that in the usual gas discharge plasma the Debye radius is very small, of the order $10^{-2} - 10^{-3}$ cm (which corresponds to a quite high degree of plasma charge: 10^{-5}), the terms $4\pi e n_0 \mu_1$ and $4\pi e n_0 \mu_2$ in the equation are much larger than the remaining terms. We then obtain

$$\left(D_1 \frac{\mu_2}{\mu_1} + D_2\right) k^2 + (i\omega - \beta)\left(1 + \frac{\mu_2}{\mu_1}\right) = 0 . \qquad (8)$$

$$|\nu_1 - \nu_2| \ll |\nu_1| .$$

Under the condition

$$k^2 = \frac{\beta\left(1 + \frac{\mu_2}{\mu_1}\right)}{D_1 \frac{\mu_2}{\mu_1} + D_2} \qquad (9)$$

we have the stable quasi-neutral stationary periodicity:*

$$l = \frac{2\pi}{\sqrt{\frac{\beta}{D_1 \frac{\mu_2}{\mu_1} + D_2}\left(1 + \frac{\mu_2}{\mu_1}\right)}} . \qquad (10)$$

Using a more complete set of equations including the equation for energy concentration of the particles and taking into account thermal diffusion, the dependence of the equation parameters on temperature, etc., we can obtain a more complicated dispersion equation which will, however, assume the indicated simpler appearance (8) when we take into account the real conditions under which striations are observed.

From a known gas pressure, electron temperature for a definite tube radius and definite gas the period of stationary striations is easily computed from (10). The results are given in Table 1 for two gases, argon and neon, in a dc discharge. In the calculation we used the known experimental dependence of electron temperature on the pressure and tube radius [9]. Because of the absence of information regarding the variation of the temperature of a neutral gas and of ions we assumed the ion mobility μ_2 to be constant. Allowance for the variation of ion mobility with gas temperature leads to a reduction of the steepness of the relation $l_T = f(r_0)$, especially for argon, in which the variation of temperature with varying tube radius is especially large. For comparison the same table contains the values of l_e for the dependence of striation period on tube radius in a high frequency discharge at constant current density as given by A. A. Zaitsev and Kh. A. Dzherpetov [5].

It should be noted that in this very simple case the dispersion equation for a high frequency discharge coincides entirely with the dispersion Equation (8). It is only necessary that the amplitude of the high frequency field E_0 be not too great, but subject to the condition

---

* The theory of Watanabe and Oleson [2] neglects the interaction between electrons and ions in a real plasma, as is especially clear in their article from the expression for the wave velocity. If the $4\pi e n \mu_2$ and $4\pi e n \mu_1$ are taken to be much larger than the remaining terms of the expression, the denominator of the fraction is very large and the wave velocity vanishes independently of the magnitude of the striation period. Thus the conclusions of Watanabe and Oleson refer to weakly charged plasmas in which the Debye radius is of the order of the striation period and much greater than the mean free path.

$$\frac{\mu_1 E_0}{c_1} < \frac{\lambda_1}{l}, \qquad (11)$$

where λ_1 is the mean free path for electrons and c_1 is their thermal velocity. A comparison shows the same character of dependence and closeness of the experimental and calculated striation periods.

TABLE 1

	Argon $p = 10$ мм Hg						Neon $p = 10$ мм Hg					
r_0, cm	0.1	0.2	0.4	0.6	0.8	1.0	0.1	0.2	0.4	0.6	0.8	1.0
l_T, cm	0.35	1.5	3.6	4.8	5.7	—	0.5	1.14	2.2	3,0	3,9	4.82
l_s, cm	0.77	1.4	2.46	3.46	4.4	—	0.85	1.53	2.7	3,8	4.8	5.8

Table 2 shows the dependence of the striation period in neon on the temperature of the electron gas (varying with the discharge current) at constant pressure. For comparison the same table contains experimental data for neon obtained by Zaitsev and Dzherpetov within about the same range of electron temperature and showing the same type of dependence.

TABLE 2

Neon, $p = 1.8$ mm Hg, $r_0 = 3.1$ cm

	T_1, °K			
	$3.5 \cdot 10^4$	$3.3 \cdot 10^4$	$2.85 \cdot 10^4$	$2 \cdot 10^4$
l_T, cm	1.3	1.8	2.3	4.5
l_s, cm	3.6	4.0	4.5	—

The correspondence between the discharge current density and the electron temperature was established by us through the graphs published in references [7, 8]. Because of the small scale of the graphs and the different experimental conditions this correspondence can be regarded as appoximate.

M. V. Lomonosov Moscow
State University

Received November 12, 1956

LITERATURE CITED

[1] M. F. Shirokov, Doklady Akad. Nauk SSSR 89, 837(1953).

[2] S. Wantanabe, and N. L. Oleson, Phys. Rev. 99, 1701(1955).

[3] J. Druyvesteyn, Physica 1, 273, 1003(1934).

[4] I. M. Chapnik, Doklady Akad. Nauk SSSR 107, 4, 529(1956).

[5] A. A. Zaitsev and Kh. A. Dzherpetov, Doklady Akad. Nauk SSSR 89, 825(1953).

[6] A. A. Zaitsev and Kh. A. Dzherpetov, J. Exptl.-Theoret. Phys. (U.S.S.R.) 24, 5, 516(1953).

[7] R. Seeliger, and R. Hirchert, Ann. d. Phys. 11, 817(1932).

[8] A. A. Zaitsev and E. I. Iankovskaia, Doklady Akad. Nauk SSSR 29, 563(1940).

[9] A. von Engel and M. Steenbeck, Elektrische Gasentladungen (Russian Translation)(Moscow, 1936).

ON THE SHAPE OF ABSORPTION AND LUMINESCENCE BANDS OF COMPLEX MOLECULES

Academician B. I. Stepanov of the Academy of Sciences, Byelorussian SSR, and L. P. Kazachenko

In the articles of S. N. Vavilov [1] it was frequently emphasized that the universal shape of the absorption and luminescence bands of complex molecules can be accounted for by purely statistical considerations. By this time a number of attempts have been made to solve this problem [2-8]. In the present article we derive a general relation which associates the absorption coefficient or emissive power for frequencies $\nu > \nu_{el}$ with the same quantities for frequencies $\nu < \nu_{el}$. The results apply only to molecules which exhibit the mirror reflection symmetry of the absorption and luminescence spectra which was observed by Levshin [9].

Stepanov [10] has proved that the emissive power of complex molecules in a solution is associated with the absorption coefficient at the same frequency by the following universal relation:

$$W_\nu^{\mathrm{lum}} = d(T)\,\nu^3 e^{-\frac{h\nu}{kT}} \varkappa_\nu. \tag{1}$$

On the other hand, for molecules with mirror symmetry of the absorption and luminescence spectra the following relation holds [11, 12]:

$$\frac{W^{\mathrm{lum}}_{\nu_{el}-\Delta\nu}}{(\nu_{el}-\Delta\nu)^4} = \alpha \frac{\varkappa_{\nu_{el}+\Delta\nu}}{\nu_{el}+\Delta\nu}, \tag{2}$$

where α is a proportionality factor that is independent of frequency. Rewriting (1) in the form

$$\frac{W^{\mathrm{lum}}_{\nu_{el}-\Delta\nu}}{(\nu_{el}-\Delta\nu)^4} = d(T)\, e^{-\frac{h(\nu_{el}-\Delta\nu)}{kT}} \frac{\varkappa_{\nu_{el}-\Delta\nu}}{\nu_{el}-\Delta\nu}, \tag{3}$$

and comparing (2) and (3) we obtain

$$\alpha \frac{\varkappa_{\nu_{el}+\Delta\nu}}{\nu_{el}+\Delta\nu} = de^{-\frac{h\nu_{el}}{kT}} e^{\frac{h\Delta\nu}{kT}} \frac{\varkappa_{\nu_{el}-\Delta\nu}}{\nu_{el}-\Delta\nu}, \tag{4}$$

This formula is valid for any $\Delta\nu$ and in particular for $\Delta\nu = 0$

$$\alpha = de^{-\frac{h\nu_{el}}{kT}} \tag{5}$$

and thus

$$\frac{\varkappa_{\nu_{el}-\Delta\nu}}{\nu_{el}-\Delta\nu}=\frac{\varkappa_{\nu_{el}+\Delta\nu}}{\nu_{el}+\Delta\nu}e^{-\frac{h\Delta\nu}{kT}} \qquad (6)$$

Equation (6) can be derived in a different manner, by writing the explicit expressions for the absorption coefficient and the luminescence emission power.

For the shape of a luminescence band we obtain from (2), (3) and (5) the similar relation:

$$\frac{W^{lum}_{\nu_{el}+\Delta\nu}}{(\nu_{el}+\Delta\nu)^4}=\frac{W^{lum}_{\nu_{el}-\Delta\nu}}{(\nu_{el}-\Delta\nu)^4}e^{-\frac{h\Delta\nu}{kT}} \qquad (7)$$

The Expressions (6) and (7) possess a large degree of generality and may be invalid only for those molecules in which there is a departure from mirror symmetry of the absorption and luminescence spectra (on the frequency scale). They are inapplicable also when during the time that the molecules are in an excited electronic state an equilibrium distribution cannot be established among the vibrational energy levels (see [10]).

TABLE 1

$\Delta\nu$, cm^{-1}	$\frac{\varkappa_{\nu_{el}+\Delta\nu}}{\nu_{el}+\Delta\nu}:\frac{\varkappa_{\nu_{el}-\Delta\nu}}{\nu_{el}-\Delta\nu}$	$h\Delta\nu/kT$
225	3.0	2.9
425	7.0	7.6
625	21.0	21.0
825	55.0	51.8
1025	127.5	134.8

$\nu_{el} = 24475$ cm^{-1}

As a check of the derived relations we used experimental data [13] on the spectra of the phthalimides given in tables. The results of a calculation for absorption by a solution of 3-aminophthalimide are given in Table 1.

The table shows that (6) is in good agreement with experiment.

Equation (6) can be put into a form which is more suitable for comparison with experiment. Taking the logarithm of (6) we obtain

$$\ln\frac{\varkappa_{\nu_{el}+\Delta\nu}}{\nu_{el}+\Delta\nu}-\ln\frac{\varkappa_{\nu_{el}-\Delta\nu}}{\nu_{el}-\Delta\nu}=\frac{h\Delta\nu}{kT}. \qquad (8)$$

Figure 1 gives the values of $\ln\frac{\kappa_\nu}{\nu}$ as a function of $\frac{\nu}{kT}$ for the absorption spectrum of a solution of 3-aminophthalimide in benzene. The solid lines give values which correspond to the left-hand side of (8) for different $\Delta\nu$; the dashed lines give the values of $\frac{\Delta\nu}{kT}$. As the figure shows, the solid and dashed lines are strictly identical in length, thus confirming (6). The construction employed in Fig. 1 can be used advantageously for the determination of ν_{el} from a single absorption band without measuring the luminescence spectrum (assuming that the law of mirror symmetry is approximately satisfied).

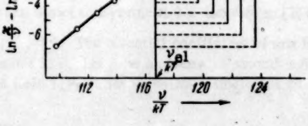

Fig 1.

Similar calculations and constructions for a few phthalimides have shown that (6) is satisfied at all times, either rigorously or approximately. The best results were obtained for absorption and somewhat poorer results for luminescence. It is characteristic that appreciable departure from mirror symmetry does not result in serious violation of (6). For the spectra of vapors (6) is less well satisfied. This is quite natural since the initial Relation (1) is not satisfied for vapors.

V. I. Lenin Byelorussian State University

Received June 4, 1956

LITERATURE CITED

[1] S. I. Vavilov, Col. Works 2, 1956, p. 190.

[2] S. I. Pekar, Progr. Phys. Sci. (USSR) 50, 197 (1953); M. A. Krivoglaz and S. I. Pekar, Trans. Phys. Inst. Acad. Sci. Ukrainian SSR, 4, 37 (1953).

[3] V. M. Agranovich and A. S. Davydov, Sci. Repts. Kiev State Univ., Coll. Phys. Fac. No. 7 (1955).

[4] B. S. Neporent, J. Exptl.-Theoret. Phys. (USSR) 21, 172 (1952); Bull. Acad. Sci. USSR, Phys. Ser. 15, 533 (1951).

[5] B. I. Stepanov and A. M. Samson, Bull. Acad. Sci. Byelorussian SSR, Phys. Ser. No. 1, (1956).

[6] B. I. Stepanov and L. P. Kazachenko, Bull. Acad. Sci. Byelorussian SSR 3, 53 (1955).

[7] F. E. Williams, Phys. Rev. 80, 306 (1950); J. Chem. Phys. 19, 457 (1951); Phys. Rev. 82, 281 (1951); 83, 877 (1951); 84, 1181 (1951).

[8] C. C. Klick, Phys. Rev. 85, 154 (1952); J. Phys. Chem. 57, 776 (1953).

[9] V. P. Levshin, J. Phys. Chem. (USSR) 2, 641 (1931); 6, 1 (1935); 9, 1 (1937); Doklady Akad. Nauk SSSR 2, 405 (1934); 1, 474 (1935).

[10] B. I. Stepanov, Doklady Akad. Nauk SSSR 112, 5, (1957), [Soviet Physics-Doklady, p. 81].

[11] D. I. Blokhintsev, J. Exptl.-Theoret. Phys. (USSR) 9, 459 (1939).

[12] B. I. Stepanov, Luminescence of Complex Molecules, Acad. Sci. Byelorussian SSR Press, 1955 (In Russian).

[13] N. A. Borisevich, Dissertation, State Optical Institute (1954).

THE GENERALIZED STOCHASTIC PROBLEM OF PARTICLE MOTION

N. A. Chernikov

(Presented by Academician V. A. Fok October 29, 1956)

The usual formulation of the stochastic problem of particle motion in which the time t is given a special part is ill-adapted to the theory of relativity and especially to gravitational theory.* The natural generalization of the usual problem which is proposed here eliminates this defect and provides a canonical formulation of problems which are analogous to the problem of the probability of two-particle collision.

Unlike the usual procedure the state of a mass point will be given by its space-time position and velocity. We shall assume that the space F of states of a mass point is a simple differentiable manifold. This will be the case, for example, if the space of events is Galilean. The space F is of dimension 7, but everywhere where it is only important that it be finite we shall denote this by n, with possible generalizations in mind.

The motion of a mass point in a given external force field is given by the set of equations

$$\frac{dx_i}{d\tau} = f_i(x_1, \ldots, x_n), \quad i = 1, 2, \ldots, n, \tag{1}$$

where $x_1, \ldots, x_n$ are the coordinates in F. The set of functions $\left\{f_1(x_1, \ldots, x_n), \ldots, f_n(x_1, \ldots, x_n)\right\}$ forms in F the vector field f(P), $P \in F$. The entire manifold of possible motions of a mass point in the given field f(P) is a family of vector lines of this field. On each of these lines the separation $\tau = \tau(P_1, P_2)$ is given between any of its points P_1 and P_2, which is the proper time of the mass point required to replace its state P_1 with the state P_2; then $\tau(P_1, P_2) = -\tau(P_2, P_1)$. The problem of mechanics is then formulated as follows: given a field f(P) and the initial state P_0 of a material point: to find its state $P = \varphi(\tau;\ P_0)$ after the lapse of proper time τ. This is equivalent to the problem of solving Equations (1) subject to the initial conditions $x_i|_{\tau=0} = x_i^0$, $i = 1, \ldots, n$.

We shall investigate the motion of a particle of a specific kind. The particle is created in some definite state $P_1 \in F$ and after existing for the time $\tau > 0$ has "lived through" the set of states $P = \varphi(\eta;\ P_1)$, $0 < \eta < \tau$, after which it decays in the state $P_2 = \varphi(\tau;\ P_1)$. This set of states will be called the world line of the particle. We shall assume that a particle starting from an arbitrary state of P decays with the probability $\frac{\tau}{T(p)} + o(\tau)$ $\left(\lim\limits_{\tau \to 0} \frac{o(\tau)}{\tau} = 0\right)$ into one of the states $P' = \varphi(\eta;\ P)$, $0 < \eta < \tau$.

Let the probability W(D) of the production of the particle in a state of the region $D \subset F$ which is defined by the skew (antisymmetric) n-lined form [2] $Q(P;\ \xi_1, \ldots, \xi_n)$ be given by the fomula $W(D) = \int\int\limits_{D}\ldots\int Q(P;\ d_1, \ldots, d_n)$. The essential coefficient of this form is, generally speaking, a generalized function of the coordinates in F. Let S be a piecewise-smooth hypersurface in F such that it has in common with any vector line of the field f(P) either no point, a single point or a single segment.

---

* We have retained Fok's terminology [1].

The probability $w(S)$ that the world line of a particle will intersect the hypersurface S is expressed by the integral $w(S) = \int \ldots_S \int \Omega_0(P;\ d_1, \ldots, d_{n-1})$ over S of the $(n-1)$-lined skew form $\Omega_0(P;\ \xi_1, \ldots, \xi_{n-1}) = A_0(P;\ f(P),\ \xi_1 \ldots, \xi_{n-1})$. The essential coefficient of the n-lined skew form $A_0(P;\ \xi_1, \ldots, \xi_n)$ is the curvilinear integral

$$A^0_{12\ldots n}(x_1, \ldots, x) = \int_0^\infty Q_{12\ldots n}(x_1', \ldots, x_n') \frac{\partial(x_1', \ldots, x_n')}{\partial(x_1, \ldots, x_n)} \exp\left[-\int_0^\tau \frac{d\eta}{T(\varphi(-\eta;\ P))}\right] d\tau, \qquad (2)$$

where $x_1, \ldots, x_n$ and $x'_1, \ldots, x'_n$ are the coordinates of the points P and $\varphi(-\tau;\ P)$.

The decaying particle can be recreated. Let the probability of reestablishment of a particle in a state of the region $D \subset F$ on the condition that it decayed into a state P^* be given by the integral $\iint \ldots_D \int K(P;\ d_1, \ldots, d_n;\ P^*)$. The skew form $K(P;\ \xi_1, \ldots, \xi_n;\ P^*)$ is a scalar function of the point parameter P^*. A particle can decay and be regenerated an infinite number of times. If the process of decay and regeneration does not change the quantities $f(P)$, $T(P)$ and $K(P;\ \xi_1, \ldots, \xi_n;\ P^*)$, the probability of the k-th regeneration is defined by the skew form

$$Q_k(P;\ \xi_1, \ldots, \xi_n) = \iint_F \cdots \int \frac{K(P;\ \xi_1, \ldots, \xi_n;\ P^*)}{T(P^*)} A_{k-1}(P^*;\ d_1^*, \ldots, d_n^*), \qquad (3)$$

where $A_{k-1}(P^*;\ d_1^*, \ldots, d^*_n)$ defines the probability of intersection with the hypersurface S by the world line of a $k-1$ times regenerated particle. The form $A_{k-1}(P;\ \xi_1, \ldots, \xi_n)$, depends on $Q_{k-1}(P';\ \xi'_1, \ldots, \xi'_n)$ in exactly the same way as $A_0(P;\ \xi_1, \ldots, \xi_n)$ depends on $Q(P';\ \xi'_1, \ldots, \xi'_n)$. From this and from (2) it follows that the skew form $A(P;\ \xi_1, \ldots, \xi_n;\ \lambda) = \sum_{k=0}^{\infty} \lambda^k A_k(P;\ \xi_1, \ldots, \xi_n)$ obeys the kinetic equation:

$$\Omega'(P;\ \xi_1 \ldots, \xi_n) + \frac{A(P;\ \xi_1, \ldots, \xi_n)}{T(P)} = \lambda \iint_F \cdots \int \frac{K(P; \xi_1, \ldots, \xi_n; P^*) A(P^*; d_1^*, \ldots, d_n^*)}{T(P^*)} + Q(P;\ \xi_1, \ldots, \xi_n) \qquad (4)$$

subject to the condition $\lim_{\tau \to \infty} \Omega(\varphi(-\tau;\ P);\ \xi_1, \ldots, \xi_{n-1};\ \lambda) = 0$, $\Omega'(P; \xi, \xi_1, \ldots, \xi_{n-1};\ \lambda)$ is the external derivative of the $(n-1)$-lined skew form $\Omega(P; \xi_1, \ldots, \xi_{n-1};\ \lambda) = A(P;\ f(P),\ \xi_1, \ldots, \xi_{n-1};\ \lambda)$. The essential coefficient of the derivative of the form is

$$\Omega'_{12\ldots n}(x_1, \ldots, x_n) = \sum_{i=1}^{n} \frac{\partial}{\partial x_i} [A_{12\ldots n}(x_1, \ldots, x_n) f_i(x_1, \ldots, x_n)].$$

The probability of intersection with the hypersurface S by the world line of a particle without regard for the number of times that the particle has decayed and has been regenerated is defined by the formula

$$\Omega(P;\ \xi_1, \ldots, \xi_{n-1}) = \sum_{k=0}^{\infty} \Omega_k(P;\ \xi_1, \ldots, \xi_{n-1}) = \Omega(P; \xi_1, \ldots, \xi_{n-1};\ 1).$$

The usual formulation of the problem is derived from the above if S is part of the hypersurface t = const. In the formulation given above it is easy to take account of gravitation, but its advantages over the usual formulation are also obvious in the theory of relativity since the hyper-surface t=const is not invariant with respect to Lorentz transformations. In the latter case as coordinates in F we can select the Galilean coordinates x, y, z, t of the particle with the components u_1, u_2, u_3 of its velocity equal to the ratios of the spatial components of its momentum to the rest mass. As a volume element in F it is convenient to take the skew form $\epsilon(P; d_1, \ldots, d_7)$, which in vectors of elementary displacements along the coordinate lines becomes

$$\varepsilon(P; d_1, \ldots, d_7) = dx\,dy\,dz\,dt\,\frac{du_1du_2du_3}{u_4}, \quad u_4 = \sqrt{1 + \frac{u_1^2+u_2^2+u_3^2}{c^2}},$$

and as element of area on the hypersurface S the 6-line skew form $\epsilon(P; f(P), d_1, \ldots, d_6)$.

Since $f(P) = \{u_1, u_2, u_3, u_4, \omega_1(P), \omega_2(P), \omega_3(P)\}$ the element of area on the hypersurface t = const is $\epsilon(P; f(P), d_1, \ldots, d_6) = dx\ dy\ dz du_1 du_2 du_3$. Any 7-lined skew form $B(P; \xi_1, \ldots, \xi_7)$ differs from $\epsilon(P; \xi_1, \ldots, \xi_7)$ by only a scalar factor: $B(P; \xi_1, \ldots, \xi_7) = B(P)\,\epsilon(P; \xi_1, \ldots, \xi_7)$. The scalar function Q(P) obtained from this formula is the probability density that the particle under consideration is formed in the state P. The scalar function $A_k(P)$ on any hypersurface S is the probability density that the world line of a k-times regenerated particle will intersect this hypersurface (at the point P). By a transition from skew forms to scalar functions we obtain the kinetic equation of relativity theory in the form

$$\begin{aligned} &u_4\frac{\partial A(P)}{\partial t} + u_1\frac{\partial A(P)}{\partial x} + u_2\frac{\partial A(P)}{\partial y} + u_3\frac{\partial A(P)}{\partial z} + \\ &+ u_4\sum_{l=1}^{3}\frac{\partial}{\partial u_l}\left[\frac{\omega_l(P)A(P)}{u_4}\right] + \frac{A(P)}{T(P)} = \\ &= \lambda\iint_{-\infty}^{+\infty}\cdots\int\frac{A(P^*)K(P;P^*)}{T(P^*)}\,dx^*dy^*dz^*dt^*\,\frac{du_1^*du_2^*du_3^*}{u_4^*} + Q(P) \end{aligned} \tag{5}$$

subject to the condition $\lim\limits_{\tau\to\infty} A(\varphi(-\tau; P)) = 0$.

Usually $T^{-1}(P^*)K(P;P^*) = L(P;a^*)\,\delta(x-x^*)\,\delta(y-y^*)\,\delta(z-z^*)\,\delta(t-t^*)$, where a^* is the velocity of the particle in the state P^*. This approach to the problem makes Lorentz invariance obvious.

The author is deeply grateful to Academician V. A. Fok for valuable suggestions.

Theoretical Physics Laboratory,
United Institute for Nuclear Research

Received October 13, 1956

LITERATURE CITED

[1] V. A. Fok, Theory of Space, Time and Gravitation, 1955.

[2] P. K. Rashevskii, Geometrical Theory of Partial Differential Equations, 1947.

The point [illegible] of the photon is [illegible] the [illegible] part of the [illegible] [illegible] of the particle with the components [illegible] of its velocity equal to the ratios of the spatial components of [illegible]

[illegible]

[illegible]

[illegible]

Clearly [illegible] where [illegible] is the velocity of the particle of the mass [illegible]

[illegible]

Theoretical Physics Laboratory, [illegible] Received October 18, 1958

[illegible]

LITERATURE CITED

[1] [illegible] Theory of [illegible] Time and [illegible]

[2] [illegible]

SOVIET PHYSICS-DOKLADY VOL. 2, NO. 1 JANUARY-FEBRUARY, 1957

(Translation of all papers in the "Physics" Sections of the Proceedings of the Academy of Sciences of the USSR, Vol. 112, Nos. 1-6, published by the American Institute of Physics, November, 1957)

CONTENTS

		Russian	
	Page	Issue No.	Page
A Study of the Explosive Showers Produced by High-Energy Cosmic Rays. V. V. Alpers, I. I. Gurevich, V. M. Kutukova, A. P. Mishakova, B. A. Nikol'skii and L. V. Surkova	1	1	33
The Dependence of π^0-Photomeson Production Cross Sections on Atomic Number. B. B. Govorkov, V. I. Gol'danskii, O. A. Karpukhin, A. V. Kutsenko and V. V. Pavlovskaia	4	1	37
Fine Structure and Lamb Shift of the $2s_{1/2}$ Level of the Tritium $T\alpha$ Line λ 6560 A. P. S. Kireev	8	1	41
On the Role of Bound States in Photoproduction. A. A. Logunov, B. M. Stepanov and A. N. Tavkhelidze	12	1	45
On the Observation of Magnetic Viscosity in Ferrites at Low Temperatures. R. V. Telesnin and I. A. Lednev	15	1	48
On the Solution of a Problem with the Schroedinger Equation in Infinite Three-Dimensional Space. M. Burnat	16	2	224
Photoluminescence of Thallous Chloride. A. S. Vysochanskii	20	2	228
π^+-Production in Carbon by 308-Mev π^--Mesons. V. V. Krivitskii and A. A. Reut	24	2	232
Phases of Meson-Nucleon Scattering up to 310-Mev. A. I. Mukhin, I. V. Popova and G. N. Tentiukova	27	2	236
Proton Relaxation in H_2O-D_2O Mixtures Containing Paramagnetic Ions. A. I. Rivkind	30	2	239
The Effect of Gas Absorption on the Luminescence of Zinc Oxide. K. V. Tagantsev and A. N. Terenin	32	2	241
The Nuclear Isomerism of Hf^{180m}. V. S. Gvozdev and L. I. Rusinov	35	3	401
Radioactive Rare Earth Isotopes Produced by Spallation. G. M. Gorodinskii, A. N. Murin, V. N. Pokrovskii, B. K. Preobrazhenskii and N. E. Titov	39	3	405
A Theory of the Interaction Between Evaporating or Growing Droplets at Large Distances. S. S. Dukhin and B. V. Deriagin	41	3	407
On the Interaction of Antiprotons and Nuclei. P. E. Nemirovskii	45	3	411
α-Decay Fine Structure of Even-Even Nuclei. V. G. Nosov	48	3	414
On Crystallization in Statistical Physics. E. A. Arinshtein	54	4	615
On the Causes of Retrograde Arc Cathode Spot Motion in a Magnetic Field. I. G. Kesaev	60	4	619
Paramagnetic Resonance Hyperfine Structure, Nuclear Spin and the Magnetic Moment of the 5.3-Year Radioactive Isotope Eu^{152}. A. A. Manenkov, A. M. Prokhorov, P. S. Trukhliaev and G. N. Iakovlev	64	4	623

(Continued on the following page)

CONTENTS (continued)

		Russian	
	Page	Issue No.	Page
On the Theory of Magnetostriction of Nickel Single Crystals. W. F. Brown, Jr.	67	5	827
Concerning the Note of W. F. Brown, Jr. Regarding the Theory of Magnetostriction of Nickel Single Crystals. N. S. Akulov	68	5	828
The Invariance Principle for a Homogeneous Medium of any Geometic Form. B. B. Kadomtsev	71	5	831
Depolarization and Intensities in the Raman Spectra of Benzene and Hexadeuterobenzene. M. A. Kovner and B. N. Snegirev	76	5	835
A Universal Relation Between the Absorption and Luminescence Spectra of Complex Molecules. B. I. Stepanov	81	5	839
Time Correlation in Classical Statistical Systems Consisting of a Large Number of Interacting Particles. V. V. Tolmachev	85	5	842
π^0-Photomeson Production on Complex Nuclei. A. S. Belousov, E. I. Tamm and E. V. Shitov	90	6	1017
Ionizing Energy of Electrons in Germanium Crystals. V. S. Vavilov, L. S. Smirnov and V. M. Patskevich	93	6	1020
On the Theory of Stationary Striations in the Positive Column of a Gas Discharge. O. V. Prudkovskaia and M. F. Shirokov	96	6	1023
On the Shape of Absorption and Luminescence Bands of Complex Molecules. B. I. Stepanov and L. P. Kazachenko	100	6	1027
The Generalized Stochastic Problem of Particle Motion. N. A. Chernikov	103	6	1030

SIGNIFICANCE OF ABBREVIATIONS MOST FREQUENTLY ENCOUNTERED IN SOVIET PHYSICS PERIODICALS

AN SSSR	*Academy of Sciences, USSR*
FIAN	*Physics Institute, Academy of Sciences USSR*
GITI	*State Scientific and Technical Press*
GITTL	*State Press for Technical and Theoretical Literature*
GOI	*State Optical Institute*
GONTI	*State United Scientific and Technical Press*
Gosenergoizdat	*State Power Press*
Gosfizkhimizdat	*State Physical Chemistry Press*
Gozkhimizdat	*State Chemistry Press*
GOST	*All-Union State Standard*
Goztekhizdat	*State Technical Press*
GTTI	*State Technical and Theoretical Press*
GUPIAE	*State Office for Utilization of Atomic Energy*
IF KhI	*Institute of Physical Chemistry Research*
IFP	*Institute of Physical Problems*
IL	*Foreign Literature Press*
IPF	*Institute of Applied Physics*
IPM	*Institute of Applied Mathematics*
IREA	*Institute of Chemical Reagents*
ISN (Izd. Sov. Nauk)	*Soviet Science Press*
I YaP	*Institute of Nuclear Studies*
Izd	*Press (publishing house)*
KISO	*Solar Research Commission*
LETI	*Leningrad Electrotechnical Institute*
LFTI	*Leningrad Institute of Physics and Technology*
LIM	*Leningrad Institute of Metals*
LITMiO	*Leningrad Institute of Precision Instruments and Optics*
Mashgiz	*State Scientific-Technical Press for Machine Construction Literature*
MATI	*Moscow Aviation Technology Institute*
MGU	*Moscow State University*
Metallurgizdat	*Metallurgy Press*
MOPI	*Moscow Regional Institute of Physics*
NIAFIZ	*Scientific Research Association for Physics*
NIFI	*Scientific Research Institute of Physics*
NIIMM	*Scientific Research Institute of Mathematics and Mechanics*
NII ZVUKSZAPIOI	*Scientific Research Institute of Sound Recording*
NIKFI	*Scientific Institute of Motion Picture Photography*
OIYaI	*Joint Institute of Nuclear Studies*
ONTI	*United Scientific and Technical Press*
OTI	*Division of Technical Information*
OTN	*Division of Technical Science*
RIAN	*Radium Institute, Academy of Sciences of the USSR*
SPB	*All-Union Special Planning Office*
Stroiizdat	*Construction Press*
URALFTI	*Ural Institute of Physics and Technology*

NOTE: Abbreviations not on this list and not explained in the translation have been transliterated, no further information about their significance being available to us.—*Publisher.*

The expanded program of the American Institute of Physics comprises translation of four leading Soviet physics journals, as listed below. These translations, by competent, qualified scientists, provide all research laboratories and libraries with accurate and up-to-date information of the results of research in the U.S.S.R.

Soviet Physics — Technical Physics

A translation of the "Journal of Technical Physics" of the Academy of Sciences of the U.S.S.R. The translation began with the 1956 issues, and is being continued. Twelve issues per year, approximately 3,000 Russian pages. Annually $90.00 domestic, $95.00 foreign.

Soviet Physics — Acoustics

A translation of the "Journal of Acoustics" of the Academy of Sciences of the U.S.S.R. The translation began with the 1955 issues. Four issues per year, approximately 400 Russian pages. Annual price, beginning with the 1957 issues, $12.00 domestic, $14.00 foreign. Prices for each volume prior to 1957, $20.00 domestic, $22.00 foreign.

Soviet Physics — "Doklady"

A translation of the "Physics Section" of the Proceedings of the Academy of Sciences of the U.S.S.R. The translation began with the 1956 issues. Six issues per year, approximately 900 Russian pages. Annually $25.00 domestic, $27.50 foreign.

Soviet Physics — JETP

A translation of the "Journal of Experimental and Theoretical Physics" of the Academy of Sciences of the U.S.S.R. Translation began with the 1955 issues. Twelve issues per year, approximately 4,000 Russian pages. Annual price, beginning with the 1957 issues, $75.00 domestic, $79.00 foreign. Prices for back volumes may be obtained from the American Institute of Physics upon request.

Subscriptions should be addressed to the American Institute of Physics, 335 East 45th Street, New York 17, N. Y.